School of Civil and Mechanical Engineering

Study of the use of ferronickel slag in concrete

Muhammad Ashiqur Rahman

This thesis is presented for the Degree of

Doctor of Philosophy

of

Curtin University

June 2019

Declaration

To the best of my knowledge and belief this thesis contains no material previously published by any other person except where due acknowledgement has been made.

This thesis contains no material which has been accepted for the award of any other degree or diploma in any university.

Signature:

Name: Muhammad Ashiqur Rahman

Date: 28-06-2019

ACKNOWLEDGEMENTS

All praise to Allah. Finally, I could accomplish my PhD study. Many thanks for your great blessings during this heroic journey.

I would like to acknowledge a number of people who helped and supported me to accomplish this study.

Firstly, I would like to express my gratitude to Associate Professor Prabir Kumar Sarker, the best supervisor that I have ever had, for his invaluable support, encouragement, assistance and guidance throughout this PhD study. I have learned a lot during this learning process mainly from the opportunities that were introduced by him. I would also like to acknowledge the support from my co-supervisor Associate Professor Faiz Ahmed Shaikh during this study.

This research was funded and supported by SLN, New Caledonia. I would like to gratefully acknowledge the contribution and continuous support from SLN through its research department and its consultant, Mr. D.J. Sassoon Gubbay. I am also grateful to Dr. Michael G Remias (Previous BGC-Cemtech Manager, Western Australia) for his continuous support to the work.

I received help and support from many wonderful technical staff in the School of Civil and Mechanical Engineering, Curtin University of Technology. Thank you very much to Mr Ashley Hughes, Mr Michael Ellis, Mr Robert Cutter, Mr Mark Whittaker, Mr Luke English, Mr Craig Gwyther, Ms Dianne Garth, Ms Sucy Leong, Mr Frankie Sia. Thank you very much to Mr. Ashish Kumer Saha for your great help in experimental work. I would like to thank Dr. Pradip Nath and Partha Sarathi Deb for their help during my research.

I acknowledge the use of equipment, scientific and technical assistance of the Curtin University Electron Microscope Facility, which has been partially funded by the

University, State and Commonwealth Governments. I like to thank Ms Elaine Miller, Dr Catherine Kealley and Angela Halfpenny for helping in microstructural tests and analyses.

I am grateful to my parents for their constant support, prayers and love for me. I would like to thank my brother and sister for their encouragement and love for me throughout the journey. I am thankful to my wife, Afshana Jaman Ananna, who sincerely supported me in crucial moments of my study. I also like to thank my parents-in-law for their encouragement and support.

Abstract: Ferronickel slag (FNS) is a by-product of the production of ferronickel alloy. About 12 tonnes of FNS is produced in the production of one tonne of ferronickel alloy. This research evaluates the suitability of using ground granulated high magnesium ferronickel slag (FNS) as a cement replacement in concrete. The FNS used in this study was obtained from smelting of garnierite ore and the molten slag was granulated by water cooling. The main elements of the slag are silicon (Si), magnesium (Mg) and iron (Fe). A series of tests were conducted to investigate the strength and durability properties of concrete using ferronickel slag as a supplementary binder with cement. Tests on fresh and early age properties show that water demand and setting times were not significantly changed by use of the FNS as a cement replacement of up to 50%. The 28-day strength activity index of the FNS was 84%. The Le-Chatelier soundness test, the autoclave expansion test and accelerated curing at 80 ^{o}C for 120 days showed no increase of expansion for using FNS at up to 65% of the binder despite its high magnesium content. Leaching assessment of ground FNS showed that the concentrations of the leachable heavy metals were below the limits set by regulatory authorities. Developments of compressive, flexural and tensile strengths of FNS blended mortar and concrete mixtures were found to be similar to those containing class F fly ash. Drying shrinkage of concrete using FNS did not show noticeable change after 90 days of age. Drying shrinkage decreased considerably at 20% FNS content and then showed increasing trend with the increase of FNS content while compressive strength decreased with the increase of FNS content. Water absorption, volume of permeable voids (VPV) and sorptivity coefficient of the FNS blended concrete specimens varied in the ranges of 3.29% to 4.17%, 8.14% to 9.65% and 0.005-0.009 mm/s$^{1/2}$, respectively. Chloride ion penetrability of the FNS blended concrete specimens was found to be either very low or low. The presence of Mg was found in the form of stable forsterite ferroan that did not take part in the hydration reaction. Therefore, expansive $Mg(OH)_2$ (brucite) was not found in the scanning electron microscopic (SEM) images of the microstructure and powder X-ray diffraction (XRD). Reinforced concrete beams were cast using 30% FNS in the binder and the specimens were steam cured at 80 ^{o}C for 8 weeks after 28 days of standard curing. High temperature and humidity were applied as an accelerated condition for any possible reaction of the Mg present in FNS to occur and

show any resulting expansive behaviour. No sign of cracks was observed in the beams after the end of this accelerated condition. The beams were then tested to investigate flexural, shear and bond behaviours. The experimental failure loads were in good agreement with the results predicted by using design standards. Overall, the soundness, strength and durability properties of ground FNS blended binder were found comparable to those of binders blended with other commonly used supplementary cementitious materials such as class F fly ash.

List of Publications:

Published:

1. Rahman, M.A., Sarker, P.K. and Shaikh, F.A.U. (2015). Fresh and Early-Age Properties of Cement Pastes and Mortars Blended with Nickel Slag. *27th Biennial National Conference of the Concrete Institute of Australia in conjunction with the 69th RILEM Week*, Aug 30 2015. Melbourne, Australia.

2. Rahman, M.A., Sarker, P.K., Shaikh, F.A.U., Saha, A.K. (2017). Soundness and compressive strength of Portland cement blended with ground granulated ferronickel Slag. *Construction and Building Materials*, 140: 194-202.

Submitted for review:

1. Rahman, M.A. and Sarker, P.K. (2020). Structural performance of reinforced concrete beams using ground ferronickel slag as a partial replacement of cement. *Materials and Structures*.

Table of Contents

List of Tables

List of Figures

Chapter 1: INTRODUCTION

1.1 Background

Unmanaged waste is increasing day by day having a critical impact on the environment. By recycling industrial waste and using it as construction materials could be a better solution from both ecological and economical points of view. About 5% of the global carbon footprint comes from the cement industry (Lamond & Pielert, 2006). Approximately one tonne of carbon dioxide is emitted to the environment while producing one tonne of cement (Lamond & Pielert, 2006). Due to the rising price of cement and higher carbon dioxide emission from cement production, it is necessary to utilize more industrial byproducts as supplementary cementitious materials (SCM). SCMs can reduce bleeding, increase plastic viscosity, and improve the hardened properties and durability of concrete. In this context, researchers have successfully used silica fume, fly ash, rice husk ash and ground granulated blast furnace slag (GGBFS) in concrete productions. In the last decade, global warming has raised a big concern and the Australian Government is taking necessary steps to reduce Australia's carbon emissions (AS 3972, 2010).

Cement is the conventional binder for concrete and is recognized as one of the energy intensive materials. Concrete is the most widely used material (Siddique & Khan, 2011) for construction due to the availability of raw materials, versatile properties, strength and durability. There has been enough pressure from consumers and government to reduce the environmental impact in terms of greenhouse gas emission reduction. Hence, the existing Australian standard, AS 3972, 2010, is being revised by allowing increased use of the proportion of mineral additions. The Government is aspiring to increase the use of supplementary cementing materials (SCMs) within the existing performance based specifications. This will reduce the 'carbon footprint' from cement manufacturing companies and help meet the Government's requirement for reducing greenhouse gas emissions.

Pozzolanicity is an important characteristic of supplementary cementitious materials (SCMs). Most SCMs used in concrete are pozzolanic in nature. The pozzolanic activity of a SCM with cement is assessed by the term pozzolanic activity index (Neville, 1996). When a pozzolan is used as a SCM, the chemical reactions take place in two steps. In the first step, the hydration reaction between C_2S or C_3S of cement and water produces $Ca(OH)_2$ and the primary calcium silicate hydrate (C-S-H) gel (Hakkari, 2011). The reaction is as follows:

C_2S or $C_3S + H_2O \rightarrow$ primary C-S-H + $Ca(OH)_2$

In the second step, the $Ca(OH)_2$ starts reacting with the silica (SiO_2) of SCM and water to produce the secondary C-S-H gel. The reaction is as follows:

$Ca(OH)_2 + SiO_2 + H_2O \rightarrow$ secondary C-S-H

The additional C-S-H makes the concrete microstructure denser and improves the strength, transport properties and durability of concrete (Zhang et al., 1996; Ganesan et al., 2007). Some SCMs such as GGBFS, fly ash and rice husk ash possess a considerable amount of silica, which acts to enhance the hardened properties of concrete (Zhang et al., 1996; Ganesan eta al., 2007; Xie et al., 2002). Similarly, ferronickel slag contains a significant amount of SiO_2 (about 53%), which may make a similar contribution. Hence, it is essential to determine the properties of concrete utilizing FNS as a SCM.

Researchers are continuously working to produce concrete with better engineering properties by using SCMs and chemical admixtures (Muhl, 2003). These can be added individually with Portland or blended cement or in different combinations. SCMs are often used to make concrete more economical, durable and stronger. These materials can reduce the amount of required cement and enhance strength, workability and durability through hydraulic and pozzolanic activity (CSA A3001-03, 2003). Typical examples of SCMs are silica fume, fly ash, GGBFS, metakaoline, rice husk ash, and

natural pozzolans such as calcined shale and calcined clay which could be incorporated in concrete as an addition or as a partial cement replacement. Over the last 20 years, the use of SCM in concrete has been steadily increasing in Australia. At present, more than 90% of concrete contains at least one SCM. Detailed standards and procedures for using fly ash, slag and amorphous silica as SCMs have been included in AS 3582.1 (2016), AS 3582.2 (2001) and AS 3582.3 (2002), respectively.

A major subject of this research is the possible reactivity of magnesium present in the ferronickel slag. X-ray florescence (XRF) analysis shows that FNS contains about 32% MgO. According to AS 3583.9 (1991), the value of MgO in an SCM is reported to be less than 15%. However, MgO is not always harmful for concrete. The delayed expansion caused by slow hydration of MgO in cement had compensated for the thermal shrinkage of concrete (Mo et al., 2012). The authors have used MgO powder as an expansive agent (MEA) by 5-10% weight of cement. Besides, minerals of dolomite, serpentine and magnesite containing about 20-40% MgO, have been used successfully for producing MEA (Lingling & Min, 2005). The reactivity of MgO depends on its calcination temperature. If the burning temperature is higher, the magnitude of early age expansion is smaller and the hydration process of MgO lasts longer. The quenching temperature of the FNS used in this study is in the range of 1200 ^{o}C to 1300 ^{o}C. Magnesium produced at this quenching temperature range may go into the hydration reaction for a longer period of time.

Using fly ash together with ferronickel slag can have dual benefits. Fly ash reduces the heat of hydration. It reacts with the hydration products of the expansive materials and cement. It absorbs expansion stress and thus reduces expansion cracking of the concrete. Deng et al. (1990) reported that using of fly ash could lower the supersaturation of Mg2+ and OH– in pore solution and form $Mg(OH)_2$, thus resulting in reduction of expansion and the corresponding expansive force. Fly ash also fills the interstitial pores of the cement pastes which reduces the permeability and shrinkage cracking of the matrix.

The performance of MgO in concrete can be improved by carbonation. Carbonation of cement paste specimens containing 0-40% MgO was effectively accelerated (Liwu & Daman, 2012) under the condition of 98% relative humidity, 99.9% CO_2 and 23±2 ^oC temperature. The experimental results showed that paste specimens with 40% reactive MgO showed a 32% reduction of the total pore volume, and a 39% higher mean microhardness after 56 days of carbonation curing in comparison with 100% general purpose Portland cement pastes. Hence, it is important to study the effect of using high magnesium FNS in concrete as partial cement replacement.

It is evident that the chemical compositions of ferronickel slags from different sources showed a significant variation in composition. Therefore, the properties of the concrete using ferronickel slag from one source can be different from those using the slag from another source. This research is aimed to investigate the properties of concrete using high magnesium ferronickel slag produced from the smelting of garnierite nickel ore as a part of the binder. Use of the ground FNS with Ordinary Portland cement (OPC) was studied.

1.2 Aim and objectives

This research is focused on assessing the suitability of using ferronickel slag from a specific source as a cement replacing material. Chemical composition of FNS varies with the source and the method of processing. Hence, the performance of the individual material is unique when compared with materials from other sources. The primary objective of this study is to determine the properties of cement binder using ground FNS as a partial cement replacement.

The aims of the research are as follows:

- Investigate the fresh and early age properties of FNS blended cement binders
- Study the expansion behaviour of the high magnesium content of FNS in ambient and accelerated heat curing conditions

- Determine the strength properties and long-term durability of cement mortar and concrete containing different percentages of FNS
- Evaluate the flexure, shear and bond behaviours of reinforced concrete beams manufactured using FNS as a partial cement replacement

1.3 Significance of the research

About 12 tonnes of FNS is produced as a by-product to produce one tonne of ferronickel alloy. SLN is one of the major nickel producers around the world. Despite the current limited uses in various construction works, a huge amount of FNS is available in the premises of nickel smelting plants. For instance, 25 million tonnes of FNS is currently available in the premises of SLN in New Caledonia. Therefore, the use of ferronickel slag as a partial cement replacement has the potential to contribute greatly in production of green concrete. This will help sustainable management of the by-product reducing environmental issues. Development of an alternate supplementary cementing material will also contribute to the durability of concrete and may reduce the cost of concrete production. This research will add valuable knowledge on using the high magnesium FNS as a supplementary cementing material. The experimental results on the reactivity of ground FNS and its effects on the fresh and hardened properties of concrete are essential for the development of FNS as a SCM. Very limited research are available to address the specific issue on using high magnesium ferronickel slag as cement replacing material.

The behaviour of concrete specimens in the short and long term are studied. The flexure, shear and bond behaviours of reinforced concrete beams are also investigated. Overall, this study will add essential knowledge on the behaviour of concrete made using ferronickel slag blended cement binder.

1.4 Thesis outline

The remaining part of the thesis is outlined as below:

Chapter 2 presents a review of previous research on different supplementary cementitious materials. It presents the behaviour of concrete using fly ash, GGBFS and other SCMs.

Chapter 3 describes the short term and long term behaviour of magnesium in supplementary cementing materials. Research methodology is developed to investigate the effects with ferronickel slag as a SCM. Material properties, mix design, and experimental methods are also described.

Chapter 4 presents the experimental results on soundness, fresh and hardened properties, strength properties and durability of ferronickel slag blended cement paste and concrete mixtures.

Chapter 5 includes the flexural, shear and bond behaviour of reinforced concrete beams made using ferronickel slag blended cement binder.

Chapter 6 presents the conclusions of the research. Future recommendations are also included in this section.

A list of references and appendices are added at the end of this thesis.

Chapter 2: LITERATURE REVIEW

2.1 Background

The strategy for utilization of supplementary cementing material was developed over the last decades by considering environmental and energy benefits. Portland cement production by grinding and calcination of raw materials is a highly energy-intensive process. Fly ash and silica fume usually do not need any grinding while slags may need grinding to use as SCM. However, using SCMs can substantially reduce the energy consumption for producing concrete binders. The uses of solid industrial waste (silica fume, fly ash, slags) and natural pozzolans (volcanic ash) as SCM are increasing day by day because of their environmental benefits and the improvement of various properties and durability of concrete (Pappadakis et al., 2002). Supplementary cementing materials can help reduce the expansion due to the alkali-aggregate reaction by producing more calcium silicate hydrates (Duchesne & Berubet, 1995). Additional C-S-H decreases the amount of available alkali ion in the matrix for reacting with the reactive aggregates. Since this study is an investigation of FNS as a SCM, some of the established SCMs that are commonly used for replacing cement partially are presented below.

2.2 Properties and usage of fly ash

Fly ash is produced from the coal-fired power plants as a byproduct. Fly ash could be characterized as aluminosilicate with cementitious/pozzolanic properties. Cementitious fly ash is labelled as Class C which contains at least 50% SiO_2+Al_2O_3+Fe_2O_3 of the mass (Scheetz & Earle, 1998) with more than 10% CaO. In pozzolanic or Class F fly ash, the mass of SiO_2+Al_2O_3+Fe_2O_3 is found to be more than 70% of the fly ash with low (less than 10%) CaO. The particle size of fly ash generally ranges between 10 to 100 μm and the specific gravity varies between 1.94 and 2.94. Some of the particles of fly ash are found to be hollow and spherical. These are known as cenospheres. Cenospheres are mainly composed of silica, alumina and iron sized from 1 to 500 μm.

X-ray diffraction analysis (XRD) of the fly ash shows the main phases are mullite, glass, quartz, hematite and magnetite and anhydrite (Helmuth, 1987).

Pozzolanicity of the fly ash mainly depends on the fineness, microstructure, calcium content and the loss on ignition (LOI). Pozzolanic activity generally enhances with the increase of fineness but the enhancement is insignificant beyond 600 m^2/kg. Cement hydration produces calcium hydroxide and fly ash silicate phases react with calcium hydroxide which produces additional calcium silicate hydrates. Additional calcium silicate hydrate gives additional strength. Additional calcium silicate hydrate (CSH) formation is time-dependent and the strength gain can be attained up to 90 days or longer. Using fly ash in concrete has many benefits (Malhotra & Mehta, 2005; Bendapudi, 2011; Hemalatha & Ramaswamy, 2017):

1. Increase of workability by the spherical and glassy particles reduces water demand of the binder.
2. Fly ash improves the resistance to bleeding and segregation in concrete.
3. The additional CSH makes the microstructure denser and less permeable.
4. Fly ash adds long-term strength to the cement products by reducing the heat of hydration.
5. Resistance to corrosion and sulphate attack are increased due to the denser microstructure and less availability of portlandite in the product.
6. Class F fly ash is used to compensate for the expansion caused by alkali silica reaction (ASR) of the reactive aggregates.

Extensive research is available on the incorporation of fly ash in concrete. The major parameters affecting the strength of concrete with fly ash are the fly ash percentage, source of the fly ash, chemical compositions and curing condition. Low calcium fly ash exhibits slow strength development at the early ages due to its low calcium content (Hemmings & Berry, 1988). Scanning electron microscope images (SEM) and energy dispersive spectrum (EDS) are usually used to analyze the hydration products. It has been reported (Hemalatha & Ramaswamy, 2017) that low calcium fly ash shows

unhydrated spots and unreacted fly ash particles at 28 days. The sensitivity of the class C fly ash is relatively less due to the curing condition (Poon et al., 1997). Moreover, it provides better strength by reacting faster at an early age. The limitation of class C fly ash is that it is not effective enough in compensating for the expansion due to sulphate attack and ASR compared with the class F fly ash. The typical application of fly ash as SCM is about 15-20% by mass (Bendapudi, 2011). A maximum of 35% by mass of coal fly ash as a SCM can be used as per BS EN 197-1 (2011), and ASTM C 595 (2018) allows substitutions up to 40%. However, ASTM C 618 (2017a) reports that the amount of fly ash or natural pozzolan replacement as supplementary cementing materials should be established by testing against the required concrete properties. Malhotra (1990) established concrete incorporating high volume fly ash by replacing more than 50% cement with good strength and durability. However, American Concrete Institute (2011) limits the usage of fly ash by up to 35% in structural concrete. Oner et al. (2007) investigated the strength development of the fly ash and the optimum usage in concrete. It has been noted that the fly ash to cement ratio plays an important role in determining fly ash efficiency. Strength was increased with the increase of fly ash up to a certain percentage, beyond that the strength decreased. The optimum level of fly ash usage was reported to be 40%.

The reactivity and strength of the fly ash depends mainly on the water/binder (w/b) ratio, replacement amount and curing condition (Kobayakawa et al., 1998). It was reported (Lam et al., 1998) that 45% replacement of fly ash with a water/binder ratio of 0.3 and 0.5 showed strengths of 72 MPa and 36 MPa, respectively. It has also been established that 45% replacement of fly ash with a water/binder ratio of 0.24 can gain strength as high as 80 MPa (Poon et al., 2000). Curing at high temperature does not always lead to higher strength gain. Research shows that fly ash at temperatures below 35°C, accelerates hydration of the cement (Narmluk & Nawa, 2011) but when curing at higher temperature, fly ash shows a retarding effect in strength gain (Escalante & Sharp, 1998).

2.3 Properties and usage of blast furnace slag

Ground granulated blast furnace slag (GGBFS) is produced as a by-product during production of iron using blast-furnaces. When iron ore, coke and limestone are fed into the furnace, molten iron and the slag are produced. At 1500 ^{o}C to 1600 ^{o}C temperature, the molten slag normally floats above the molten iron. GGBFS contains about 30%-40% of SiO_2 and 40% of CaO which is similar to the normal Portland cement. When the molten slag is cooled down rapidly using water jets or water in a pond, it produces fine granular non crystalline glassy calcium-aluminosilicates. After drying, a rotating ball mill is used for grinding and further processing the granulated slag to very fine powder of GGBFS. GGBFS can be used for replacing the normal Portland cement from 30% up to 85%. Generally, 50% is used in most cases. Replacement up to 85% can be used to reduce the heat of hydration in harsh environments. Typical compositions of GGBFS and comparison with OPC (Hanson, 2010) are given in the Table 2.1 below.

Table 2.1: Typical composition of GGBFS and OPC

Components	% in GGBFS	% in OPC
Calcium oxide (CaO)	40%	60-67%
Silica (SiO_2)	35%	17-25%
Alumina (Al_2O_3)	16%	3-8%
Magnesia (MgO)	6%	0.1-4%
Other - Fe_2O_3, etc.	3%	0.5-6%

GGBFS is a fine glassy powder. The colour can vary from dark to off-white. The specific gravity of GGBFS (2.87-2.9) is less than that of cement (3.15). The chemical composition of GGBFS varies based on the ores, fluxing stone and amount of coke impurities. Physical properties, surface area (m^2/kg) and average diameter (μm) of GGBFS used in the previous research are shown in Tables 2.2 and 2.3 below.

Table 2.2: Physical properties of GGBFS

Properties	Oner and Akyuz (2007)	Hui-sheng et al. (2009)	Tasong et al. (1999)
Specific gravity	2.87	2.89	2.9
Specific surface (m^2/kg)	425	371	425-470

Table 2.3: Surface area and average diameter of GGBFS (Wan et al., 2004)

Samples	Ball-mill (A)	Vibromill (B)	Airflow mill (C)	Ball-mill (D)
Specific surface (m^2/kg)	510	685	515	512
Diameter (μm)	13.69	9.12	11.72	13.15

It can be noted from Table 2.2 that the surface area of the GGBFS varied from 371 to 470 m^2/kg. Table 2.3 shows the surface area and diameter of the GGBFS prepared from different grinding techniques. Sample A is ground in an industrial ball mill with a diameter of 2.2 m and 6.5 m long. Steel balls are used as the grinding medium inside the ball mill. Sample B is prepared using a laboratory vibromill. A vibromill consists of a driving device with circular steel vessel which is filled with samples. For crushing the material, a steel ring and a cylinder are placed in the vessel with filled samples. Type C is generated from the industrial airflow mill created by Alpine, Germany. A similar ball mill as used in sample A, was used for sample D. To increase the output, grinding assistant agent (0.05% ZS) is added in the ball mill. As shown in Table 2.3 the diameter of the GGBFS particles varied from 9.12-13.69 μm and the surface area was between 510-685 m^2/kg. Wan et al. (2004) also investigated the SEM image of the samples ground by the above (A-D) procedure and concluded that GGBFS particle shape is not spherical; rather, it varies based on a different grinding procedure.

Yim et al. (2015) reported that the specific density of GGBFS and Portland cement was 2.95 and 3.14, respectively. Their surface area was 414 m^2/kg and 335 m^2/kg, respectively. The particle size distributions of both powders showed the maximum

particle size is about 200 μm for both. The median particle size for cement is higher than 20 μm and for GGBFS is lower than 20 μm. It was also observed that cement is more normally distributed compared with GGBFS, but the overall distributions are similar for both. Cement and GGBFS particle size distributions are presented in Figure 2.1.

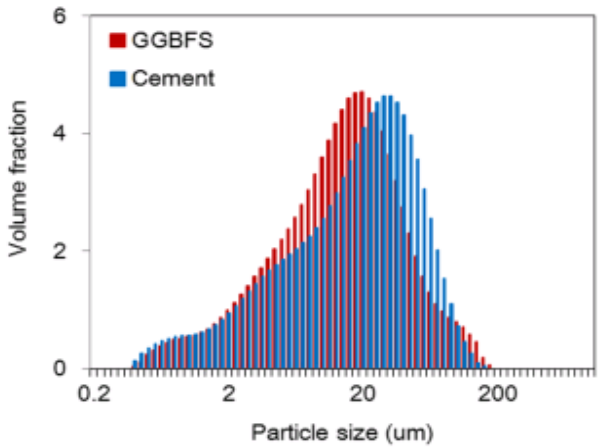

Figure 2.1: Particle size distribution of cement and GGBFS (Yim et al., 2015)

Normally, calcium, silicon, magnesium, aluminium, and oxygen constitute more than 95% mass of GGBFS. Hydraulic properties of the GGBFS are determined by basic (1) chemical composition, (2) vitreous state (Daube & Bakker, 1986) and (3) basicity index (CaO/SiO_2 ratio) (Nkinamubanzi et al., 1998). Hydraulic activity of slag is dependent on basicity. Greater hydraulic activity is associated with higher basicity. According to Cheron and Lardinois (1968), the hydraulic activity index of GGBFS can be calculated by the ratio of $CaO + 1.4\ MgO + 0.56\ Al_2O_3) / SiO_2$. Hydraulic index normally varies between 1.65 and 1.85.

GGBFS blended cement pastes usually show smaller gel pores and less large capillary pores than those in pure cement pastes. Structures with smaller pores provide GGBFS concrete lower permeability and improved durability. Bleeding characteristics of GGBFS concrete depends on the fineness of GGBFS (ACI 233 R03, 2000). It is also reduced with the increase of fineness of GGBFS. Research shows that the bleeding

capacity of the concrete increases with the increasing amount of GGBFS (Wainwright & Rey, 2000; Wainwright & Ait-Aider, 1995; Olorunsogo, 1998). At cement replacements higher than 60%, bleeding characteristics increase significantly and do not follow fineness of GGBFS. It was observed that with increasing the amount of GGBFS, the workability of concrete increased (Wainwright & Rey, 2000; Megat Johari et al., 2011). Beyond 85% cement replacement by GGBFS does not have much effect on bleeding. Morphological characteristics, smoother surface and better particle dispersion of the GGBFS increase the fluidity of concrete (ACI 233 R03, 2000). Workability of mortar increases with the increase of fineness (Wan et al., 2004). GGBFS particles fill the spaces between the larger cement particles which results in higher flow-ability of OPC-GGBFS mixtures (Ozbay et al., 2016).

The setting times of concrete blended with GGBFS depend on many factors, mainly water/cement ratio and temperature. Generally, the setting time of GGBFS concrete is longer than that of concrete with only Portland cement. By increasing the GGBFS content, setting time increases (Wainwright & Ait-Aider, 1995). The effect is more pronounced at low temperature and high levels of GGBFS. Prolonged setting time can be advantageous sometimes as the concrete will be workable for a longer period for specific applications.

At normal temperature, the hydration of GGBFS blended cement occurs in two phases. Firstly, the main part of the reaction is with alkali hydroxide and subsequently it reacts mainly with $Ca(OH)_2$. The inclusion of GGBFS refines the product and pore structure of the hardened concrete (Daube & Bakker, 1986). GGBFS reduces the porosity and pore size and changes the mineralogy of the hardened concrete. It creates a denser and more compact structure (Bouikni et al., 2009). It reduces the water penetration which decreases the mobility of the chloride ions as well. Higher GGBFS content yields higher C-S-H and improved durability of concrete. Experimental work with 70% GGBFS shows that the pore structure was improved significantly (Luo et al., 2003) at 60 days. GGBFS generates less heat of hydration, less shrinkage and less thermal cracks in concrete.

Strength development of concrete containing GGBFS depends on the GGBFS percentage in the binder, total binder content, water/binder ratio, curing condition and age. Early stage strength development of concrete with GGBFS decreases with increasing amounts of GGBFS. The strength of GGBFS concrete at 90 days increases compared with the control concrete. GGBFS content of up to 60% showed good strength and beyond 60% it was not beneficial. Research also shows that early strength gain of the GGBFS blended concrete and mortar mixes depend on the curing condition. Figure 2.2 shows that the compressive strength decreased with increasing amounts of slag percentage (Guneyisi & Gesoglu, 2008). Strength gain at 90 days was higher than that at 28 days. Wet curing condition is more effective for attaining compressive strength compared with dry curing condition. Compressive strength was increased up to 60% replacement compared to the control mix for wet curing.

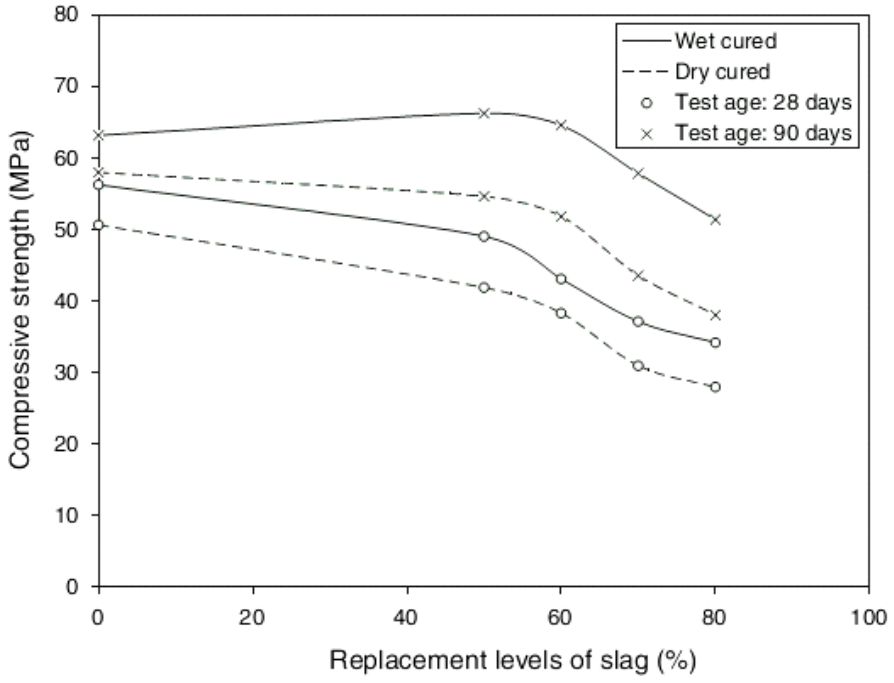

Figure 2.2: Effect of curing condition and the percentage of GGBFS on compressive strength (Guneyisi & Gesoglu, 2008)

At elevated temperature, the strength gain at 28 days of concrete made with GGBFS was found to be higher than the concrete prepared with ordinary Portland cement only

(Soutsos, 2004). The effect of temperature on strength development is shown in Figure 2.3 (Barnett et al., 2006). At higher temperature, the strength gain is higher but normal curing strength gain is slower compared to that of OPC concrete.

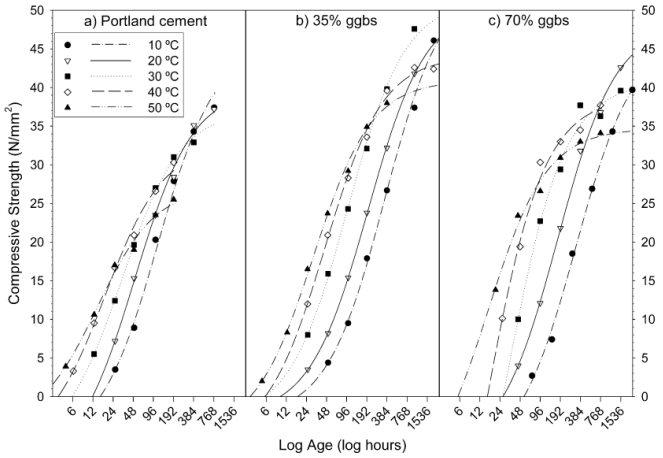

Figure 2.3: Strength development of high w/b ratio (0.5-0.6) mortars at different curing temperatures (Barnett et al., 2006)

Flexural strength of the concrete with GGBFS showed higher compared to the control specimens at 14 days (Sivasundaram & Malhotra, 1992). Khatib and Hibbert (2005) showed that flexural strength reduced with 40% and further reduced with 80% cement replacement but increased at 60% replacement. No explanation was given for such variation. Babu and Kumar (2000) investigated the effectiveness of GGBFS in concrete with different percentages of replacement (10–80%) using the concept of efficiency by establishing relationships between the water/cement ratio and strength of GGBFS concrete and normal concrete. For concretes containing up to 30% GGBFS, compressive strengths were slightly higher at 28 days compared to the normal concrete. For all other replacement percentages, the strengths were lower compared to the normal concrete. The experimental results indicated that the overall slag efficiency factor (k) has to increase by 8.6 and 19.5 for 50% and 65% replacement, respectively, in total cementing materials for gaining an equivalent strength to that of 28 days normal concrete.

Research conducted by Li and Zhao (2003) reported the combined influence of fly ash and GGBFS high-strength concrete on compressive strength development. Three different types of concretes such as (a) high-volume fly ash concrete (HFAC) (b) concrete with GGBFS and fly ash (GGFAC) and (c) Portland cement concrete (PCC) were prepared. The strength development was recorded up to 360 days. HFAC contained 300 kg/m^3 of cement and 200 kg/m^3 of fly ash. GGFAC was prepared with 300 kg/m^3 of cement and 125 kg/m^3 of fly ash and 75 kg/m^3 of GGBFS. PCC was made with 500 kg/m^3 cement only. At early ages, the behaviour of HFAC (prepared with 40% fly ash) was different from the behaviour of PCC and GGFAC (containing 40% of FA). Before 56 days, it had lower strength, but highest strength was observed at the end of testing age. The strength gains of GGFAC and PCC were similar. It was slightly lower than PCC before 28 days. GGFAC was able to achieve good early-age compressive strength and higher long-term strength.

Cheng et al. (2005) investigated the influence of GGBFS on concrete compressive strength. Three concrete mixtures were prepared. One was a control with a mix proportion of 1:1.82:1.97. The water/binder ratio was 0.55. Other two were prepared by replacing 40% and 60% cement by GGBFS. Compressive strengths of the specimens at 91 days were 42.4, 45.3 and 48.6 MPa for control, 40% and 60% replacement, respectively. GGBFS concrete showed a higher value of compressive strength compared to the OPC concrete after completion of hydration and pozzolanic reaction of GGBFS. Higher replacement of GGBFS showed higher ultimate strength.

An experiment conducted by Atis and Bilim (2007) revealed the behaviour of the GGBFS concrete under various curing conditions (wet and dry). Samples were prepared with Portland cement and GGBFS with w/b ratios of 0.3, 0.4 and 0.5. The cement content was 350, 400 and 450 kg/m^3. GGBFS replacement percentages were 20-80% with an increment of 20%. Twelve cube samples were produced and demoulded the next day. Half of the samples was kept at 22±2 ^oC and 65% relative humidity (RH), and other half was placed at 22±2 ^oC and 100% RH. Compressive strength was measured using the samples at 28 days and 3 months. The result showed that wet-cured specimens with

20% and 40% GGBFS content had compressive strengths higher than the control specimen at 28 days. For 60% GGBFS replacement, compressive strength was reported to be equivalent to that of control specimen and it was found to be satisfactory at 80% GGBFS replacement. At 28 days, for the dry curing condition, 20% and 40% GGBFS replacement had an equivalent compressive strength to that of the control specimen. At 60% GGBFS replacement, compressive strength was satisfactory compared with the control concrete and at 80% GGBFS showed lower strength compared to the control concrete.

2.4 Properties and usage of silica fume

2.4.1 Physical properties of silica fume

Silica fume is an amorphous mineral containing chemically active extremely small particles of SiO_2. It is extracted as a by-product from the smelting furnaces during silicon alloy or silicon production. Raw materials such as coal, quartz, and woodchips are used in this process. Silica fume is composed of fine particles and the specific surface is about six times that of cement. Silica fume has a higher content of non-crystalline silicon dioxide and less amounts of magnesium, alkali and iron oxides. The physical characteristics of silica fume depend on the manufacturing process. Generally, it is in form of a spherical shape. The average silica fume particle size is less than 1 μm which is about 100 times smaller than the average Portland cement particle (Butterworth, 2003). The specific gravity is about 2.2. The specific surface area is about 13000-30000 m^2/kg (Khan & Siddique, 2011). The bulk density is about 200-350 kg/m^3. The colour could vary from light to dark grey depending on the manufacturing process. It is also influenced by the composition of the raw material, exhaust temperature, furnace temperature and the type of metal being produced.

2.4.2 Characteristics of silica fume

As per AASHTO M307 (2013) or ASTM C1240 (2015), silica fume can be considered as a supplementary cementing material to enhance the strength and long-term durability properties of concrete (Bhanja & Sengupta 2005). Due to higher silica content and fineness, it is classified as a highly pozzolanic material. In concrete, silica fume reacts with the $Ca(OH)_2$ and produces aluminate and silicate hydrates. These hydrates reduce permeability and increase strength by densifying the concrete structure. Generally, the reactivity of silica fume is higher than PFA or GGBFS due to its higher surface area and silica content (Atul, 2012). Silica fume enhances strength and durability by pore-size refinement, microstructure modification and cement paste and aggregate interfacial refinement. Silica fume reduces CH crystals' degree of orientation in the transition zone between the cement paste and aggregate and increases the interfacial bond strength. Silica fume adds strength to the bond between cement paste and aggregate by reducing the pores and increasing homogenous microstructure of the interfacial region. Experiments (Razak & Wong, 2004; Newman & Choo, 2003; Chung, 2002; Poon et al., 2006; Elahi et al., 2010) revealed that usage of silica fume in the concrete mix increased the strength about 30-100% based on the type of cement, silica fume percentage and curing process (Roy & Sil, 2012). The main contribution on the strength development by silica fume takes place between about 3 and 90 days. Further strength development beyond 90 days is insignificant.

2.4.3 Mechanical properties and workability of silica fume concrete

Workability of the fresh concrete mix depends mainly on the type of material, environmental condition and mix proportion. Silica fume makes concrete mix more cohesive and provides resistance to segregation. Literature reveals that workability of the concrete generally reduces (Gafoori & Diawareand, 2007; Yogendran et al., 1987; Pawade et al., 2011) with the addition of silica fume. Compressive strength was found to be increased by 6-67% for addition of 5-40% silica fume (Atul, 2012; Kadri & Duval, 1998; Sakr, 2006; Ganeshbabu & Suryaprakash, 1995; Khan & Ayers, 1995) with

various water/binder ratios. Flexural strength and tensile strength were also increased for silica fume incorporated concrete mixes due to increase of compressive strength. Application of silica fume as SCM increased the tensile strength by 22-34% (Sakr, 2006; Kathkhuda et al., 2009). Bhanja and Sengupta (2005) experimented on the variation of tensile strength of silica fume incorporated high-performance concrete at 28 days. Concrete mixes were prepared with 0-25% replacement with increments of 5%. The w/c ratios were 0.26-0.42 with increments of 0.04. Investigation revealed that splitting tensile strength was not increased significantly with higher replacement by silica fume and the increase was minimal beyond 15%. Tanyildizi and Coskun (2008) reported the contribution on the tensile strength by silica fume at high temperature exposure of lightweight concrete. The replacement was 0-30% by weight with silica fume. It was observed that the tensile strength was reduced starting from temperature 200 ◦C. The reduction with 10% silica fume was 3.11%, 11.46% and 80.15% at 200, 400 and 800 ◦C, respectively. The reduction was 5.8%, 40.62% and 75.08% at 200, 400 and 800 ◦C, respectively, for concrete with 30% silica fume. Generally, it was observed that the reduction of tensile strength in concrete was prevented by addition of silica fume.

Investigation also reveals that flexural strength could be also improved by addition of silica fume at 15-65% (Roy & Sil, 2012; Sakr, 2006; Kathkhuda et al., 2009; Ramakrishnan & Srinivasan, 1982). Bhanja and Sengupta (2005) prepared high performance concrete (HPC) with silica fume to investigate the effect on flexural strength of the mixes. The w/c ratios of mixes were 0.26-0.42 with an increment of 0.04. The replacement of silica fume was 0-25% by weight with increments of 5%. It was observed that the flexural strength increased significantly even with high percentage silica fume replacement. Silica fume was incorporated with hooked steel fibres and the flexural strength was evaluated by Koksal and Sahin (2008). A significant increase in flexural strength was observed due to incorporation of steel fibres and silica fume. Concretes containing 0.5% steel fibre had lower strength compared with the concrete with 1% steel fibre with same silica fume content.

2.5 Properties and usage of rice husk ash

Rice husk is the coating of rice seed. It contains cellulose (about 50%), lignin (25-30%), and silica (15-20%) (Ahmed et al., 2017). Lignin and cellulose are removed after burning and the only remaining is silica ash. Burning of rice husk under controlled temperature can produce rice husk ash (RHA) which has high amorphous silica content which can be treated and used as a SCM in the concrete. Open burning of rice husk produces crystalline RHA with high carbon content and low reactivity (Hwang & Chandra, 2016). It adversely affects concrete performance and is not recommended for use. Investigation shows that burning the rice husk at 500-700 °C for a period of more than 12 hours produces RHA with high reactivity and amorphous content (Nair et al., 2008). It was also reported that RHA produced at 600-700 °C has the highest pozzolanic activity (Hwang & Chandra, 2016). After burning, rice husk produces about 20% ash. It is reported that 200 kg of rice husk is produced from 1,000 kg of rice grain. After burning 200 kg of rice husk, 40 kg of ash is produced (Nair et al., 2008). The specific gravity of the RHA is reported to be 2.05-2.53 (Karim et al., 2013; Suaiam & Makul, 2013) which is lower than OPC. Research showed that grinding of RHA is required to increase the specific surface area to work as a pozzolanic material (Safiuddin, 2008) and the best pozzolanic activity can be achieved with a specific surface area of 700 kg/m^2. Previous literature (Ahmed et al., 2017) revealed that RHA is categorized the same as Class F fly ash due to similarity of their chemical compositions.

Due to its porous structure and higher surface area, water demand is found to increase with the increasing content of RHA in the concrete mix (Marthong, 2012; Rashid, 2016). Hence, more water or water reducing admixture should be used to produce RHA concrete that is workable compared to concrete without RHA. Setting times (initial and final) increase with increasing RHA content (Marthong, 2012, Dabai et al., 2009). RHA contains a good percentage of SiO_2 which reacts with $Ca(OH)_2$ and produces CSH gel. Feng et al. (2004) studied the pozzolanic actitivity of the two types of RHA. One was prepared from rice husk pretreated with hydrochloric acid and another was prepared from untreated rice husk. It was observed that the pozzlanic activity of the RHA was

enhanced due to pretreatment, had a faster rate of reaction with the $Ca(OH)_2$ and produced more CSH. After seven days, less amounts of $Ca(OH)_2$ were found in the pretreated RHA. Due to the presence of higher SiO_2 the strength was also significantly increased compared with the control and untreated specimens. It was also reported (Nguyen, 2011) that increasing the content of RHA produced finer pore structure and more CSH gel due to its higher fineness. This contributes to the pore structure refinement and as a result reduces the pore volume and porosity. Overall, RHA blended cement binder reduces the permeability and porosity of mortar and concrete compared with those not containing RHA (Kartini et al., 2010; Chopra et al., 2015).

The compressive strength of RHA concrete mainly depends on the water-binder ratio, cement replacement level and curing condition. Literature has revealed that concrete containing RHA showed higher compressive strength than specimens without RHA (Hwang et al., 2011; Mahmud et al., 2016). The compressive strength was increased with 20% RHA at 7, 28 and 90 days with water/binder ratios of 0.30-0.34 compared to the control specimens (Chindaprasirta et al., 2007; Babaiefar, 2007). Increasing the water/binder ratio caused a reduction of strength. Up to 30% RHA replacement increased concrete strength for longer curing durations at w/c ratio of 0.5 and 0.53 (Habeeb & Fayyadh, 2009; Habeeb & Mahmud, 2010). Increase of CSH, reduction of pore size and densification of matrix were reported at later ages. The reduction in early age compressive strength compared with control concrete is attributed to delayed hydration by the reduced cement content.

At 15% RHA replacement, splitting tensile strength was increased by 18% (Le et al., 2014) and 28% (Foong et al., 2015). Khassaf et al. (2014b) reported that the w/b ratio affects the splitting tensile strength of RHA concrete. The strength was increased at 28 days for 10% cement replacement by RHA. An increase of tensile strength was also reported for 20% RHA at 56 days. Flexural strength was increased with 10% (Vinothan & Baskar, 2015) and 20% (Talsanial et al., 2015) RHA. Foong et al. (2015) reported that incorporation of RHA in concrete enhanced the flexural strength by 6–15% compared to concrete without RHA.

Reduction of water absorption was reported due to incorporation of RHA by Mahmud et al. (2009) and Safiuddin and Soudki (2011). Drying shrinkage has been found to be reduced (Mahmud et al., 2009; Habeeb & Mahmud, 2010; Khassaf et al., 2014b) with the incorporation of RHA and the reduction increases with the increasing amount of RHA. Incorporation of RHA in concrete and mortar samples reduced diffusivity of chloride ions and increased chloride resistance for using up to 40% RHA compared to control specimens (Chopra et al., 2015; Chindaprasirta et al., 2007; Coutinho & Papadakis, 2011; Salas et al., 2009). Literature also reports that incorporation of RHA and fly ash with Portland cement reduced the sulphate resistance of concrete (Kadri & Duval, 1998; Chindaprasirta et al., 2007).

2.6 Application of ferronickel slag

2.6.1 Use of ferronickel slag as aggregate

An extensive literature review has been carried out to investigate the available research results and recommendations for using ferronickel slag in concrete as a binder or aggregate. Researchers attempted to use ferronickel/nickel slag as both coarse and fine aggregates in producing normal strength concrete (Sakoi et al., 2013; Behra et al., 2011), high strength concrete (Sato et al., 2011) and self-compacting concrete (Tanijaya & Hardjito, 2007; Tokuhashi et al., 2001). Experimental results indicated that the unit weight of the concrete slightly increased due to incorporating the slag as aggregate. Compressive strength, tensile strength, modulus of rupture, workability, drying shrinkage, freeze and thaw resistance and hardness of concrete increased due to incorporation of the slag as a fine aggregate in the concrete. Ferronickel slag aggregate reduced water demand of the concrete mix. However, the amount of bleeding increased with the increasing ferronickel slag aggregate volume (either fine or coarse). In terms of toxicity, ferronickel slag was found to be non-hazardous (Demotica et al., 2012) since no leaching of metal exceeded the limits recommended by the United States Environmental Protection Agency (USEPA).

Sakoi et al. (2013) studied the mechanical property and durability (freeze and thaw resistance and drying shrinkage) of concrete with natural sand and air granulated ferronickel slag as fine aggregate. Experiments with combined use of the ferronickel slag as fine aggregate (FNS) (0 and 40%) and ferronickel slag as coarse aggregate (FNG) (0, 50 and 100%) for concrete was also conducted. The compressive strength of the concrete with FNS and FNG was found to be the same as that of normal concrete. The static modulus of elasticity of the concrete containing FNS and FNG indicated higher values compared to normal concrete. FNS and FNG concrete showed high resistance against freezing and thawing action regardless of whether FNS and FNG were used. The drying shrinkage was slightly increased by the increased volume fraction of ferronickel slag aggregate. No specific reason was given for the increase of drying shrinkage.

Behera et al. (2011) investigated the variation in strength with the percentage of slag. They replaced 20-100% coarse aggregate with slag aggregate and reported that 20% replacement did not give a significant strength increase. The dead load increased only 6% when 100% coarse aggregate was replaced by ferronickel slag aggregate. Experimental results also indicated that workability, compressive strength, flexural strength and splitting tensile strength increased with the increased amount of slag up to 100%.

Tanijaya and Hardjito (2007) conducted research on using nickel slag either as coarse aggregate or as both coarse and fine aggregate. Based on their investigation, it was concluded that usage of the nickel slag as an aggregate in concrete had superior results in terms of compressive and tensile strength and modulus of rupture compared to the concrete with natural aggregates only.

Dimitrioglou et al. (2016) used ferronickel slag (FNS) as an aggregate substitute for producing H-shaped concrete paving blocks. At 28 days, the compressive strength of the paving blocks with 10% FNS aggregate was 16% higher than the reference mixture with no FNS aggregate. But the strength reduced by 20% with 30% FNS replacement. Splitting tensile strength was reduced by 7.28% and 17% for 10% and 20%

replacements, respectively. Finally, it was concluded that a mixture with 10% FNS satisfied the minimum requirements of the BS EN 1338 (2003) standard.

Saha and Sarker (2016; 2017a; 2017b; 2017c) studied the suitability of using ferronickel slag as fine aggregate. It was used for replacing 50% and 100% of natural fine aggregate (sand) (Saha & Sarker, 2017c). The binder content was 390 kg/m^3 and the w/b ratios of the mixes were constant at 0.33. Experimental results showed that 50% FNS increased the workability slightly while it decreased for 100% FNS aggregate. The compressive strengths of the concretes were 66 MPa for using 50% FNS aggregate without fly ash, and 51 MPa when containing 30% fly ash as cement replacement. The splitting tensile and flexural strength varied at 28 days in the range of 7-10% and 10-14% of the corresponding compressive, respectively, for 50% or 100% FNS aggregates. Leaching assessment of the concrete indicated that concentration of the heavy metals was far below the limit set by USEPA and the UK Environment Agency for 50% and 100% FNS replacement. In another study, FNS was classified as reactive aggregate in terms of alkali silica reaction (Saha & Sarker, 2017c). However, the ASR expansions were found to be successfully mitigated by using fly ash as a partial cement replacement. Sorptivity and chloride penetration increased with the increment of FNS (Saha & Sarker, 2017b). Up to 50% FNS aggregate, sorptivity was within the limit set by Cement Concrete & Aggregates Australia (2009). It was observed that 30% of fly ash incorporation in the binder mitigated the alkali silica reaction, reducing the sorptivity and chloride penetration of the concrete with FNS aggregate.

2.6.2 Use of ferronickel slag as SCM

Katsiotis et al. (2015) reported the properties of blended cement with ground ferronickel slag of 5-20 wt% with an increment of 5%. The blended mixes showed lower demand for water, and higher setting times than the control specimen with cement only. Addition of slag increased the workability of concrete. Due to incorporation of FNS, the strength development rate was lower compared to the control specimen. FNS seemed to delay the early age hydration of the mixtures. The strength development increased at later ages.

The 28-day compressive strength was found to be decreased by 2.2, 6.8, 10 and 13% for the mixes with 5, 10, 15 and 20 wt% FNS content, respectively. At 90 days, compressive strength of the control mix (63.5 MPa) was only 8 % and 1% higher than the 20% (58.2 MPa) and 5% (62.8 MPa) FNS content mixes, respectively. Leachability tests using TCLP and NEN 7375 confirmed that concentrations of the leachable heavy metals of the mixes were far below the standard limits.

Usage of ferronickel slag in geopolymerisation was conducted by Liu et al. (2017). Fly ash and ferronickel slag was used for producing geopolymer concrete. The chemical analyses of the ferronickel slag and fly ash are given in Table 2.4.

Table 2.4: Chemical composition of ferronickel slag and fly ash

Composition	SiO_2	Al_2O_3	Fe_2O_3	CaO	MgO	SO_3	K_2O	Na_2O	Cr_2O_3	Loss
Ferronickel slag	48.85	15.94	9.71	17.45	5.98	0.71	0.23	0.15	0.12	0.76
Fly ash	51.12	28.31	4.38	6.92	1.21	0.32	1.11	0.44	0.89	5.29

It was observed that the maximum compressive strength (110 MPa) was obtained at 60% ferronickel slag and 40% fly ash mixture. XRD analysis revealed the presence of amorphous aluminosilicate phase and SEM analysis indicated that the microstructure of the concrete containing 40% fly ash and 60% ferronickel slag was denser.

Since this slag has a higher amount of magnesium content, reviewing the effects of MgO on the soundness and strength development of the binder is critical. In the next section the effect and role of MgO in concrete are discussed.

2.7 Effect of MgO in concrete

After hydration MgO produces $Mg(OH)_2$ (Brucite). It has a 17% higher volume (Lingling & Min, 2005). Peiwei et al. (2008) studied the effect of MgO-type expansive

material for providing expansive stress for mitigating concrete deformation and fracture. MgO-type material was prepared with the solid wastes of serpentine, dolomite and magnesite. They were ground, mixed and burned for 1–1.5h at 1150–1200 °C in an electric furnace. It was noted that hydration of the particles of the MgO-type expansive material at 20 °C shows the formation of brucite at 28 days (Peiwei et al., 2008). The rate of hydration is quite slow at 20 °C. About 57% of MgO was found to be hydrated to brucite after a 180 day curing period. Excessive volume change due to unsoundness usually causes cracking and loss of strength. MgO concrete causes volume expansion at later ages.

Reactivity of the MgO depends mainly on the burning or calcination temperature. Three types of MgO could be classified based on calcination temparature: (a) lightly burnt (850-1200 ^{o}C) (b) heavily burnt (1500-1800 ^{o}C), and (c) dead burnt MgO (Periclase) (>1800 ^{o}C). Hydration of MgO in category (a) takes place within six months, category (b) up to 1000 days and category (c) could be up to 6-8 years. If the burning temperature is high, it produces MgO with lower early-age expansion. The hydration process lasts longer. A highly crystalline form of magnesia (periclase) could be produced at temperatures over 1800 °C. This form of magnesia is resistant to hydration and degradation. However, MgO is not always harmful for the concrete. This depends on the chemical bond between MgO and the matrix. Researchers found that expansion in the later ages caused by slow hydration of the MgO in cement had compensated for the thermal shrinkage of concrete during the cooling stage (Lingling & Min, 2005; Yuan & Tang, 1984). In this regard, researchers have used MgO powder as an expansive agent (MEA) (Lingling & Min, 2005; Mo & Deng, 2010a, 2010b) by 5-10% weight of cement. It has been also noted that when 8% Magnesium expansive agent (MEA) is used, the cement paste cracked causing unsoundness (Mo et al., 2010), but the concrete prisms showed very good surface and strength after the complete hydration of MEA. Moreover, their mechanical performance (flexural strength) was even better than the control prisms.

Mo et al. (2012) investigated the hydration characteristic of MgO-based expansive additive (MEA) and aluminate based expansive additive (AEA) in Portland and fly ash

cement paste under the dry curing condition. MEA mainly consisted of 91.96% MgO. The study was conducted using 5% and 8% of MEA both pastes of OPC and fly ash cement. Portland cement paste was also prepared using 5% and 8% of AEA for comparison. It was observed that shrinkage occurred at an early age in cement pastes containing MEA. Slower hydration of the MgO in MEA showed smaller early age expansion than autogenous shrinkage caused by hydration of the cement. The cement paste with 8% and 5% MEA had expansion after 21 and 55 days, respectively. Rapid compensation of autogenous shrinkage was observed in cement paste specimens having higher amounts of MEA. Pastes with fly ash also compensated the autogenous shrinkage and it seemed to delay the expansion of MgO. The thermal shrinkage of the cement paste with or without fly ash was also compensated completely using MEA. Thermal shrinkage was not compensated in the cement paste specimens containing AEA.

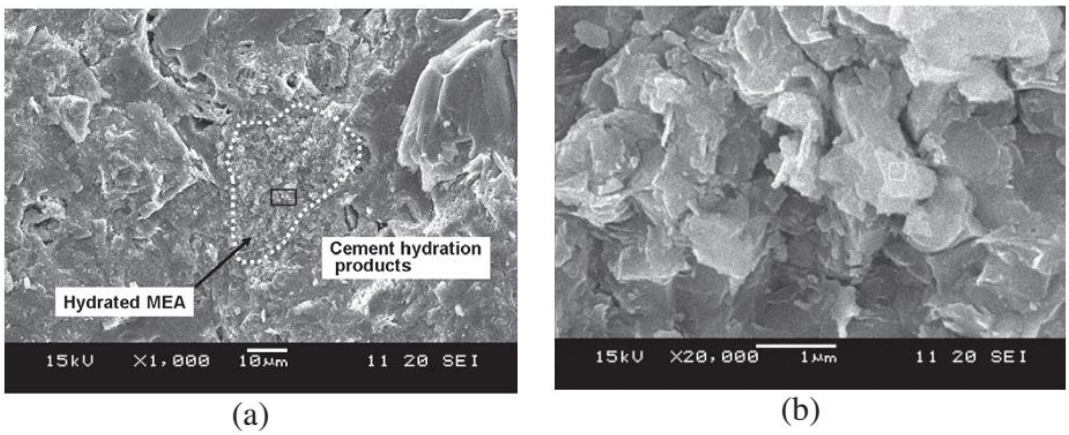

Figure 2.4: SEM image of Portland cement paste with 8% MEA (Mo et al., 2012)

SEM analysis of OPC paste with 8% MEA is presented in Figure 2.4. It shows the hydrated MEA particles. Formation of $Mg(OH)_2$ sheets and their agglomeration in the hydrated paste were observed.

Chengyou et al. (2014) investigated the effect of material ratio, citric acid and fly ash on Magnesium Oxysulfate (MOS) cement. Light burnt magnesia (LBM) was used for preparing MOS cement. The calcination temperature of the LBM was 700 to 800 °C. The total MgO amount in LBM was 80.20% though the hydration test result confirmed

only 58.50% MgO. LBM and $MgSO_4$ solution were blended together with a molar ratio of 3, 5, 7, 9, 11 and 13 to form MOS cement paste and was cast into 40mm x 40mm x 40 mm specimens. The compressive strengths were determined after curing for 28 days at room temperature. Maximum compressive strength (39.91 MPa) was obtained with a molar ratio of 5 due to formation of a new magnesium subsulphate crystal phase – $yMg(OH)_2 \cdot MgSO_4 \cdot zH_2O$ (Y phase). The compressive strength decreased from 56.89 to 33.75 MPa due to the incorporation of 40% fly ash as SiO_2 in fly ash forms hydrated magnesium silica gel and it can adsorb on the surface of the Y phase and reduce its growth. A high content of Y phase provides high strength. Addition of citric acid also enhances the growth and conversion of Y phase and increases compressive strength of the MOS cement.

Mo and Panesar (2013) studied CO_2 uptake, microstructure, carbonation mechanism, microhardness and compressive strength of cement paste mixtures containing OPC, GBFS and reactive MgO (89.67% MgO). The results revealed that at 56 days, cement pastes with 10-20% reactive MgO, had similar CO2 uptake compared to mixtures without reactive MgO. It was also found that CO_2 uptake reduces with the increase of reactive MgO. The least amount of CO_2 uptake was noticed with 40% reactive MgO. The formation of the Ca/Mg carbonates for the carbonated cement pastes decreased the pore volume and size while increasing the microhardness. Higher microhardness was achieved from the tight morphology and carbonate phase conglomeration due to incorporation of reactive MgO. It was also observed that the compressive strength decreased to a lesser degree with the increase of reactive MgO for carbonation cured mortars compared with normal atmosphere cured mortars due to the formation of magnesium calcite. Agglomeration of magnesium calcite resulted in a dense interconnected microstructure.

2.8 Summary of the literature review

Previous research revealed the potential usage of different SCMs in concrete. Fly ash can be used up to 40% and in some cases high volume fly ash can contain more than 50%

fly ash. GGBFS could be used up to 60% cement replacement, and silica fume up to 65%. Usage of RHA up to 20% increased strength at all ages, and at 30% replacement level strength was increased with prolonged curing condition.

Based on the available literature it is established that very limited research work has been conducted on the use of ferronickel slag (FNS) as a supplementary binder material in concrete. The high magnesium content of FNS can have a significant negative effect on the properties of concrete due to its possible reaction, especially to cause excessive expansion. However, this issue has not been studied adequately. Therefore, this study investigated the properties of paste, mortar and concrete in order to understand the effects of FNS when used as a partial replacement of cement. The properties include expansion, setting, strength, microstructure, durability and structural behavior. Hence, this research has significant importance for establishing the concrete properties with high magnesium FNS and its usage as a SCM.

Chapter 3: EXPERIMENTAL WORK ON FERRONICKEL SLAG BLENDED CEMENT PASTE, MORTAR AND CONCRETE

This chapter describes the materials and methods used for preparing specimens and conducting experimental works on the fresh and early-age properties, soundness, toxicity characteristics, strength and long-term durability properties. These properties are very important to understand the bahaviour of the composites using FNS as a SCM. Preparation of materials, mixing and casting of the test specimens are explained. Curing and preparation of the test specimens and procedure of conducting each test in accordance with relevant standards are described.

3.1 Materials

3.1.1 Binders

General purpose (GP) Portland cement was used as the main binder complying with AS 3972 (2010). Ground ferronickel slag, fly ash and GGBFS were used to partially replace the main binder.

The specific ferronickel slag used in this study was collected from the smelters of Société Le Nickel (SLN) in New Caledonia. The slag is produced as a by-product in the pyro-metallurgical process of Garnierite ores in an electric arc furnace at temperatures between 1200 ^{o}C and 1300 ^{o}C. The molten slag is granulated by rapid cooling using sea water. The maximum particle size of the granulated slag was about 5 mm. It was then ground using a laboratory ball mill to a fineness of 500-530 m^2/kg. The specific surface area of the ground slag was determined using the Blaine's air permeability method according to the ASTM C204-11 Standard (2013). Photographs of the raw slag and ground slag are shown in Figure 3.1. Specific gravity of the ferronickel slag was 2.95, which is similar to that of Portland cement (about 3.15) or other supplementary cementitious materials such as GGBFS (2.90).

Raw slag Ground slag

Figure 3.1: Raw and ground ferronickel slag

Figure 3.2: Cement, fly ash, GGBFS and ground FNS

The chemical compositions of the ferronickel slag were determined by X-ray fluorescence (XRF) and the elements in terms of the oxides are given in Table 3.1. It is observed from the Table 3.1 that the magnesium oxide (MgO) of the slag is about 32% by mass. According to AS 3583.9 (1991), the value of MgO in a SCM should be less than 15%. Though the XRF results show the Mg content in terms of MgO, an X-ray diffraction (XRD) phase analysis of the ferronickel slag showed that the magnesium was present mainly as crystalline forsterite ferroan. The chemical compositions of the cement, fly ash and GGBFS used in the study are also given in Table 3.1. Figure 3.2 presents the images of the binders. The result of the chemical analysis of the binders is shown in Table 3.1. It shows that FNS and fly ash had high amounts of SiO_2 and low amounts of CaO. On the other hand, OPC and GGBFS contained high amounts of CaO and low amounts of SiO_2. Fe_2O_3 content was higher in FNS than in the other materials.

The Blaine's fineness of the ground FNS, cement, fly ash and GGBFS were 500 m^2/kg, 370 m^2/kg, 330 m^2/kg and 450 m^2/kg, respectively.

Table 3.1: Chemical compositions of the cement, ferronickel slag, fly ash and GGBFS

Material	OPC	FNS	Fly	GGBFS
SiO_2	20.29	53.29	76.34	32.45
Al_2O_3	5.48	2.67	14.72	13.56
Fe_2O_3	2.85	11.9	3.69	0.82
MgO	1.24	31.6	0.54	5.10
SO_3	2.49	-	0.11	3.20
CaO	63.11	0.42	0.60	41.22
Na_2O	0.29	0.11	0.19	0.27
K_2O	0.45	-	0.96	0.35
Cr_2O_3	0.02	1.08	-	-
P_2O_5	0.17	-	0.10	0.03
SrO	0.05	-	-	-
TiO_2	0.27	-	0.61	0.49
Mn_2O_3	0.08	-	0.07	0.25
ZnO	0.04	-	-	-
NiO		0.1		
Co_3O_4		0.01		
LOI	3.39	- 0.83	0.53	1.11

3.1.2 Aggregates

All the mixtures were prepared using natural sand as the main source of fine aggregate. The aggregates' particle size distribution is given in the appendix A which is within the limit recommended by AS 2758.1 (2014a). Fine aggregate had a FM (fineness modulus) of 1.94 and water absorption of 0.34%.

Crushed granite was the source of coarse aggregate and the maximum sizes were 20 mm (60%) and 10 mm (40%). The water absorption of the coarse aggregate was 0.43% which meets the requirement set by AS 2758.1 (2014a). The FM of the coarse aggregate

was found to be 7.6. Figure 3.3 shows the images of the aggregates. The physical properties of fine and coarse aggregate and raw ferronickel slag are shown in Table 3.2.

Figure 3.3: Fine and coarse aggregate

Table 3.2: Physical properties of aggregates and Raw FNS

Properties	Sand	Coarse Aggregate	Raw FNS
Bulk Density (SSD) (gm/cm^3)	2.15	2.70	2.76
Apparent particle density (gm/cm^3)	2.30	2.71	2.86
Water absorption (%)	0.34	0.49	0.43
Fineness modulus (FM) (%)	1.94	7.6	4.05
Porosity (%)	7	1	2

3.1.3 Water

Normal potable tap water was added to prepare all the mixes. The water was collected from taps in the laboratory.

3.1.4 Admixture

A high-range, water reducing admixture (Rheobuild 1000) was added to produce Rheoplastic concrete which flows easily. This type of concrete also maintains high plasticity for more extended time periods than conventional concrete with normal superplasticizer. Rheobuild 1000 admixture conforms to ASTM C 494/C 494M (2017)

Type A (water-reducing) and Type F (high-range water-reducing) admixture. Rheobuild 1000 was collected from BASF chemicals, Australia and used in the concrete mixtures.

3.2 Methodology

A series of tests was conducted to assess the fresh and hardened properties of FNS blended cement paste, mortar and concrete. The test results were compared with those of the control mixtures without FNS. Comparison was also made with the results of cement paste mixtures blended with fly ash (FA) and ground granulated blast furnace slag (GGBFS). The properties of paste mixes include normal consistency, initial and final setting times, strength activity index and soundness tested by different methods. Compressive strength development and leaching characteristics of mortar specimens containing ferronickel slag were evaluated. Phase analysis by X-Ray diffraction (XRD) was carried out to have an insight into the reaction product of FNS in cement paste. Concrete specimens with and without ferronickel slag were prepared and tests were carried out for evaluating strength (compressive, flexural and tensile), drying shrinkage, chloride ion penetrability, volume of permeable voids and sulphate resistance. Reinforced concrete beams were also cast with the concrete incorporating ferronickel slag and the behaviours under flexure, shear and bond were studied. The following sections describe the mixture proportions, preparation of specimens and test methods.

3.2.1 Fresh properties

3.2.1.1 Normal consistency and setting time

Normal consistency is defined by the required quantity of water which brings the cement paste to a standard condition of wetness. This will allow the Vicat plunger to penetrate to a point about 5-7 mm from the bottom of the mould. It represents the flow behaviour of a fresh mixture. Knowledge of setting time of a cementitious mixture is required in order to determine the available time for mixing, transporting, placing and compacting the concrete effectively. Setting time tests are used to characterize how a

particular cementitious paste sets. It is affected by a number of factors such as the fineness and chemical compositions of the cementitious materials, water-binder ratio, and the admixtures if used. Setting time and soundness properties are determined at a specified consistency rather than a certain water-binder ratio (Lamond & Pielert, 2006). Therefore, the water content for normal consistency is determined as a pre-requisite for the setting time and soundness tests.

Commercial GGBFS can be used at up to 65% cement replacement and 20% is considered as the lower range of SCM dosage. Hence, the ferronickel slag was used from 20% to 65% by weight as partial replacement of cement. The normal consistencies and setting times of the mixtures were determined in accordance with the Australian Standards AS 2350.3 (2006) and AS 2350.4 (2006). The tests were conducted on freshly mixed pastes in the laboratory at a relative humidity of 70 ± 10% and temperature of 23 ± 2 ^{o}C.

3.2.1.2 Strength activity index

Strength activity index is defined as the ratio of the strength of 20% ferronickel slag-blended cement mortar to the strength of the reference cement mortar at a specific age. The control cement mortar mixture consisted of 500g of cement, 1375g of sand and 242g of water as specified in ASTM C311M (2013). The ferronickel slag blended cement mortar mixture contained 400g cement, 100g ferronickel slag, 1375g sand and 242g of water. Since the water demand for a normal consistency of 20% ferronickel slag blended paste was found to be the same as that of the control cement paste, the water contents of both the mortar mixtures were kept the same. Cube specimens of 50 mm sides were prepared and tested in accordance with ASTM C311M (2013). After pouring, the specimens were placed in a moist room at 23±2 ^{0}C for 24 hours. The specimens were then demoulded and cured by immersion in water until testing for compressive strengths at the ages of 7 and 28 days.

3.2.1.3 Workability test of concrete and mortar

A standard slump test was performed according to AS 1012.3.1 (2014) for determining the workability of OPC mixtures. After mixing, the concrete was poured to one third the height of the Abram's cone and 25 strokes were applied to it. The cone was filled following the same process for the second and third layers. After levelling the top, the cone was lifted in 3 seconds. The cone was placed up-side down and the slump value was measured. Figure 3.4 presents the slump measurement of OPC concrete.

Figure 3.4: Concrete slump test

A flow test was done according to ASTM C1437 (2015) for evaluating the workability of mortar specimens. A mortar flow test was carried out for control and FNS, GGBFS and FA blended mortar mixtures. After carefully cleaning and wiping the flow table, the flow mould was positioned at the centre of the table. About 25 mm thick mortar was placed in the flow mould and was tamped 20 times. This process was repeated until the flow mould was filled. The mortar at the top of the mould was cut off smoothly in a horizontal plane using a trowel. Immediately, after lifting the mould away, the flow table was allowed to drop 25 times in 15s through a height of 12mm. The diameter of the mortar mass was taken in different directions and the average was recorded. Flow

was determined as the percentage increase in the average base diameter of the mortar mass. A picture of mortar flow test is shown in the appendix.

3.2.2 Soundness

Magnesium content of the slag obtained by XRF analysis as shown in terms of MgO is about 32%. According to AS 3582.2 (2001), the value of MgO in SCMs should be less than 15%. Therefore, the high magnesium content of the slag could raise concerns of excessive expansion. However, the magnesium may not always be harmful for concrete depending on how it is chemically bound in the slag. The quantitative XRD result of the slag showed that the magnesium is present in the form of forsterite ferroan rather than in the form of MgO. The soundness of the ferronickel slag blended cement pastes was evaluated using the well-known Le-Chatelier soundness, autoclave expansion and accelerated heat curing tests.

The Le-Chatelier soundness test was carried out in accordance with the Australian Standard AS2350.5 (2006). The cement paste samples were prepared at normal consistency by replacing 0 to 65% of cement with the ferronickel slag. The Le-Chatelier mould was filled with the paste and submerged in water for 24 hours. After curing, it was boiled for 3.5 hours, and then left at room temperature to cool down. The distance between the pointer of the mould before and after boiling was taken as the Le-Chatelier expansion.

The autoclave expansion was determined in accordance with the Australian Standard AS 3583.4 (1991). The paste specimens used for this experiment were prisms of 25 mm square by 285 mm long, having a 250 mm effective gauge length. A paste of normal consistency was prepared, moulded and moist cured for 24 hours in a cupboard. After curing, the specimens were demoulded and the initial lengths were measured. The specimens were then placed in an autoclave containing water to maintain an atmosphere of saturated steam. The temperature of the autoclave was raised at a rate that brought the pressure of steam to 2 MPa in 45 minutes to 75 minutes. A pressure of 2000 ± 70 kPa

was maintained within the autoclave for 3 hours. Afterwards, the specimens were cooled, and the changes in length were measured.

It was reported that curing at elevated temperature such as 80 ^{o}C could accelerate the hydration of lightly burnt (1000-1250 ^{o}C) MgO and complete hydration would be achieved within 30 days (Mo & Deng, 2010b). Therefore, accelerated heat curing tests were conducted to investigate the expansion characteristics of the control and the FNS blended cement pastes. The size of the specimens of this test was same as that for the autoclave expansion test and was prepared by using 30% and 50% FNS as cement replacement. Another batch of samples was prepared by the addition of 5% and 10% MgO (minimum 95% Magnesia) with cement in order to compare the expansions of the specimens containing ferronickel slag and those with reactive MgO. The test specimens were of the same size as those for the autoclave testing. After casting, the prisms were cured for 24 hours in the laboratory at 23±2 ^{o}C. After demoulding one set of the specimens was cured at 80 ^{o}C in water for 120 days and the other set was cured in water at ambient temperature. Then the effects of normal curing and accelerated curing conditions were evaluated. Three identical specimens were tested for each condition and the average value of the expansions was calculated.

3.2.3 Toxicity Characteristics

The toxicity characteristics were evaluated for the ground FNS powder and mortar specimens containing 20% and 50% FNS. Cube mortar specimens of 50mm sides were prepared in accordance with the ASTM C109 (2013) Standard. After casting, the samples were placed in the moist room at 23±2 ^{o}C for 24 hours. The specimens were then demoulded and cured by immersion in water. After 28 days, ground fine powder was collected from the specimens for the leachability test. Australian Standard Leaching Procedure (ASLP) (AS4439.3) (1997) was used to conduct the leachability test. Initially 5.0g of the powder was mixed with 100mL water. After stirring vigorously for 5 minutes, the pH value was measured and recorded. The samples were extracted in accordance with AS 4439.3 (1997) using acetate buffer solution of pH 5 or 2.9 and the

final pH was noted. The extraction bottle was agitated using a rotator for 18 ± 2h at 30 ± 2 revolutions per minute at a temperature of 22 ± 5 ^{o}C. The filtrate was collected using a glass fibre filter of 0.6-0.7 µm. The analysis was done for the major metal ions using inductively coupled plasma atomic emission spectroscopy (ICPAES) and the trace-metals were identified by inductively coupled plasma mass spectroscopy (ICPMS).

3.2.4 Strength and durability properties

3.2.4.1 Preparation of concrete and mortar specimens

Ordinary Portland cement (OPC) concrete was prepared according to AS1012.2 (2014). The concrete specimens were prepared according to the mix proportions shown in Table 3.3. The designations of the mixtures were done using the percentage of binder materials in the mix. For example, the mixture containing 40% ground FNS and 60% cement was designated as 40FNS 60C. First the aggregates were mixed for about two minutes and the binder was then added to the dry mix. Water and plasticizer were added slowly to the dry mix until a uniform mix was achieved. Soon after the mixing, a slump test on the concrete was carried out. Then the fresh concrete mixtures were poured into the steel moulds. The specimens were demoulded the next day. After demoulding those were immersed in water and allowed to cure for a period of 28 days. The specimens were removed from the water after 28 days and allowed for air curing until the test date.

Table 3.3: Concrete mix proportions

Type of mix	Coarse aggregate kg/m^3	Fine aggregate Kg/m^3	Binder Kg/m^3			Water Kg/m^3	Plasticizer Kg/m^3
			Cement	FNS	GGBFS		
Control	1142	793	400	0	0	130	6.85
20FNS 80C	1142	793	320	80	0	130	4.6
30FNS 70C	1142	793	280	120	0	130	4.6
40FNS 60C	1142	793	240	160	0	130	4.6
40FNS 10GGBFS 50C	1142	793	200	160	40	130	4.6
50FNS 50C	1142	793	200	200	0	130	4.6
65FNS 35C	1142	793	140	260	0	130	4.6

The mortar mixtures consisted of one part of binder and three parts of sand by mass with a water-binder ratio of 0.50. A control mixture was prepared by mixing 450g of cement, 1350g of sand and 225g of water according to AS2350.12 (2006). Ferronickel slag was used to replace 20, 30, 40 and 50% of cement in the other mixtures. The mix proportions of the mortars are given in Table 3.4 and designated in the same way as the concrete mixtures.

Table 3.4: Mortar mix proportions

Type of mix	Fine aggregate (g)	Binder (g)		Water (g)
		Cement	FNS	
0FNS 100C	1350	450	0	225
20FNS 80C	1350	360	90	225
30FNS 70C	1350	315	135	225
40FNS 60C	1350	270	180	225
50FNS 50C	1350	225	225	225

A mixer was used to mix each batch of mortar mechanically. While keeping the mixer in the operating position, the binder was added after pouring the water into the bowl. Immediately after adding the cement, the mixer was operated at low speed (140 ± 5

r/min). After 30 s the sand was added to the mix steadily during the next 30 s. The mixer was set to high speed (285 ± 10 r/min) and continued the mixing for another 30 s. Then the mixer was stopped for 90 s. Within first 15 s, all of the mortar adhering to the bottom of the bowl and wall was removed by means of a scraper and was placed in the middle of the bowl. Finally, the mixing was finished at high speed for 60 s.

Demoulding of the mortar specimen was done after 24 hours. After demoulding, the specimens were placed in water for curing at 23 ± 2 ^{o}C with 70 ± 10% relative humidity until the test date.

3.2.4.2 Compressive strength of the concrete and mortar

Compressive strength tests were performed on cylindrical (diameter = 100 mm and height = 200 mm) concrete and cubic (50×50×50 mm^3) mortar samples. The test was conducted following AS 1012.9 (1999). A compression machine with a multifunctional control console (MCC8) was used for compressive strength testing. The machine had a capacity of 3000 kN. The top of the cylinder surface was capped using either sulphur or rubber for distributing the load evenly on the samples. The loading was applied constantly at 0.333 MPa/sec for all the compressive strength tests. Gradually the load was applied to the specimen until failure. The failure load was noted. The compressive strength was determined from the load and average cross-sectional area of the specimen.

Three samples were tested for each mix at 3, 7, 14 and 28 days of age and the average compressive strength was calculated. The specimens for compressive strength testing are shown in Figure 3.5.

Figure 3.5: Compressive strength test

3.2.4.3 Flexural and splitting tensile strengths

Flexural strength refers to the tension properties of concrete which are associated with cracking of concrete. The test for flexural strength of the concrete was done as described in AS 1012.11 (2000b). The specimen dimensions were 100 mm wide × 100 mm deep × 400 mm long. The specimens were allowed to fail due to flexural stress. Testing of specimens in a MCC8 machine is shown in Figure 3.6. Three specimens were used to test for each mix. The specimens were placed on supporting blocks of the MCC8 machine. A two-point loading roller was brought into contact with the specimens and a load was applied constantly at a rate of 0.017 MPa/sec. The distance between the loading roller and from each supporting roller to the loading roller was one third of the span. The ultimate loads of the specimens were noted. The average area at the failure surface was also recorded. Equation 3.1 was used for calculating the modulus of rupture or flexural strength.

$$f_{cf} = \frac{1000\ \text{PL}}{\text{BD}^2} \quad \ldots\ldots\ldots\ldots\ldots\ldots\ldots\ldots\ldots\ldots\ldots\ldots\ldots\ldots \quad 3.1$$

where f_{cf} = modulus of rupture (MPa)

P = applied maximum load (kN)

L = span (mm)

B = average specimen width at the section of failure (mm)

D = average specimen depth at the section of failure (mm)

Figure 3.6: Test for flexural strength

AS 1012.10 (2000) was used for the splitting tensile strength tests of the specimens. The specimens were 150 mm × 300 mm cylinders. Each test was performed using two samples and the average of the results was noted. The test was completed using the MCC8 machine. The loading rate was of 0.067 MPa/min and sensitivity was set to 50 kN. The specimen was placed, and the load was applied along the length of the cylinder. Splitting tensile failure occurred along the applied load on the plane with high compressive force. Splitting tensile strength was calculated using equation 3.2. Splitting tensile tested specimens are shown in Figure 3.7. Equation 3.2 was used to calculate the indirect tensile strength.

$$T = \frac{2000P}{\pi LD} \quad \ldots\ldots\ldots\ldots\ldots\ldots\ldots\ldots\ldots\ldots \; 3.2$$

where,

T = splitting tensile strength, in MPa

P = maximum applied load, in kN

L = length, in mm

D = diameter, in mm

Figure 3.7: Splitting tensile strength test

3.2.4.4 Drying shrinkage

A drying shrinkage test of the concrete was done in accordance with AS 1012.13 (1992). Specimens were prepared using prismatic (75 mm × 75 mm × 280 mm) moulds. Three specimens were prepared from the same concrete mix that was used for the other properties. Stainless steel studs were attached to the ends of the prism specimens along the horizontal axis before casting. The gauge length of the prism was set to 250mm. After casting of the specimens, the moulds were placed in a curing chamber (about 23 ^{o}C and 70±10% RH) for 24 h before demoulding. Demoulded specimens were cured under water for 7 days. At the 7th day, all the specimens were taken out of the water and wiped to achieve a surface dry condition. Then the initial length was measured using a horizontal length comparator which was used as the reference length for the subsequent length changes. The subsequent readings were taken at 7 day intervals for a specific period of time. Afterwards, the readings were taken at monthly intervals. The drying shrinkage was calculated using equation 3.3.

$$L_{ds} = \frac{(L_t - L_i)}{L} \times 10^6 \quad \ldots \ldots \ldots \quad 3.3$$

where,

L_{ds} = drying shrinkage in microstrain

L_t = specimen length in mm at specified time t

L_i = initial specimen length in mm

L = gauge length, 250 mm

3.2.4.5 Volume of permeable voids (VPV)

The VPV test was carried out according to AS 1012.21 (1999a). This test was done at 28 and 90 days. Four samples were cut from a cylinder (100 mm × 200 mm) with an equal size of 45mm for the VPV test. After wiping, the samples were placed inside an oven at 105 °C temperature for a minimum period of 24 hours. All the samples were then cooled and weighed. This method was repeated every 24 hours. When the difference between two successive weights was less than 1g, the weight was recorded as M_1.

Then, the samples were submerged in a water bath maintaining the temperature at 23 ± 2 °C. Every 24 hours the surface dry weight of the sample was recorded until a constant value was achieved. This weight was recorded as *M2i*.

Afterwards, the samples were boiled in a water bath for 5.5 ± 0.5 hours. Those were then cooled to room temperature in submerging conditions. The specimens were taken out of the bath at least 14h later, surface dried and weighed. The weight was recorded as M_{3b}. At room temperature, the suspended weights of the samples were also measured. This was denoted as M_{4ib}. The immersed absorption (A_i), boiled absorption (A_b) and apparent volume of permeable voids (VPV) were calculated using Equations 3.4 to 3.6.

$$A_i = \frac{(M_{2i} - M_1)}{M_1} \quad \text{……3.4}$$

$$A_b = \frac{(M_{3b} - M_1)}{M_1} \times 100\% \quad \text{……3.5}$$

$$VPV = \frac{(M_{3b} - M_1)}{(M_{3b} - M_{4ib})} \times 100\% \quad \text{……. 3.6}$$

where,

M_1 = Oven dried sample weight (g)

M_{2i} = Saturated immersed weight (g)

M_{3b}= Boiled sample weight (g)

M_{4ib} = Submerged weight of the sample (g)

3.2.4.6 Sorptivity

Sorptivity is used to measure the rate of water absorption by concrete. The sorptivity test was performed according to ASTM C 1585 (2013). Two samples of 50 mm deep and 100 mm diameter were prepared from the top of a cylinder of 200 mm deep and 100 mm diameter. Two specimens were used from each type concrete mixture. The samples were first placed in an environmental chamber at 60 ºC temperature and 70 ± 5% RH for 3 days until a constant mass was achieved. After oven drying, these were kept in the sealable container for minimum 14 days at a temperature of 23 °C. The specimens were sealed with silicon gel leaving a selected 100 mm face submerged in 1-3 mm depth of water. The weight of the sealed specimen was recorded as the initial weight. The weight of the sample was taken at 1, 5, 10, 20, 30 min and each hour for up to six hours and then every 24h up to one week. For every weighing, the specimens were taken out of the water, wiped using cloth, weighed quickly and then returned to the tray. The specimens used for the sorptivity test are shown in Figure 3.8. The water absorption (I) was determined using Equation 3.7.

$$I = \frac{M_t}{A \times \delta} \quad \text{……3.7}$$

where,

I = absorption in mm

M_t = mass change in gram at time t

A = exposed specimen area in mm^2

δ = density of water in g/mm^3

The rate of absorption can be expressed by Equation 3.8.

$$I = C + St^{0.5} \quad \text{……3.8}$$

where, S is the rate of absorption (sorptivity) which is the slope of I vs $t^{0.5}$ and could be obtained from linear regression analysis.

Figure 3.8: Specimens for sorptivity test

3.2.4.7 Rapid chloride penetration test (RCPT)

The rapid chloride penetration test was done according to ASTM C1202 (2012). The samples were cut to 50 mm thick slices with 100 mm nominal diameter from cylindrical specimens of 100 mm x 200 mm. A potential difference of 60V direct current (DC) was maintained during a 6-h period across each end of the specimen. One of the ends was immersed in a NaCl solution, the other in a NaOH solution. The test set up is shown in Figure 3.9. The amount of electrical current passed in coulombs was recorded and related to the resistance of the specimen to chloride ion penetration.

After cutting the specimens, the side was coated with sealant and cured until dry. Then the specimens were placed directly in a vacuum desiccator. Both end faces of the specimen were kept exposed. The desiccator was sealed, and the vacuum pump was started. Pressure was decreased to less than 50 mm Hg (6650 Pa) within a few minutes. After vacuuming for 3 hours, water was added, and vacuuming was continued for another hour. When the vacuuming was finished, the samples were soaked for 18 hours

under water. The side of the cell was filled using 3% NaCl solution (negative terminal) and 0.3 N NaOH solution (positive terminal). The first reading was taken when the test was initiated, and every other reading was taken at 30 minute intervals for up to 6h. The total charge passed was determined by the Equation 3.9 given below.

$$Q = 900(I_0 + 2I_{30} + 2I_{60} + \ldots\ldots\ldots\ldots + 2I_{330} + I_{360}) \ldots\ldots\ldots\ldots\ldots\ldots\ldots\ldots\ldots\ldots 3.9$$

where,

Q = charge passed in coulombs

I_o = current in amperes immediately after the voltage is applied

I_t = current in amperes at t min after the voltage is applied

Figure 3.9: Rapid chloride penetration test

3.3 Summary

The properties of different materials used in this study are presented in this chapter. The mix proportions and methodology for investigating the fresh properties, soundness, strength, durability and toxicity characteristics of the paste, mortar and concrete are described. The experimental works are illustrated by using photographs of the conducted tests and methods of calculations are explained by equations.

Chapter 4: RESULTS AND DISCUSSION

This chapter presents the test results and discussion of the results. The effects of different mix variables are studied by drawing graphs using the test results. Specifications given in standards were used to evaluate the performance of the slag in different mixtures. Performance of the slag was also evaluated by comparison of the test results of different mixtures.

4.1 Fresh properties

4.1.1 Normal consistency and setting time

The normal consistency results of the pastes containing up to 65% ferronickel slag are shown in Figure 4.1. The water contents required to achieve normal consistency of the pastes are plotted against the percentage of ferronickel slag in this figure.

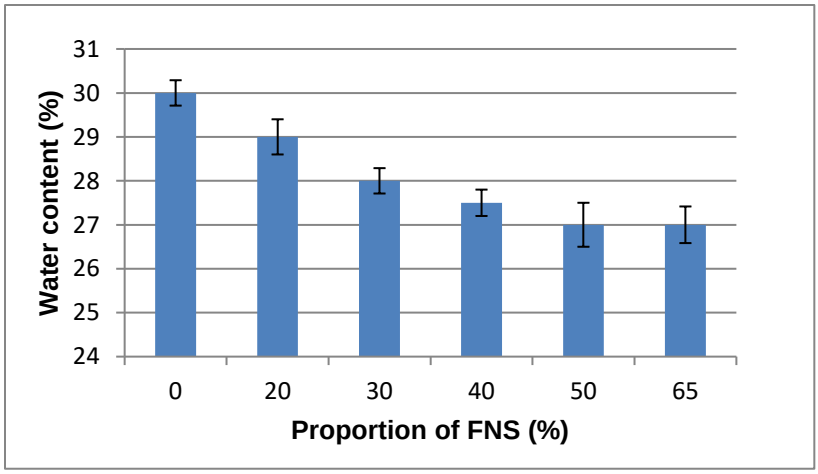

Figure 4.1: Variation of water content for normal consistency of paste with the percentage of ferronickel slag.

The results in Figure 4.1 show that the amount of water required for normal consistency of the paste slightly decreased with the inclusion of ferronickel slag. The water content

required for normal consistency of the control mixture was 30% and that of the mixtures with ferronickel slag varied from 29% to 27%. Therefore, the required water content decreased from 30% to 27% with the inclusion of up to 65% ferronickel slag in the paste. The ratios of the water requirement of the control mix to those of the mixes containing 30% and 65% ferronickel slag were 1.07 and 1.11, respectively. ASTM Standard C618.12a (2012) recommends the maximum ratios of 1.05 and 1.15 for fly ash and natural pozzolans, respectively. Thus, the water requirements of ferronickel slag are comparable to those of other supplementary cementitious materials. The observed decrease in water requirement of the ferronickel slag is attributed to its low water absorption characteristics and the inert behaviour at the initial stage of mixing.

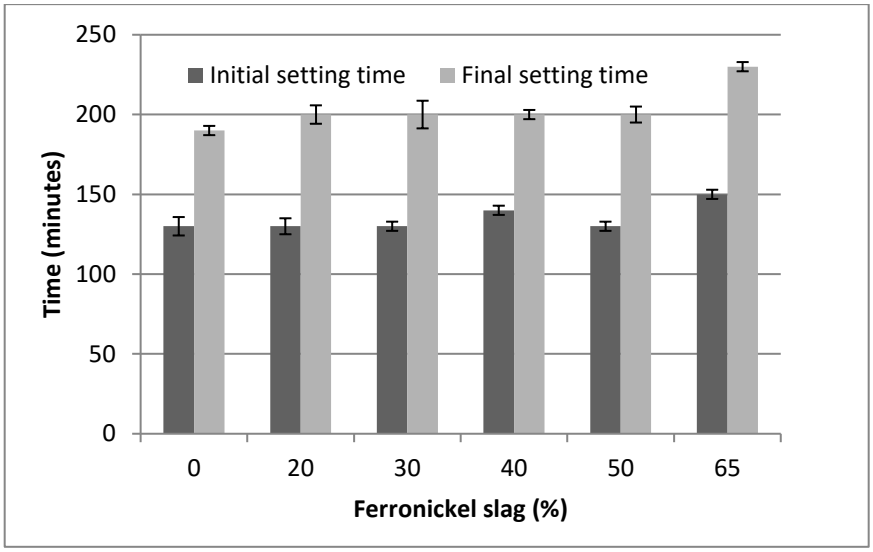

Figure 4.2: Variation of setting times with the addition of ferronickel slag.

The initial and final setting time results of the control cement paste and the mixtures with up to 65% ferronickel slag are shown in Figure 4.2. It can be seen that the initial setting times of the mixtures varied from 130 minutes to 150 minutes and the final setting time varied from 190 minutes to 230 minutes. According to ASTM C150 (2012) specification, the initial setting time shall not be less than 45 minutes. A very long final setting time is not usually preferred because this may cause large expenditures on the formworks. Therefore, the initial and final setting times of the mixtures containing up to 65% ferronickel slag are considered suitable for general applications of concrete.

No significant difference in the setting times was observed due to the incorporation of ground ferronickel slag as a cement replacement by up to 50%. At the cement replacement level of 65%, the ferronickel slag was found to retard the initial setting time by 20 minutes and the final setting time by 40 minutes. This is consistent with the usual observation that increasing the amount of supplementary cementitious materials such as silica fume, fly ash and GGBFS retards the setting time of concrete (Brooks et al., 2000). Cement replacement by GGBFS at a rate of more than 40% was shown to significantly increase the setting time (Erdogan & Mustafa, 2016). The initial and final setting times of the concrete produced without GGBFS were 332 and 449 minutes, respectively, whereas concrete with 60% GGBFS had an initial setting time of 913 minutes and a final setting time of 1021 minutes.

The normal setting time of Portland cement is related to the hydration of C_3S and C_3A, and the formations of CSH gel and ettringite (Snelson & Wild, 2011). High levels of cement replacement cause reductions of the hydrated products from C_3S and C_3A. Also, the increased percentage of cement replacement by SCMs causes an increase of the separation distance between hydrated cement particles that eventually delays the formation of interlocking networks between the particles. It should also be noted that the ferronickel slag has a very low (0.42%) calcium content. Thus, the setting time is increased at a high percentage of cement replacement such as 65% by the low calcium ferronickel slag.

4.1.2 Workability of mortar and concrete mixtures

Workability of mortar was determined by flow tests of fresh mixtures using 20% to 50% FNS, GGBFS and FA. It was observed that the flow of mortar slightly increased with increase of SCM content. The control mix (100% OPC) had a flow of about 70%. By using FNS, GGBFS and FA as 20-50% of cement replacement, the flow values varied in the ranges of 75-80%, 60-65% and 70-83%, respectively. It was seen that cement replacement by FNS and FA resulted in a slightly increased flow compared with the

control mix. Use of GGBFS slightly reduced the flow compared with the control mix. The flow results for each mixture are given in Table B.2 of the Appendix.

Workability of the concrete mixtures was evaluated using the slump test. The control mix had a slump of 160 mm. The superplasticiser dosage was reduced in the other mixtures to achieve a slump value of around 100 mm. For 20-50% FNS, the slump of fresh concrete mixtures varied from 80 mm to 130 mm. It was observed that the slump of concrete slightly increased with the increase of FNS content except for 50% FNS content. The concrete mixture containing GGBFS had the lowest slump value (75 mm). The slump values of all the concrete mixtures are given in Table C.2 of the Appendix.

4.1.3 Strength activity index

The pozzolanic activity of ferronickel slag was quantified by determination of the strength activity index. The strength activity index of any material depends on the surface area, particle size distribution and silica content. The strength activity index can be increased by reducing the particle size thus increasing the fineness. The average compressive strengths obtained from three specimens were used to determine the strength activity index. The results are presented in Table 4.1.

Table 4.1: Strength activity index of ferronickel slag

SI No	Composition	Mean 7 days strength (MPa)	Mean 28 days strength (MPa)	Strength activity index	
				7 days	28 days
1	Control	31	37	74%	84%
2	20% FNS	23	31		

Table 4.1 shows that the strength activity indices at 7 days and 28 days were found to be 74% and 84%, respectively. ASTM C618-08a (2006) recommends a minimum strength activity index of 75% for fly ash and natural pozzolans at 7 or 28 days. Since the value for the ferronickel slag at 28 days is above 75% and that at 7 days is very close to 75%,

the effect of the ferronickel slag on strength development may be considered comparable to those of other common supplementary cementitious materials.

4.2 Soundness evaluation

4.2.1 Le-Chatelier expansion

The Le-Chatelier expansion results are plotted against the percentage of ferronickel slag in Figure 4.3. Expansions of two additional mixtures containing 40% fly ash and 40% GGBFS were also tested for comparison with the expansion of the mixture containing 40% ferronickel slag. Besides, two other types of samples were prepared using 5% MgO and 10% MgO with the FNS and cement to investigate the effect of reactive MgO on expansion. These were tested for evaluating the reactivity of the magnesium present in FNS by comparing the expansion of mixtures containing ground FNS with those containing reactive MgO.

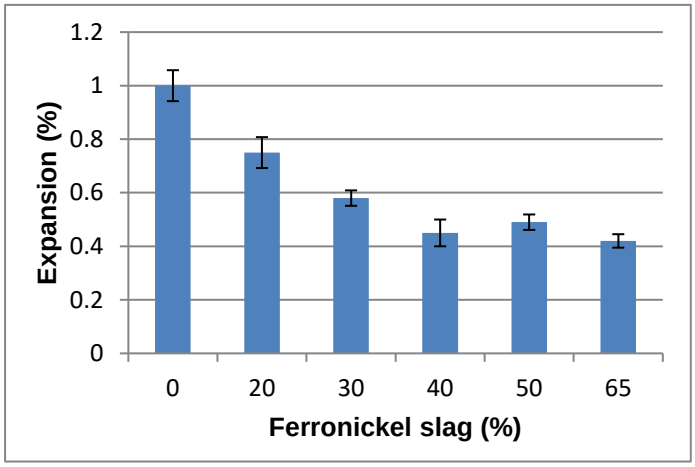

Figure 4.3: Variation of Le-Chatelier expansion with the percentages of ferronickel slag

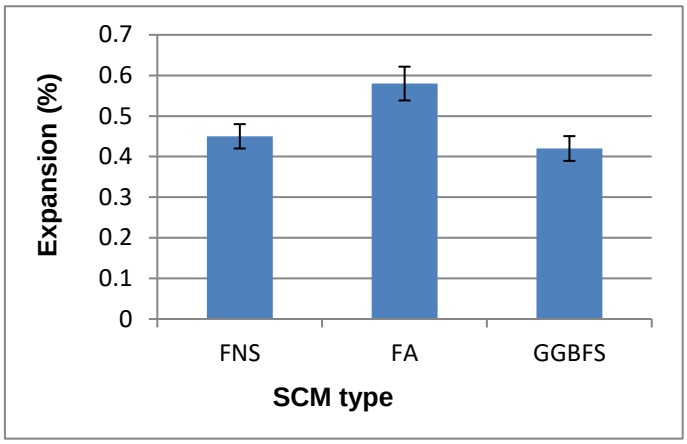

Figure 4.4: Le-Chatelier expansions of pastes containing 40% FNS, 40% fly ash and 40% GGBFS

It is observed from the results that Le-Chatelier expansions of the mixtures containing 0% to 65% ferronickel slag varied between 0.42% and 1%. These values are well below 5%, which is specified as the limiting value of Le-Chatelier expansion in Australian Standard (AS 3972, 2010). It can be seen from Figure 4.3 that the values generally decreased with the increase of cement replacement by the slag. The value decreased from 0.75% to 0.42% when the cement replacement by FNS increased from 20% to 65%.

Figure 4.4 shows the Le-Chatelier expansions of the mixtures of 40% cement replacement by the ferronickel slag, class F fly ash and GGBFS. The mean expansions of the specimens using 40% ferronickel slag, 40% fly ash and 40% GGBFS were 0.45%, 0.58% and 0.42%, respectively. All these expansion values are well below the 5% limit of AS 3972 (2010). Though the ground FNS had the highest fineness (500 m^2/kg) compared to the fly ash (330 m^2/kg) and GGBFS (450 m^2/kg), the reaction of the FNS did not show excessive expansion of the specimens. Thus, the Le-Chatelier expansion of the mixture containing 40% ferronickel slag is similar to that of the mixtures containing the same percentage of other common supplementary cementitious materials such as fly ash and GGBFS.

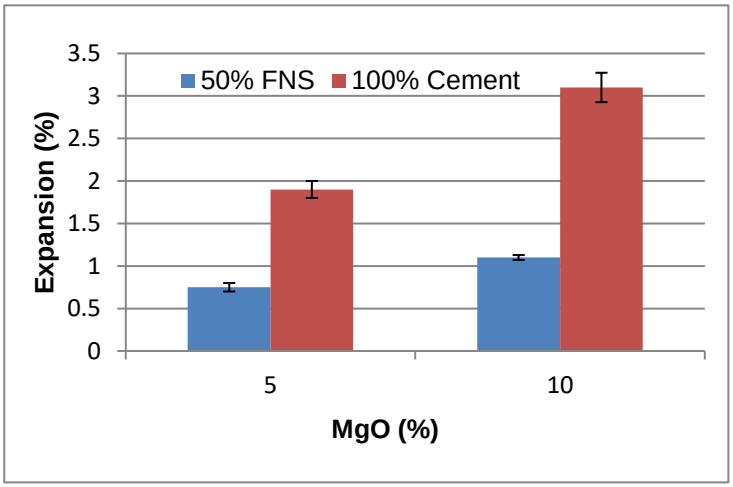

Figure 4.5: Le-Chatelier expansions of pastes containing 5% MgO and 10% MgO with and without ferronickel slag

Expansions of four other mixtures containing 5% or 10% reactive MgO were also determined in order to evaluate the sensitivity of the Le-Chatelier test to expansions caused by the reaction product of reactive MgO. MgO powder was added to the mixtures of 100% cement or 50% cement with 50% ferronickel slag. The expansions of these four mixtures are plotted in Figure 4.5. When reactive MgO was added to the FNS blended cement mixture, expansion increased with the increase of MgO. It was observed that the expansion increased from 0.75% to 1.1% by increasing the MgO content from 5% to 10%, respectively. The increase of expansion is expected because of the formation of expansive $Mg(OH)_2$ by hydration of MgO. It can also be seen that expansions of the mixtures without FNS blending were 1.9% and 3.1% for using 5% and 10% MgO, respectively. Expansions of the mixtures with 50% cement replacement by ferronickel slag were much less than the expansions of corresponding mixtures without ferronickel slag. This is because of the less quantity of available lime in the mixtures with 50% ferronickel slag as cement replacement. This indicates that the magnesium of ferronickel slag did not produce the expansive reaction product that is produced by reactive MgO.

Thus, the Le-Chatelier expansions of the pastes containing ferronickel slag up to 65% were found to be well below the 5% limit of the Australian Standard and were less than

those of the control mixture. Expansions of the mixtures containing 40% FNS are comparable with expansions of the mixtures containing the same percentage of other common supplementary cementitious materials such as fly ash and GGBFS.

4.2.2 Autoclave expansion

Autoclave expansion tests were conducted on specimens containing 0%, 20%, 30%, 40% and 50% ferronickel slag as cement replacement. The expansion results are given in Table 4.2 and Figure 4.7. No cracks, disintegration or warping were observed in the specimens after completion of the tests. The specimens for the autoclave test are shown in Figure 4.6.

Figure 4.6: Set up for autoclave testing and specimens after testing

Table 4.2: Autoclave expansion of ferronickel slag blended cement paste prisms

FNS content (%)	Autoclave expansion (%)
0	0.08
20	0.01
30	0.06
40	0.03
50	0.08

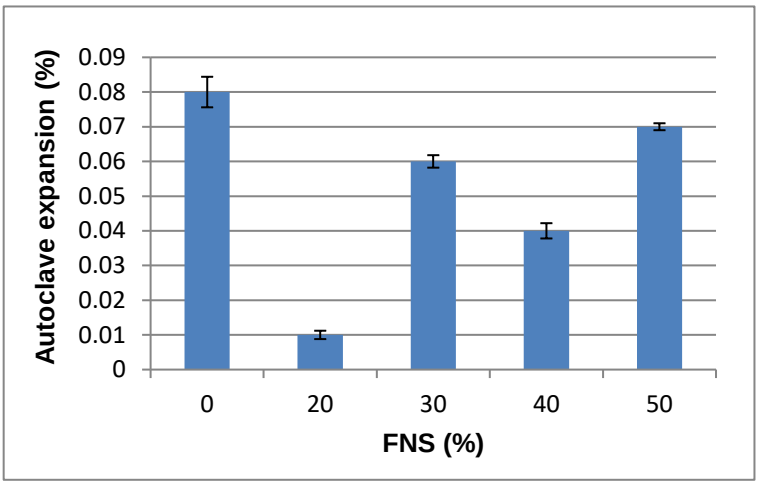

Figure 4.7: Expansion results of autoclave testing

The results show that the autoclave expansion values were scattered between 0.01% and 0.08% with no definite trend for the increase of ferronickel slag up to 50%. ASTM Standards C150 (2012) and C618-98 (1999) limit the autoclave expansion of a cement or blended mix by 0.8%. Therefore, the expansions of these mixtures are very small compared to the limit of the ASTM Standards. The expansion in cement or any blended mixture occurs due to the presence of free lime or magnesia (periclase). The autoclave test is especially designed for measuring the expansion due to periclase. The results do not show any increase in the expansion by the increase of ferronickel slag in the mixture. This is because the magnesium present in the ferronickel slag is in the form of forsterite ferroan rather than periclase. Thus, the autoclave expansion was not increased by the use high magnesium ferronickel slag.

4.2.3 Expansion by accelerated heat curing

Prism specimens of FNS and MgO blended cement pastes were subjected to accelerated heat curing at 80 ^{o}C and 100% relative humidity. The changes in length of the specimens were measured weekly for 120 days of curing. The variations of the expansion for individual ambient and heat-cured specimens are plotted in Figure 4.8.

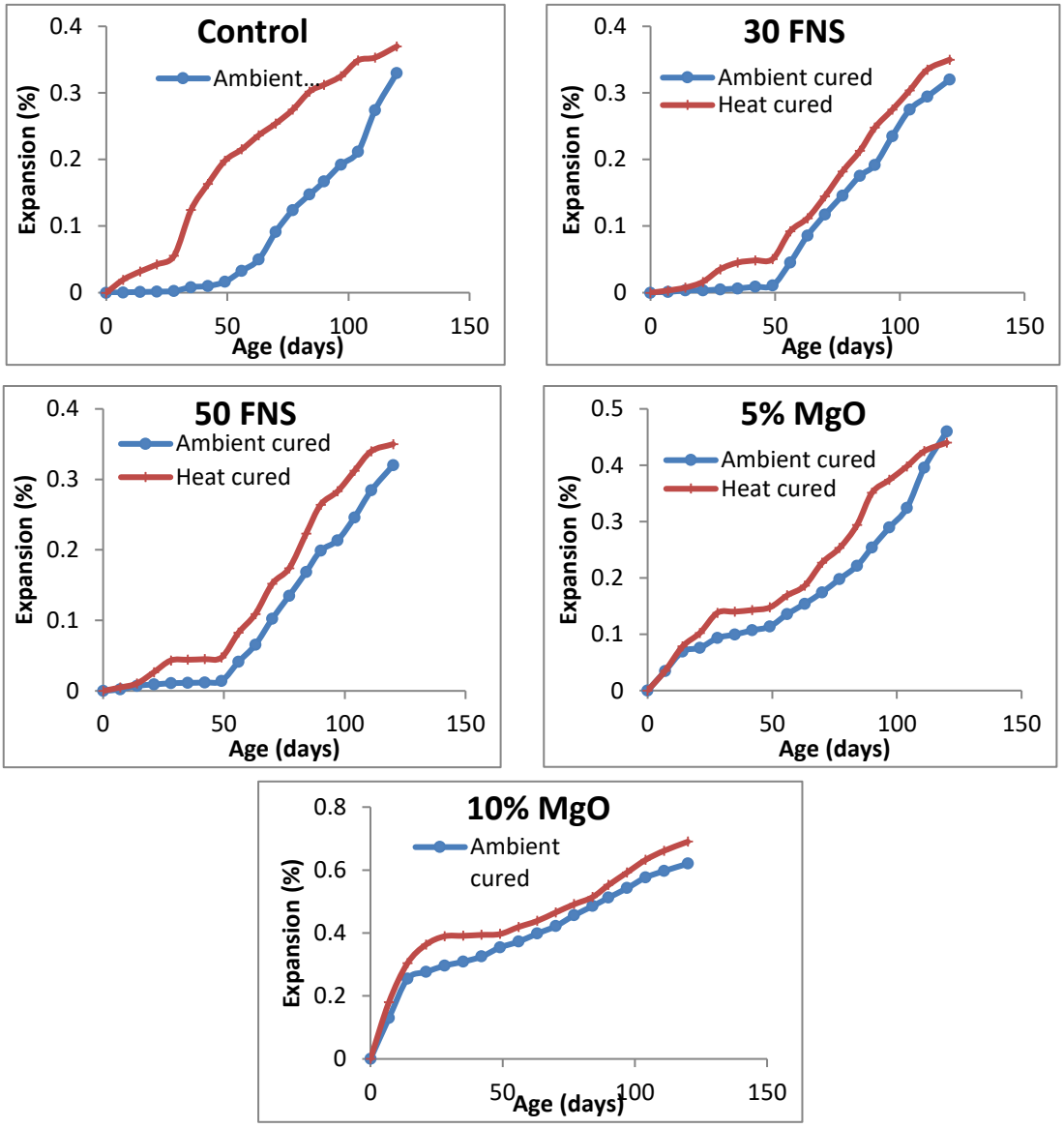

Figure 4.8: Expansion results of ferronickel slag and MgO blended cement paste prisms

From Figure 4.8, it is observed that the heat-cured specimens generally showed higher expansions than the corresponding ambient-cured specimens. The control specimens and FNS containing ambient-cured specimens did not show much expansion until 50 days, while the heat-cured specimens showed appreciable expansions from the early ages. This confirms that accelerated curing by heat increased expansion of the specimens. On the other hand, specimens containing MgO had higher expansion from

the beginning for both ambient and heat cured specimens. The tests were discontinued after 120 days as the control and FNS blended specimens had similar expansions.

The expansions of the specimens at 120 days of curing in ambient conditions and in accelerated heat curing at 80 ^{o}C are compared in Figure 4.9. It can be seen that 120-day expansion of the ambient-cured control specimen was 0.33% and that of the specimens with either 30% or 50% ferronickel slag was 0.32%. Similarly, the expansion of the heat-cured control specimen was 0.37% and that of the specimens containing ferronickel slag was 0.35%. Thus, the 120-day expansions of the specimens containing ferronickel slag were similar to those of the control specimen. Generally, heat curing at 80 ^{o}C increased expansion of the specimens with or without ferronickel slag. The results show that the specimens containing MgO had higher expansions compared to the control specimens and the specimens containing ferronickel slag. The expansions of the ambient-cured specimens with 5% MgO and 10% MgO were 0.46% and 0.62%, respectively. Thus, the expansion increased by about 39% and 94% by the use of 5% and 10% reactive MgO, respectively. Similarly, 38% and 86% increases in expansion of the specimens were also observed by the use of 5% and 10% MgO, respectively, for the heat curing condition. Therefore, while the use of reactive MgO increased expansion, the use of ground ferronickel slag up to 50% did not increase expansion compared to the control specimens. This shows the difference between the reactivity of Mg in MgO and that in FNS. Thus, the effect of ferronickel slag on expansion in these tests is similar to that shown by the Le-Chattelier test.

Therefore, the use of ferronickel slag as a cement replacement did not increase expansion as observed by the results of Le-Chattelier soundness test, autoclave expansion test and the accelerated heat curing test.

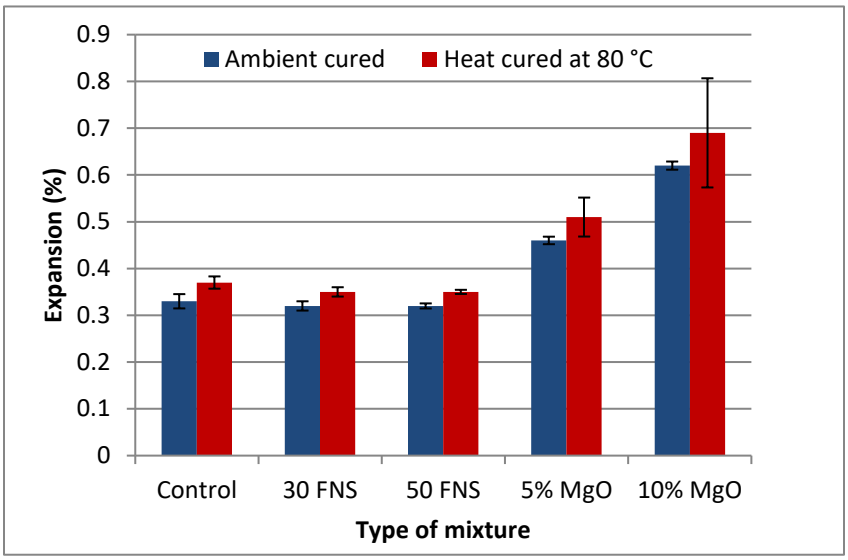

Figure 4.9: Ambient and heat cured expansion test results

4.3 Leachability of raw FNS and blended mortar specimens

The leachability test results for ground ferronickel slag, and mortar specimens containing 20% and 50% FNS are given in Table 4.3. The mortar samples were cured in water for 28 days before the leachability test. The limits of leaching of the metals set by regulatory authorities are also given in the Table 4.3 for comparison with the test results. Australian standard leaching procedure (ASLP) (AS 4439.3) test results are compared broadly with different regulatory levels set by different authorities. It is observed from Table 4.3 that the concentrations of heavy metals leached from ground ferronickel slag are less than the regulatory limits set by toxicity characteristics leaching procedure (TCLP) (US EPA -1311), ASLP and DENR administrative order no. 35 (DAO-35). When ferronickel slag was blended with cement in mortar mixtures, leaching of metals was further reduced. Thus, the metals were immobilised in the mortar specimens. Specimens with 50% ferronickel slag showed higher leaching of Ni, Co, As and lower leaching of Cr, Cu and Fe compared to the specimen with 20% nickel slag. Overall, the concentrations of leachable heavy metals were far below the limits set by regulatory authorities. Therefore, use of ferronickel slag alone or blended with cement in mortar

are considered to be environmentally safe in accordance with the limits of leachable metals set by these regulatory authorities.

Table 4.3: Concentration of heavy metal in ground ferronickel slag

Heavy metal	Concentration (mg/L)			Regulatory limit (mg/L)		
	Ground FNS	Mortar specimen at 28 days				
		20 FNS 80C	50 FNS 50C	TCLP	ASLP (Category C)	DAO- 35 (Protected water)
As	0.002	0.001	0.004	5	0.7	0.2
Cd	0.0005	0.0009	0.0009	1	0.2	0.05
Co	0.095	0.0005	0.001	NRL	NRL	NRL
Cr	0.21	0.11	0.075	5	5	0.1
Cu	0.0014	0.005	0.0039	NRL	200	NRL
Fe	41	0.021	<0.005	NRL	NRL	NRL
Ni	1.9	0.002	0.023	NRL	2	NRL
Pb	0.005	<0.0001	<0.0001	5	1	0.2
Zn	0.24	<0.001	<0.001	NRL	300	NRL
pH	5.4	>10	8.4	-	-	-
NRL = no regulatory limit						

4.4 Strength properties and durability

4.4.1 Compressive strength of mortar

The strength developments of mortar specimens containing 0% to 50% ferronickel slag as cement replacement are shown in Figure 4.11. The pictures of the tested specimens are shown in Figure 4.10.

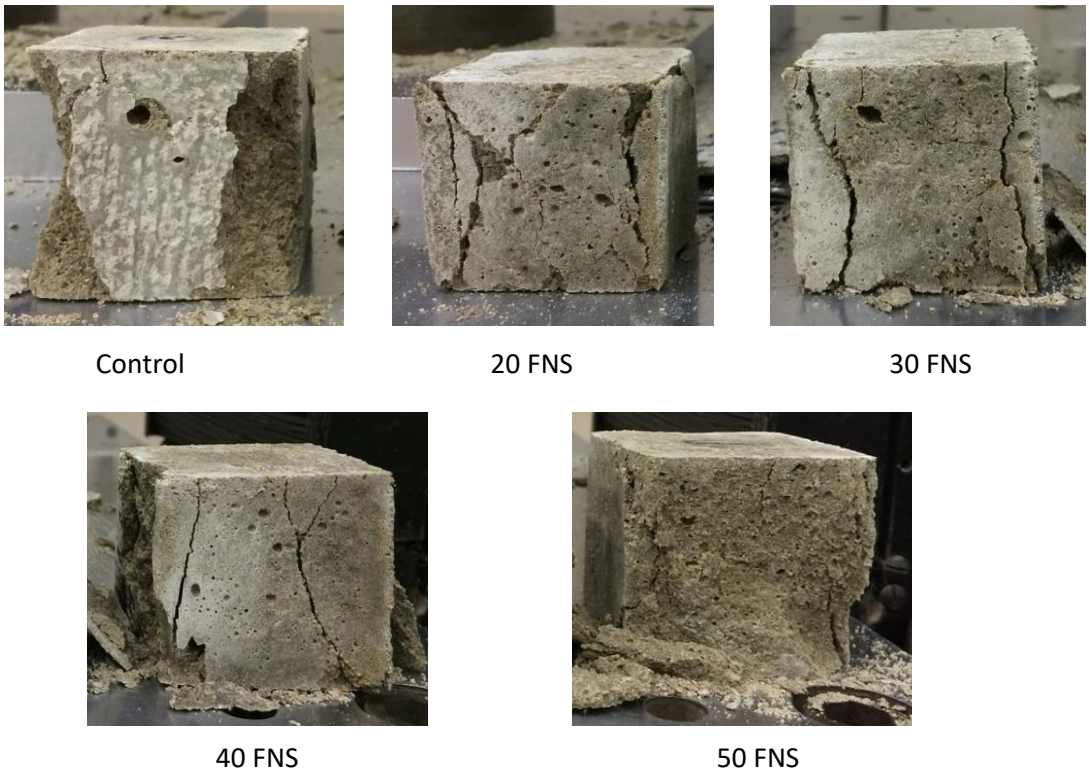

Figure 4.10: Failure mode of mortar specimens

From Figure 4.10, it is seen that control and 20-40% FNS mortar had similar types of failure modes. With the increase of the applied load a vertical crack started to appear in the specimens. When the load reached the bearing capacity of the mortar specimens, the lateral surface of the specimens collapsed. With 50% FNS, the specimens did not have any specific pattern of failure. Those failed by peeling of the side surface of the specimens.

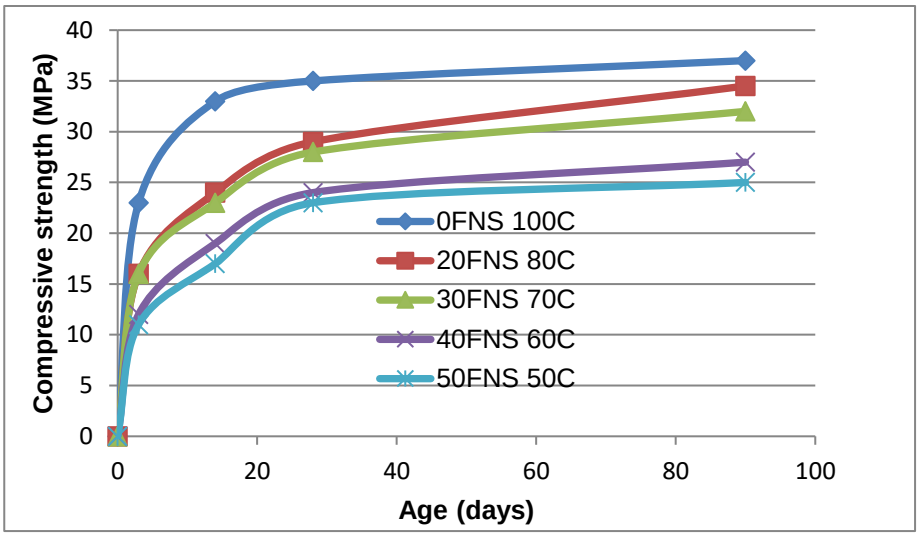

Figure 4.11: Compressive strength of mortars containing different percentages of ferronickel slag as cement replacement

It can be seen from Figure 4.11 that the early-age strength of mortar was decreased by the use of ferronickel slag as cement replacement. The rates of strength development of the ferronickel slag blended mortars were higher during 14 to 28 days compared to those of the control mix. The strength development of the ferronickel slag blended mortars showed an increasing trend up to the age of 90 days. The control mortars of 100% cement developed to 35 MPa and 37 MPa compressive strengths at 28 and 90 days, respectively. At 28 days, the mortar specimens using 20%, 30%, 40% and 50% ferronickel slag as cement replacement gained 83%, 80%, 69% and 66% strength of the control mix, respectively. At 90 days, the specimens of 20%, 30%, 40% and 50% ferronickel slag gained 93%, 86%, 73% and 68% strength of the control specimen, respectively. Therefore, the rates of strength gain of the specimens using ferronickel slag during 28 days to 90 days were significantly higher than those of the control specimens. The difference between the later-age strength development rates between the control specimens and those using ferronickel slag is more pronounced for 20% and 20% cement replacement levels. Thus, the strength development behaviours of ferronickel slag blended mixtures are similar to the general behaviour of concrete containing pozzolanic materials such as class F fly ash.

4.4.2 Compressive strength of concrete

The failure modes of the concrete cylinder specimens are shown in Figure 4.12. The cylinders were prepared from concrete containing 0% to 65% FNS as cement replacement. One ternary mixture was prepared with 10% GGBFS and 40% FNS for comparison.

Figure 4.12: Failure mode of concrete cylinder specimens

From Figure 4.12, it is observed that the control and 50% FNS specimen failed in shear mode, with the 20 and 30% FNS specimens failing by creating cones at both ends. Specimens with 40% FNS, 40% FNS and 10% GGBFS, and 65% FNS failed in compression mode with vertical cracks. Overall, specimens up to 30% FNS, had a common mode of failure. With higher cement replacement by FNS, the cylinders failed either by shear or compression.

The compressive strength developments of concrete cylinders are presented in Table 4.4 and Figure 4.13.

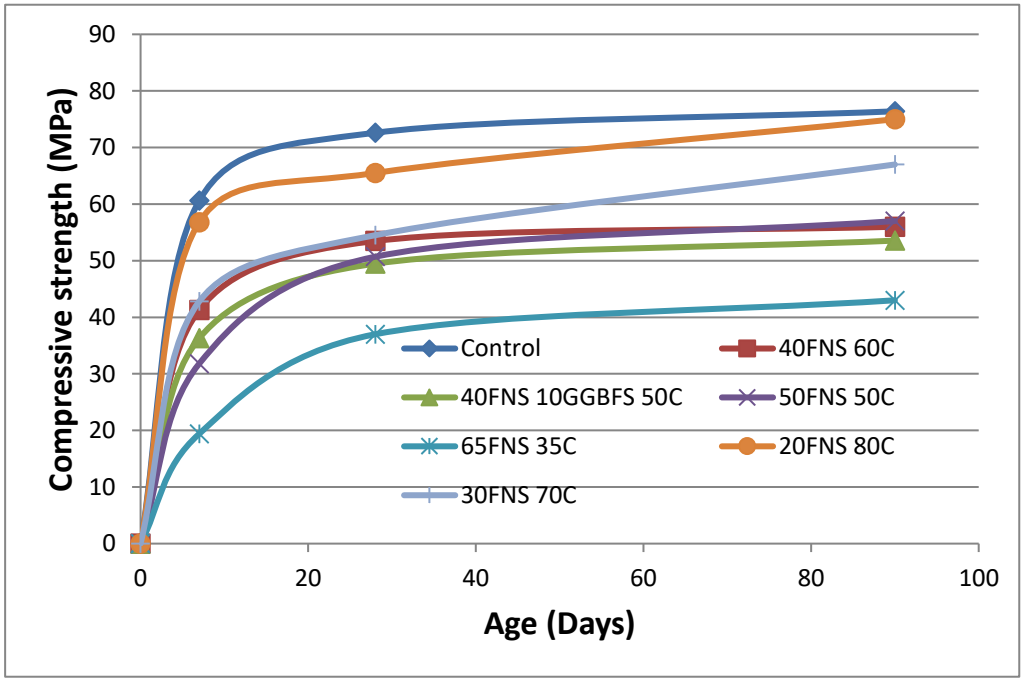

Figure 4.13: Compressive strength of concrete cylinder specimens

From Figure 4.13, it can be seen that the early age strength of concrete was reduced by the cement replacement by ferronickel slag. However, the strength gain rate from 28 days to 90 days was higher in the specimens using ferronickel slag compared to that of the control specimens. Similar to the observation in mortar mixtures, the late-age strength gain of the concrete specimens was more pronounced for 20% and 30% cement replacement by ferronickel slag. The 90-day concrete compressive strengths were 98%, 88%, 75%, 70% and 56% of the control concrete's strength for using 20%, 30%, 40%,

50% and 65% ferronickel slag as cement replacement, respectively. Therefore, use of up to 30% ferronickel slag as a cement replacement can be considered to provide an ultimate strength close to that of the control concrete by the pozzolanic activity. The strength development of the ternary mix of 40% FNS, 10% GGBFS and 50% OPC was similar to that of the binary mix of 50% FNS and 50% OPC.

4.4.3 Flexural strength of concrete

Tensile strength of concrete indicates its resistance to cracking. Higher tensile strength can reduce cracking of concrete due to external load, drying shrinkage and corrosion of embedded steel reinforcement. The tensile strength of concrete is determined by flexural tests and splitting tensile tests. The mean flexural strengths of concrete specimens using 0% to 65% FNS are presented in Figure 4.14 and Table 4.4.

It can be seen from Figure 4.14 that flexural strength generally decreased with the increase of FNS content. The effect of FNS content on flexural strength is similar to that on compressive strength. At 90 days, flexural strengths for 20% FNS content were the same as those for the control mixture. However, at 30% FNS replacement the flexural strength was highest among all the mixtures at both 28 days and 90 days. Flexural strength then gradually decreased at both 28 days and 90 days with further increase of the FNS content.

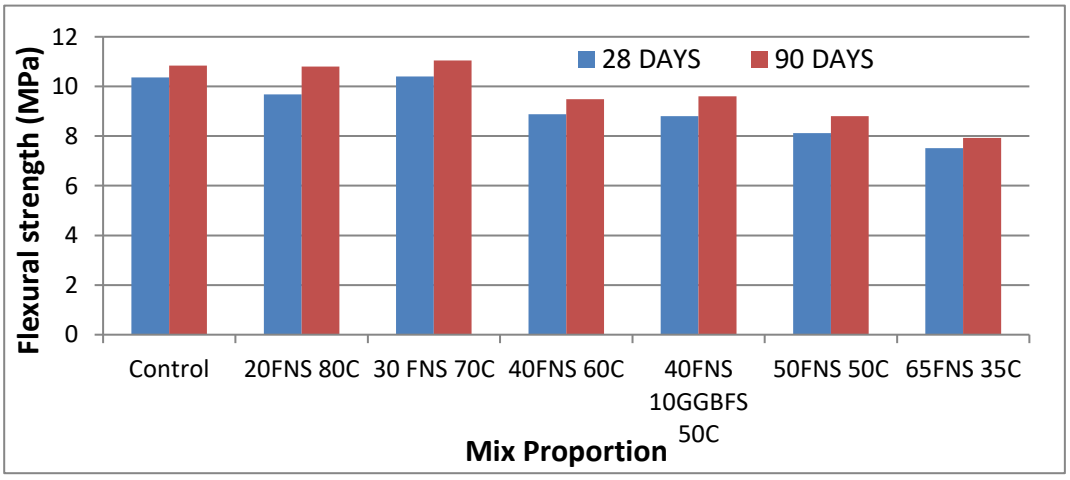

Figure 4.14: Variation of flexural strength of concrete with 0-65% FNS

Table 4.4: Experimental and predicted flexural strengths of FNS concrete

Mix	Mean compressive strength (MPa) f_{cm}		Mean flexural strength, $f_{ct.f}$ (MPa)					
			28 days			90 days		
	28 days	**90 days**	**Exp**	**Predict. AS 3600**	**Exp/ AS 3600**	**Exp**	**Predict. AS 3600**	**Exp/ AS 3600**
0FNS 100C	73	76	10.36	7.0	1.48	10.84	7.2	1.51
20FNS 80C	66	75	9.68	6.6	1.46	10.8	7.1	1.52
30FNS 70C	55	67	10.4	6.0	1.73	11.04	6.7	1.64
40FNS 60C	54	56	8.88	6.0	1.49	9.48	6.1	1.55
40FNS 10GGBFS 50C	50	54	8.8	5.7	1.54	9.6	6.0	1.61
50FNS 50C	51	57	8.12	5.8	1.40	8.8	6.2	1.43
65FNS 35C	37	43	7.52	4.9	1.54	7.92	5.3	1.49

4.4.3.1 Prediction of flexural strength from compressive strength

Usually a correlation is observed between flexural strength and compressive strength of concrete. Based on this correlation, design codes and standards recommended equations to predict flexural strength from the known values of compressive strengths. Australian Standard AS 3600 (2009) recommends Equation 4.1 for prediction of the characteristic flexural tensile strength($f'_{ct.f}$) from compressive strength of OPC concrete. The mean and upper characteristic values are found by multiplying the value obtained from Equation 4.1 by 1.4 and 1.8, respectively.

$$f'_{ct.f} = 0.6\sqrt{f_c'} \quad \ldots\ldots 4.1$$

where, f_c' is the characteristic compressive strength which is the specific compressive strength grade, or it could be determined statistically from compressive strength tests carried out in accordance with AS 1012.9 (1999). Alternatively, the relationship

between mean and characteristic compressive strengths for concretes of different grades recommended in AS3600 can be used.

Equation 4.1 was used to calculate the flexural strengths of concrete from the experimentally determined compressive strengths and the values are given in Table 4.4. The ratios of experimental and predicted flexural strengths are also given in the table. The mean values of the 28-day experimental to predicted flexural strengths ratio varied from 1.4 to 1.73 for all the mixtures. Similarly, the ratio varied between 1.43 and 1.64 for the 90-day flexural strengths. These ratios are greater than 1.0 indicating that the relationship of flexural strength to compressive strength recommended in AS3600 can be used for conservative prediction of flexural strength of concrete using ground FNS as a cement replacement up to 65%. No effect of using ground FNS as a cement replacement could be observed on the relationship.

4.4.4 Splitting tensile strength of concrete specimens

The mean splitting tensile strength of the concrete specimens using 0% to 65% FNS are presented in Table 4.5 and Figure 4.15. It can be seen from Figure 4.15 that splitting tensile strength generally decreased with the increase of FNS content. The effect of FNS content on splitting tensile strength is similar to that on compressive strength. At 90 days, splitting tensile strengths for 20% FNS content were 93% of the control specimens. Splitting tensile strength gradually decreased at both 28 days and 90 days with increase of the FNS content.

4.4.4.1 Prediction of splitting tensile strength from compressive strength

Usually an indirect correlation is observed between splitting tensile strength and compressive strength of concrete. Based on this, design codes and standards recommended equations to predict splitting tensile strength from the known values of compressive strengths. Australian Standard AS 3600 (2009) recommends Equation 4.3 for prediction of the characteristic splitting tensile strength ($f_{ct.sp}$) from the uniaxial

tensile strength of concrete (f_{ct}). Uniaxial tensile strength could be determined from compressive strength of OPC concrete according to equation 4.2. The mean and upper characteristic values are found by multiplying the value obtained from Equation 4. by 1.4 and 1.8, respectively.

$$f_{ct} = 0.36\sqrt{f_c'} \quad \ldots\ldots 4.2$$

$$f_{ct} = 0.9 f_{ct.sp} \quad \ldots\ldots 4.3$$

where, f_c' is the characteristic compressive strength which is specific compressive strength grade, or it could be determined statistically from compressive strength tests carried out in accordance with AS 1012.9. Alternatively, the relationship between mean and characteristic compressive strengths for concretes of different grades recommended in AS3600 can be used.

Equations 4.2 and 4.3 were used to calculate the splitting tensile strength of concrete from the experimentally determined compressive strengths and the values are given in Table 4.5. The ratios of between experimental and predicted splitting tensile strengths are also given in the table. The mean values of the 28-day experimental to predicted flexural strengths ratio varied from 0.92 to 1.24 for all the mixtures. Similarly, the ratios varied between 0.9 and 1.25 for the 90-day splitting tensile strength. These ratios are greater than 1.0 for FNS replacement from 0% to 40% indicating that the relationship of splitting tensile strength to compressive strength recommended in AS3600 can be used for the conservative prediction of flexural strength of concrete using ground FNS as a cement replacement up to 40%. A slight negative effect could be observed on the relationship for 50 and 65% FNS replacement.

Table 4.5: Experimental and predicted splitting tensile strengths of FNS concrete

Mix	Mean compressive strength (MPa) f_{cm}		Mean splitting tensile strength, $f_{ct.sp}$ (MPa)					
			28 days			90 days		
	28 days	**90 days**	**Exp**	**Predict. AS 3600**	**Exp/ AS 3600**	**Exp**	**Predict. AS 3600**	**Exp/ AS 3600**
0FNS 100C	72.6	76.4	5.78	4.67	1.24	6.00	4.80	1.25
20FNS 80C	65.5	74.5	4.84	4.43	1.09	5.58	4.74	1.18
30FNS 70C	54.5	67	4.63	4.02	1.15	5.5	4.48	1.23
40FNS 60C	53.5	56	4.39	3.98	1.10	4.72	4.08	1.16
40FNS 10GGBFS 50C	49.5	53.5	4.15	3.82	1.09	4.35	3.98	1.09
50FNS 50C	50.7	57	3.54	3.87	0.92	3.72	4.12	0.90
35FNS 65C	37	43	3.06	3.27	0.94	3.29	3.54	0.93

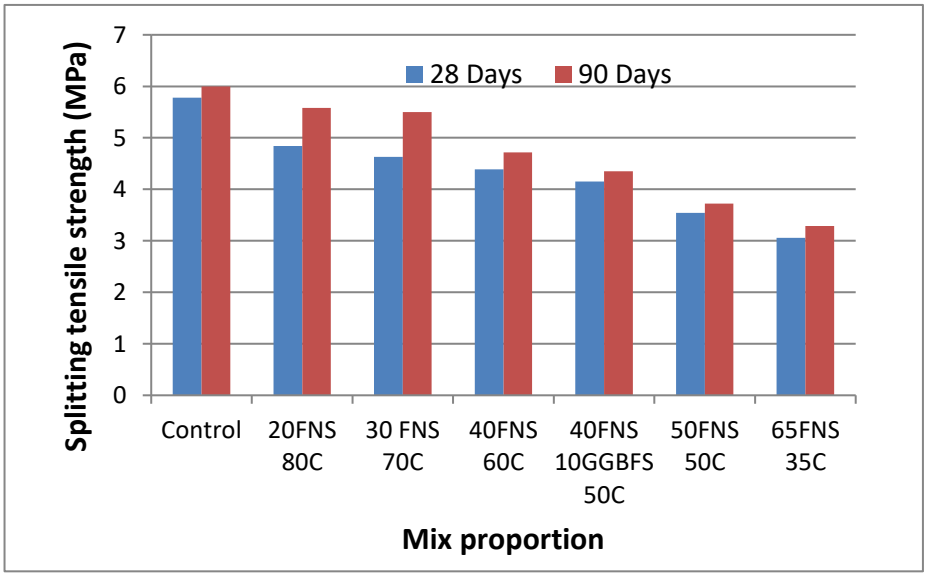

Figure 4.15: Variation of splitting tensile strength with 0-65% FNS in concrete mixtures

It can be seen that the mean ratio of the experimental splitting tensile strength to predicted values are 1.07 and 1.11 at 28 days and 90 days, respectively. Therefore, the

equations of the Australian Standard can be used to conservatively predict the splitting tensile strength of concrete using ground FNS as partial cement replacement.

4.4.5 Drying shrinkage

Drying shrinkage can increase the tensile stress in concrete, which may lead to cracking, internal warping and external deflection. This occurs mostly due to the reduction of water in the concrete or cement paste. It is affected by the amount of water and admixture used in the concrete, and the temperature and placement and curing. The types of cement and aggregate also contribute to shrinkage of concrete. Drying shrinkage occurs mostly due to the evaporation of the free water in the concrete through capillary action. Shariq et al. (2016) reported that the factors influencing the creep of concrete also affect the drying shrinkage. However, drying shrinkage does not depend on the stress conditions in concrete. Creep and drying shrinkage are both associated with the compressive strength of concrete. Lower concrete strength usually shows higher drying shrinkage strain.

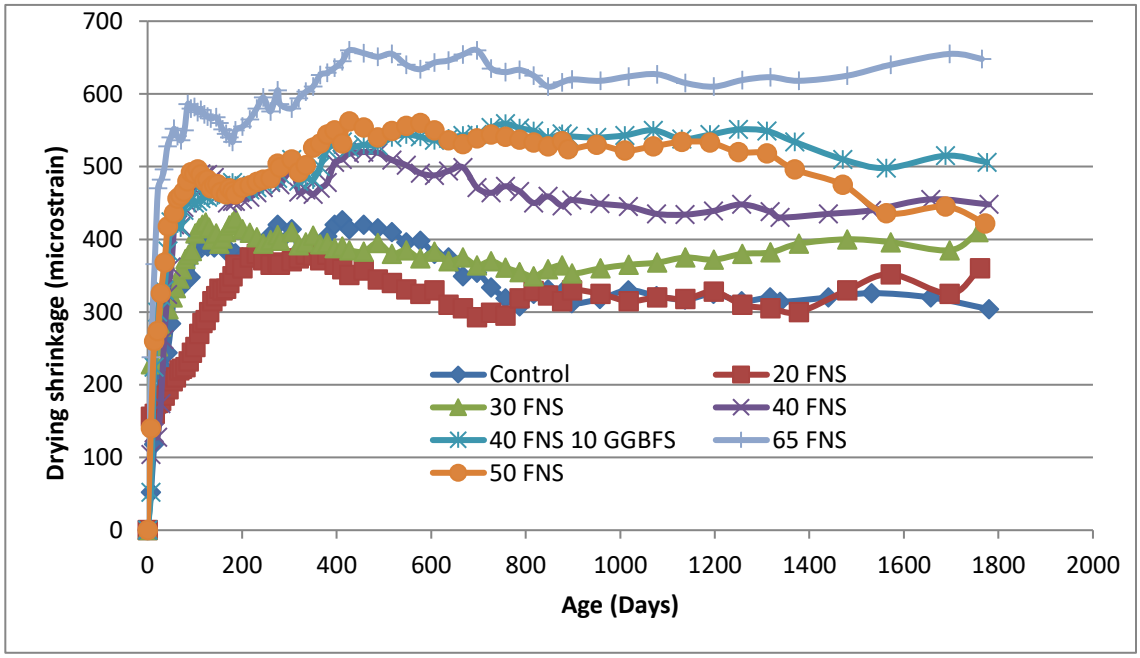

Figure 4.16: Variation of the drying shrinkage of concrete with age

In this study, drying shrinkage of concrete specimens was recorded for a period of 58 months. The long-term shrinkage measurement of the specimens was considered particularly important because the trend of shrinkage with the increase of age would reflect any expansion caused by the high magnesium content of FNS. The first reading was taken at seven days and is considered as the reference. The drying shrinkage test was carried out according to AS1012.13 (1992) and the results are plotted in Figure 4.16.

It can be seen from Figure 4.16 that the long-term drying shrinkage of the concrete specimens varied between 300 and 660 microstrains. It can also be noted that very small changes occurred in the drying shrinkage after 120 days. Some fluctuations in the magnitude of drying shrinkage with the increase of age could be observed. Drying shrinkage of concrete decreased at the early ages by incorporation of 20% FNS compared with the shrinkage of the control concrete. Generally, the trends of drying shrinkage of the specimens containing 20% and 30% FNS as cement replacement were comparable with those of the control concrete. Increasing trends of shrinkage could be observed with the increase of FNS contents beyond 30%. The higher drying shrinkage in the specimens containing higher FNS content is considered associated with a decrease of compressive strength. A similar trend was reported by Shariq et al. (2016) for use of GGBFS. As the compressive strength started to decrease considerably for using 30% to 65% FNS, drying shrinkage started to increase accordingly. However, no cracks were observed due to the higher drying shrinkage in the specimens with the higher amount of FNS. The increase of drying shrinkage with the increase of FNS content may also be attributed to the higher fineness of ground FNS than cement. It can be noted that the Blaine's fineness of FNS and cement were 500 m^2/kg and 330 m^2/kg, respectively. Shrinkage of concrete is usually found to increase with the increase of fineness of the ingredients.

4.4.5.1 Calculation of design drying shrinkage by AS3600

The design drying shrinkage at 90 days was calculated using AS3600 (2009). The calculation of design drying shrinkage is explained by the following example.

Drying shrinkage calculation for control specimen at 7 days:

L_{ds} = Drying shrinkage (microstrain)

L_i = Initial length of the specimen = 14.17 mm

L_t = Length of the specimen at specified time at 7 days = 14.146 mm

L = Gauge length = 250 mm

Drying shrinkage $L_{ds} = \frac{(L_t - L_i)}{L} \times 10^6 = 96$ microstrain

Calculation of design drying shrinkage for specimen 65FNS 35C at 90 days according to AS3600 (2009):

Drying shrinkage at 90 days was calculated according to page 39-40 of AS3600 (2009). Final drying basic shrinkage strain $\varepsilon^*_{csd.b} = 1000 \times 10^{-6}$ for elsewhere other than Sydney, Brisbane and Melbourne. The basic drying shrinkage strain,

$$\varepsilon_{csd.b} = (1 - 0.008 f_c^{'}) \times \varepsilon^*_{csd.b} = 0.000656$$

where, $f_c^{'} = 43\ MPa$ at 90 days

After commencement of drying at any time (t) the drying shrinkage strain is

$\varepsilon_{csd} = k_1 \times k_2 \times \varepsilon_{csd.b}$

At 90 days the value of $k_1$is calculated 1.56 from Figure 3.1.7.2 in page 40 of AS3600 (2009) and the value of k_2 is equal to 0.65 for an interior environment.

At 90 days the value of drying shrinkage, $\varepsilon_{csd} = 663$ microstrain.

The experimentally determined 90-day drying shrinkage of this specimen was 583 microstrains.

The design drying shrinkages at 90 days were calculated using the same procedure for all the concrete mixes and are presented in Table 4.6. Experimental 28 day drying shrinkage values are also shown in this table for comparison. It can be seen from the table that the calculated 90-day drying shrinkage increased with the increase of FNS content. The ratio of the experimental to predicted 90-day shrinkage varied between 0.73 and 0.88. This shows that the method of calculation recommended in the Australian Standard can be used for conservative prediction of design drying shrinkage of concrete using ground FNS as a partial cement replacement. AS 3972 recommends the drying shrinkage value for general purpose and blended cement at 28 days should be less than 750 microstrains. From the Table 4.6, it is observed that 28 day drying shrinkage values for all the specimens are well below the limit set by AS3972.

Table 4.6: Experimental and predicted drying shrinkage at 90 days

Mix ID	Drying shrinkage (microstrain)			Experimental/AS3600 at 90 Days
	Experimental		AS3600-2009 at 90 Days	
	28 Days	90 Days		
Control	212	348	393	0.88
20 FNS 80C	178	300	409	0.73
30 FNS 70C	280	382	469	0.81
40FNS+60C	174	454	558	0.81
40FNS+10BS+50C	322	450	578	0.77
50FNS+50C	326	490	550	0.89
65FNS+35C	482	583	663	0.88

4.4.6 Water absorption and volume of permeable voids (VPV)

Water absorption and permeability properties of the concrete mixtures were investigated using volume of permeable voids (VPV) and sorptivity tests. Water absorption can be used to measure the porosity of concrete. Higher water absorption indicates the concrete has higher porosity and higher amounts of open voids inside. The measurements of the mass were taken in oven dried, immersed saturated surface dried, boiled saturated surface dried and in suspended conditions. Figure 4.17 shows the water absorption of the specimens under immersed and oven dried conditions. It is observed that the water

absorption of the specimens under the immersed condition varied in the range of 3.29% to 4.17%. Absorption varied under the boiled condition in the range of 3.33% to 4.06%, as shown in Figure 4.18. As seen in Figures 4.17 and 4.18, there was no significant difference between the absorptions at 28 days and 90 days. According VicRoad's (2007) specification, water absorption less than 5% is considered low and according to BS1881-122 2011 water absorption in the range of 3-5% is considered average. It can be seen that there was a slight increase in absorption in the specimens using FNS, though there was no definite trend with the increase of FNS content.

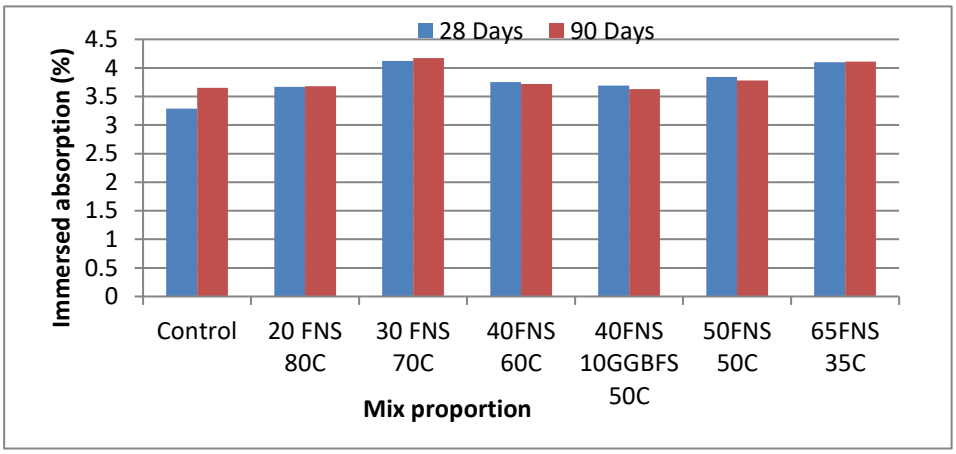

Figure 4.17: Immersed water absorption

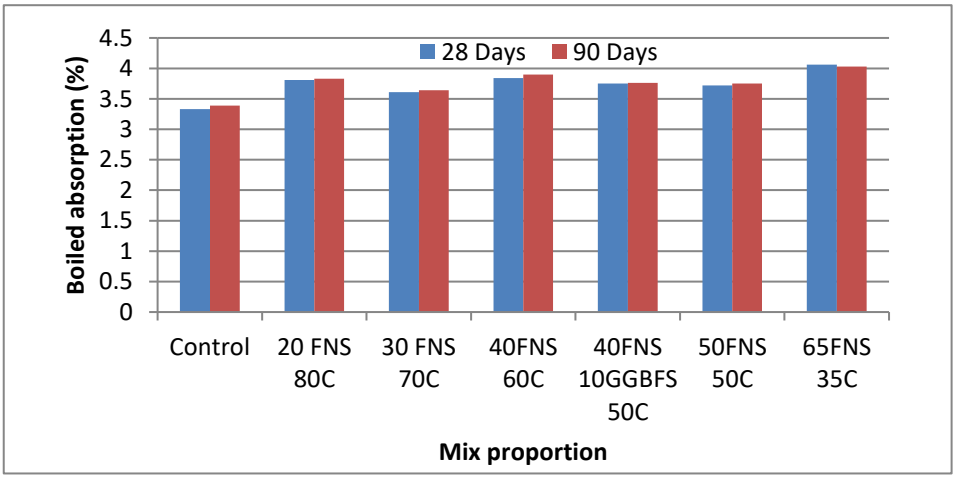

Figure 4.18: Boiled water absorption

Figure 4.19 shows the volume of permeable voids for the concrete specimens. It is observed that the volume of permeable voids of the mixes varied in the range of 8.14%

to 9.65% at 28 and 90 days. According to VicRoad's (2007) specification, concrete with VPV values of less than 11% is considered good. No significant difference in AVPV was observed for replacement of cement by FNS of up to 50%.

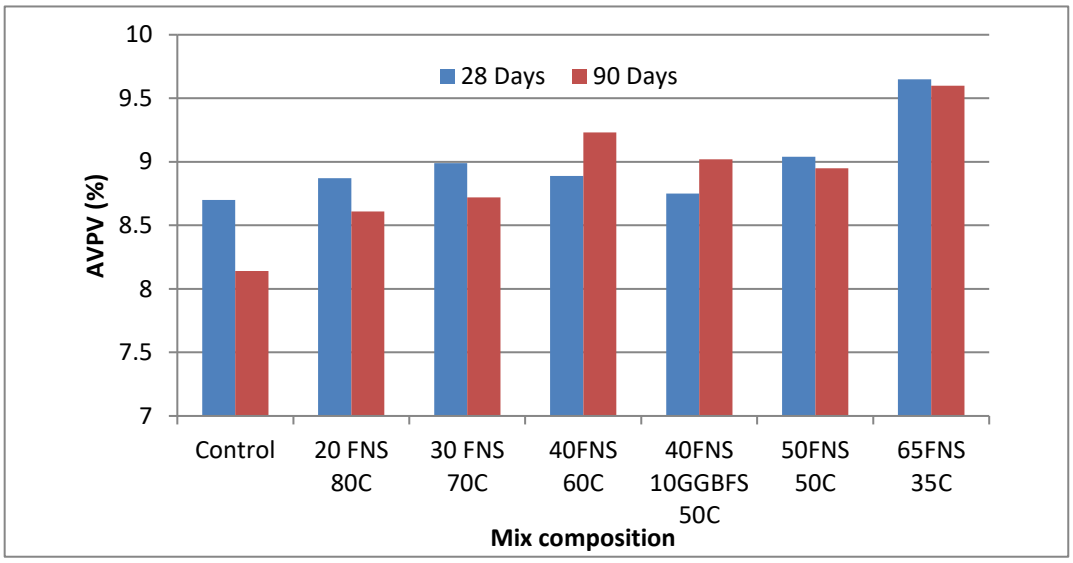

Figure 4.19: Volume of permeable voids of FNS concrete mixtures

4.4.7 Sorptivity

Sorptivity is an important property of concrete as it represents the long-term durability of concrete. Water absorption through the capillary pores in concrete is defined as sorptivity. Sorptivity is the capability to absorb and transmit water through the pore structure by capillary suction and surface tension. Surface tension is a function of the viscosity and density of the liquid and the pore structure of the porous solid. A low water/cement ratio usually produces concrete of low permeability which has small and disconnected pores that show low values of sorptivity. The sorptivity results are shown in Figure 4.20. It shows the initial sorptivity of the mixtures at 28 and 90 days. It can be seen that initial sorptivity of the concrete with FNS generally decreased with the increasing amount of FNS. This characteristic is true for both 28 and 90 day sorptivity values. The value of sorptivity was within the range of 0.005 to 0.009 ($mm/min^{0.5}$) which is considered very low. It can be seen that sorptivity at 90 days was less than the value at 28 days in all the mixtures except that with 65% FNS as cement replacement.

The decrease of sorptivity with the increase of age is attributed to the continued hydration of the binder with the increase of age. The increase of sorptivity with age was not observed for a mix of 65% FNS because the FNS content was very high and there was a small quantity of portlandite for pozzolanic reaction of FNS. However, the sorptivity of this mix was less than those of the other mixtures. The low sorptivity of this mix is attributed to the higher fineness of FNS than cement.

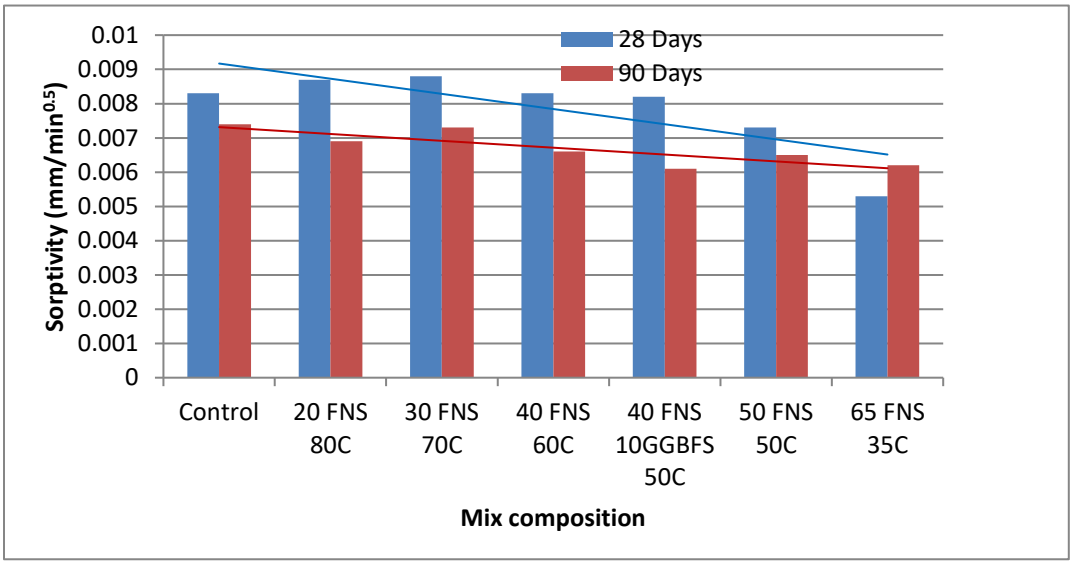

Figure 4.20: Sorptivity of concrete specimens

4.4.8 Chloride permeability

Chloride ion penetrability is a major factor for concrete in terms of long-term durability and serviceability, especially for concrete structures exposed to a marine environment. If the chloride ion penetrates through concrete to reach the reinforcing steel, it initiates corrosion of steel in the presence of moisture and air. Since the volume of rust is much higher than the original volume of steel, it exerts a high pressure on the cover concrete that can result in expansion and spalling of the concrete. A rapid chloride permeability test (RCPT) was conducted to investigate the chloride ion penetrability of concrete containing ground FNS as partial cement replacement. The RCPT results are shown in Figure 4.21. Generally, chloride ion penetrability reduced with the increase of FNS content in the concrete mix. The total amount of charge passed through the specimens at

90 days was less than that at 28 days for all the mixtures. At 28 days, chloride ion penetrability of all the mixtures was classified as low and at 90 days those were considered very low except for the control mix and that using 40% FNS according to ASTM C1202 as shown in Table 4.7. The reduction of charge passed through the specimens is attributed to the improvement of the microstructure by pozzolanic reaction of FNS at 90 days. Inclusion of FNS produced additional CSH gel that densified the microstructure which reduced the chloride ion penetrability in the specimens.

Table 4.7: Chloride ion penetrability based on charge passed (ASTM C1202)

Charge passed (Coulombs)	Chloride Ion Penetrability
>4000	High
2000-4000	Moderate
1000-2000	Low
100-1000	Very low
<100	Negligible

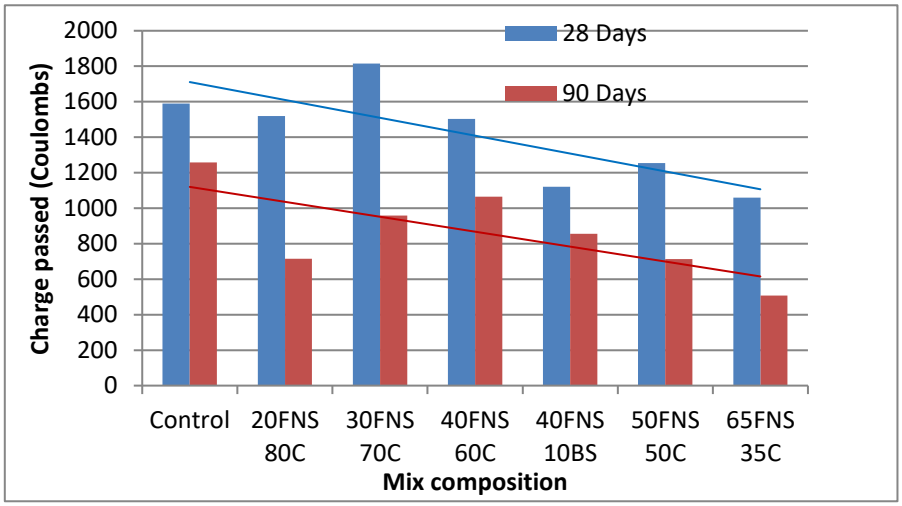

Figure 4.21: Chloride ion penetrability of the concrete mix with FNS

4.5 XRD and microstructure analysis by SEM and EDS

4.5.1 Phase identification by XRD

The formation of different phases by the hydration process was identified using quantitative XRD analysis. The XRD results of the raw ferronickel slag and the cement paste specimens containing 20% and 50% ferronickel slag are shown in Figure 4.22. It is evident from the figure that the major crystalline components in raw ferronickel slag were forsterite ferroan with very small amounts of quartz and enstatite. Quantitative analysis showed that raw ferronickel slag contained about 48 wt% forsterite ferroan, 2.2 wt% enstatite and 0.4 wt% quartz. The amorphous content of the FNS is about 50%. Most of the silica is present in the amorphous phase. This amorphous silica has participated in the pozzolanic reaction and contributed to the late-age strength development of the mixtures containing ferronickel slag, as shown in Figure 4.13.

In Figure 4.22, the cement mineral hatrurite and the FNS mineral forsterite can be observed in both the paste samples containing ferronickel slag. It can be seen that the intensity of the peaks of forsterite ferroan, contributed by the ferronickel slag, is higher in the sample with 50% ferronickel slag compared to that of the sample with 20% ferronickel slag. This means that the magnesium containing crystalline phase of ferronickel slag is stable in the hydration process. Since no brucite was identified in the XRD, it can be said that the magnesium content of FNS did not take part in the reaction process and it did not contribute to the expansion of the specimens. For this reason, the expansions determined by the Le-Chatelier test, autoclave test and extended heat curing test of the specimens containing ferronickel slag were not higher than those of the control specimens despite the high magnesium content of the slag. Also, no expansion was observed in the specimens containing ground FNS in the shrinkage tests up to 50 months. The other hydration products found were melanterite and small amounts of ettringite and gypsum.

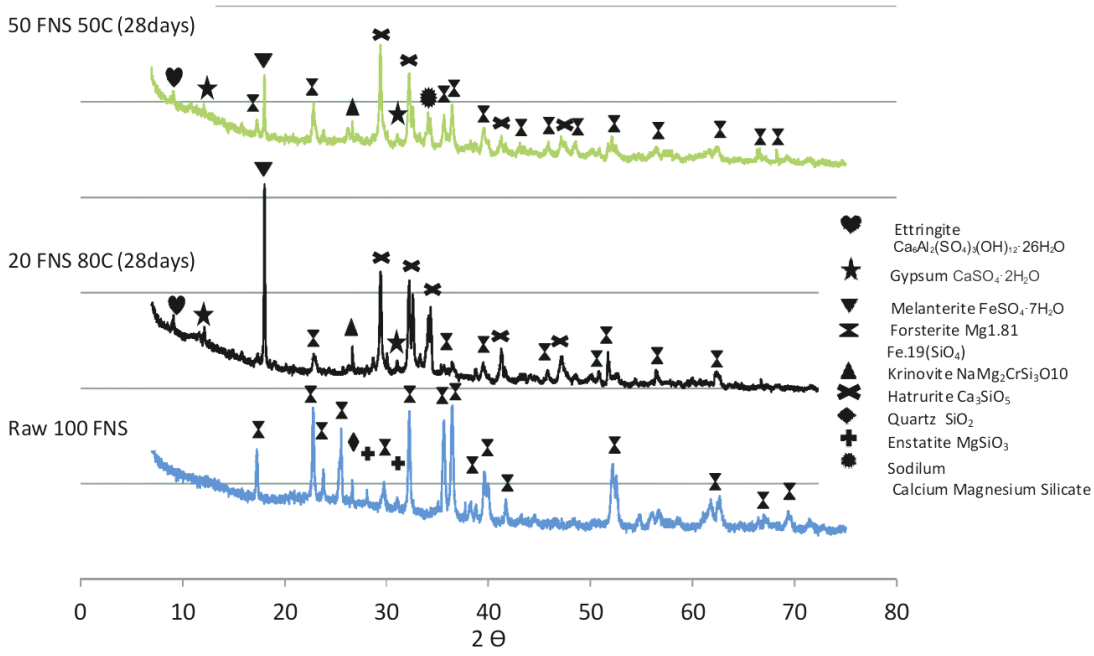

Figure 4.22: Phase analysis of raw FNS and FNS blended cement pastes by XRD

4.5.2 Investigation of the microstructure by SEM and EDS

Further to the XRD, microstructures of the hardened paste specimens were investigated by SEM images and EDS in order to identify if there was any expansive Brucite present in the specimens containing 20% and 50% ferronickel slag. Figure 4.23(a) shows the SEM image and corresponding EDS of the specimen with 20% FNS and Figure 4.23(b) shows the SEM image and corresponding EDS of the specimen containing 50% FNS.

Generally, a compact microstructure can be observed in both the specimens. It was shown by several researchers (Kumar et al., 2009; Yu et al., 2004; Henrist et al., 2003; Wu et al., 2008) that the formation of Brucite or $Mg(OH)_2$ is identified as hexagonal plate shaped crystals that may be often found agglomerated in spherical shaped morphology when observed by SEM. This type of morphological shape was not found in the SEM images as shown in Figures 4.23(a) and 4.23(b). Thus no $Mg(OH)_2$ was visible in SEM images of the specimens containing 20% and 50% FNS. This observation is consistent with the XRD results shown in Figure 4.22 that no $Mg(OH)_2$

was found in the powder samples. As shown in Figures 4.23(a) and 4.23(b), the EDS identified the presence of mainly Mg, Si, O, Fe and Ca in both cases. These elements refer to the formation of calcium silicate hydrate (C-S-H) and the stable forsterite ferroan phase of the FNS. The ratio of Mg:Si for 20% and 50% FNS were found as 0.70 and 0.75 respectively. The amorphous silica of the FNS participated in a pozzolanic reaction to continue the strength gain as shown in Figure 4.13.

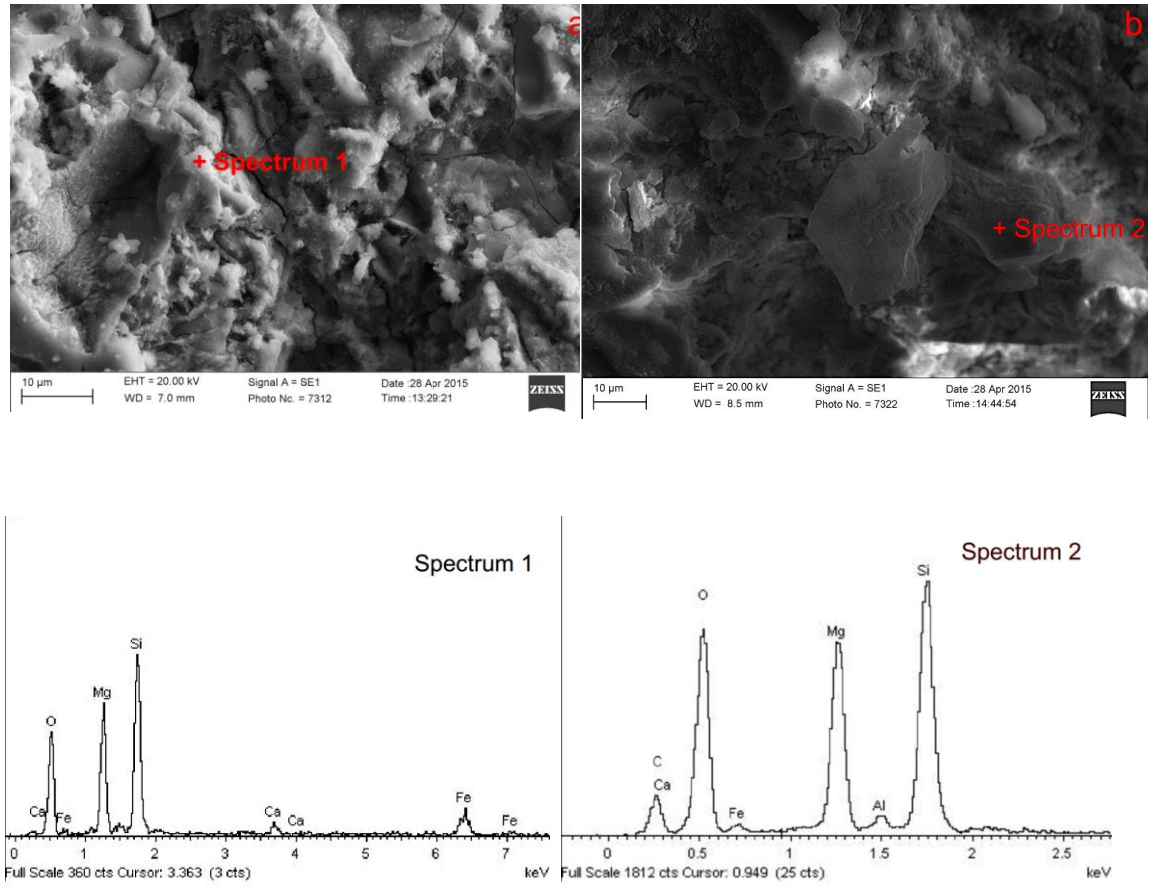

Figure 4.23: SEM and EDS of hardened paste samples containing 20% (a) and 50% (b) ferronickel slag

4.6 Summary

This chapter describes the experimental results of the concrete or mortar specimens. The specimens were prepared and tested for fresh properties, strength and durability

properties, soundness evaluation, leaching and toxicity characteristics and microstructure analysis.

Overall, water demand was reduced with the increase of FNS in paste specimens. No significant difference in the setting times was observed due to the incorporation of ground ferronickel slag as a cement replacement by up to 50%. Flow of the mortars containing FNS was slightly increased compared with the control specimen. Strength activity indices met the requirement set by ASTM C618-08a (2006).

Le-Chattelier soundness test, autoclave expansion test and the accelerated heat curing test showed that use of ferronickel slag as cement replacement did not increase expansion.

Strength development of FNS blended mortar mixtures are similar to the general behaviour of concrete containing pozzolanic materials such as class F fly ash. The 90-day concrete compressive strengths were 98%, 88%, 75%, 70% and 56% of the control concrete's strength for using 20%, 30%, 40%, 50% and 65% ferronickel slag as cement replacement, respectively. The effect of FNS content on flexural and splitting tensile strength is similar to that on compressive strength.

The drying shrinkage of the specimens containing 20% and 30% FNS as cement replacement were comparable with that of the control concrete. Increasing trends of shrinkage could be observed with the increase of FNS contents beyond 30%.

Water absorption of the specimens containing FNS was well below the limit recommended by VicRoad's (2007) and BS1881-122 (2011). No significant difference in AVPV was observed for replacement of cement by FNS up to 50%. FNS reduced the chloride ion penetrability and all the mixtures with FNS were either in low or very low category according to the ASTM C1202 (2012) classification. The XRD, SEM and EDS analysis showed no trace of expansive $Mg(OH)_2$ in the hydration product though the FNS had a high magnesium content.

Chapter 5: BEHAVIOUR OF REINFORCED CONCRETE BEAMS CONTAINING FERRONICKEL SLAG AS PARTIAL CEMENT REPLACEMENT

The effect of using ground FNS as a partial cement replacement on the structural performance of concrete members was investigated by load testing of reinforced concrete beams to failure by flexure, shear and bond between concrete and reinforcing steel. The beams were steam-cured at 80 ^{o}C for eight weeks to accelerate any possible long-term reaction of the high magnesium content of the ferronickel slag. An accelerated curing environment was created by the high temperature and humidity that would favour any possible reaction of magnesium to occur which may produce expansive brucite. It was expected that if the magnesium of ferronickel slag went into the hydration reaction to produce brucite, it would cause expansion in the concrete. Thus, the restraining effect of the internal reinforcement against the force created by the expansion of the concrete might cause cracks in the specimens if the magnesium went into the hydration reaction. The concrete beams were visually inspected for occurrence of any crack during the accelerated curing environment. The beams were then load tested to failure. The load-deflection behaviours and failure loads under different failure modes were studied. Comparison was made between the experimentally determined failure loads with those predicted by the methods of Australian Standard AS 3600, 2009 in order to evaluate the suitability of using the standard to design reinforced concrete beams containing high magnesium ferronickel slag as partial cement replacement.

5.1 Materials and mix proportions

The concrete was mixed in a commercial concrete mixing truck in the plant and delivered to the laboratory for casting of the reinforced concrete beams. Natural river sand and crushed granite were used as the fine and coarse aggregates, respectively. The main binder was ordinary Portland cement (OPC) and ground FNS was used as a 30% cement replacement in the concrete mix. The concrete mix proportions are given in

Table 5.1. The total binder content was 400 kg/m^3 and the water to cement ratio was 0.6. The measured slump value was 150 mm.

The properties of the reinforcing steel used in the beams are given in Table 5.2. 6 mm and 10 mm diameter bars were used as lateral reinforcements and 12 mm to 24 mm diameter bars were used as longitudinal reinforcements.

Table 5.1: Mix proportion of concrete mix for beam specimens

Coarse aggregate kg/m^3	Fine aggregate kg/m^3	Cement kg/m^3	FNS kg/m^3	Water kg/m^3
1050	730	280	120	240

Table 5.2: Properties of reinforcement

Diameter (mm)	Area (mm^2)	Yield strength (MPa)
6	28	250
10	78	500
12	113	500
16	200	500
20	314	500
24	452	500

5.2 Specimen details

A total of 11 beams were cast and tested. All the beam specimens were 150 mm wide, 250 mm deep and had a total length of 2000 mm. A cross section of a typical beam is shown in Figure 5.1.

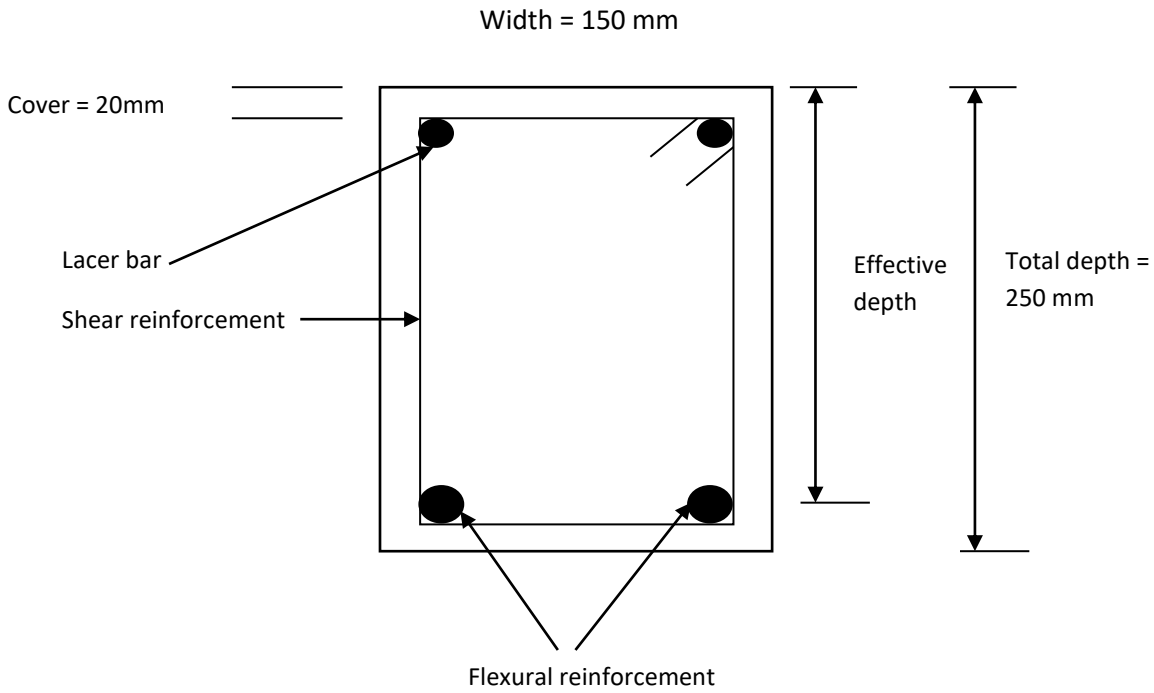

Figure 5.1: Typical cross section of beams

5.2.1 Specimens for flexure test

Three beams were prepared for flexural behaviour testing with varying steel reinforcing ratios of 0.6%, 1.26% and 1.99%. The effective span was 1800 mm and the shear span to depth ratio was 3.0. Shear reinforcement of the flexural beam was designed in a way to avoid shear failure. Shear reinforcement was provided by closed ties of 10 mm diameter bars at a centre-to-centre spacing of 75 mm. Two 12 mm bars were used as a lacer bar at the top. The details of the flexural specimens are given in the Table 5.3 and the prepared cages are shown in Figure 5.2.

Table 5.3: Details of the beams tested for flexural behaviour

Beam ID	Main Bar mm	Reinforcement ratio (%)	Effective span (m)	Shear span/depth	Shear reinforcement
F-2ϕ12	2N12	0.6	1.8	3.0	N10 @ 75mm c/c
F-2ϕ16	2N16	1.26	1.8	3.0	N10 @ 75mm c/c
F-2ϕ20	2N20	1.99	1.8	3.0	N10 @ 75mm c/c

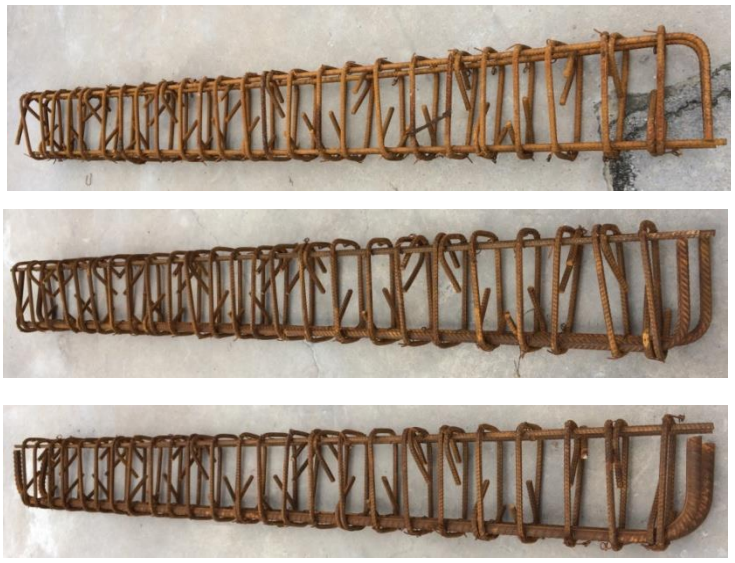

Figure 5.2: Prepared reinforcing cages for flexural beams

5.2.2 Specimens for shear test

Four beams were designed for shear failure. The tensile reinforcement consisted of two N24 bars in all the beams in order to prevent failure by flexure. The shear links were provided such that the beams failed in shear. The shear reinforcement and shear span to depth ratio was varied in the beams. The shear reinforcement consisted of closed ties made from 6 mm bars placed at 125 mm or 175 mm spacings along the length of the beams. The effective span was 1800mm and the shear span to depth ratio was either 2.3 or 3.0. The details of the shear beams are given in the Table 5.4 and the prepared cages are shown in Figure 5.3.

Table 5.4: Beam specimen detail for shear behaviour

Beam ID	Main bar mm	Effective span m	Shear span/depth	Shear reinforcement
S-125-2.3	2N24	1.8	2.3	R6 @ 125mm c/c
S-125-3.0	2N24	1.8	3.0	R6 @ 125mm c/c
S-175-2.3	2N24	1.8	2.3	R6 @ 175mm c/c
S-175-3.0	2N24	1.8	3.0	R6 @ 175mm c/c

Cage with shear reinforcement spacing of 175mm c/c

Cage with shear reinforcement spacing of 125mm c/c

Figure 5.3: Reinforcing cages prepared for shear beams

5.2.3 Specimens for bond test

Four beams were cast and tested to investigate the bond behaviour between the reinforcing steel and concrete. Tensile reinforcement ratio and splice length were varied for the test beams. Shear failure was prevented by using sufficient shear reinforcement which was closed ties of 10 mm bars at 75 mm centre-to-centre in the shear spans of the beam. No stirrups were used in the spliced region to avoid any confinement of the concrete against splitting. Details of the beams tested for bond failure are given in Table 5.5 and the prepared cages are shown in Figures 5.4a-5.4d. The effective span was 1800mm and the shear span to depth ratio was 3.0.

Table 5.5: Beam specimen detail for bond tests

Beam ID	Main Bar mm	Effective span m	Shear span/depth	Splice length mm	Shear reinforcement
B-2ϕ12-200	2N12	1.8	3.0	200	N10 @ 75mm c/c
B-2ϕ12-300	2N12	1.8	3.0	300	N10 @ 75mm c/c
B-2ϕ16-200	2N16	1.8	3.0	200	N10 @ 75mm c/c
B-2ϕ16-300	2N16	1.8	3.0	300	N10 @ 75mm c/c

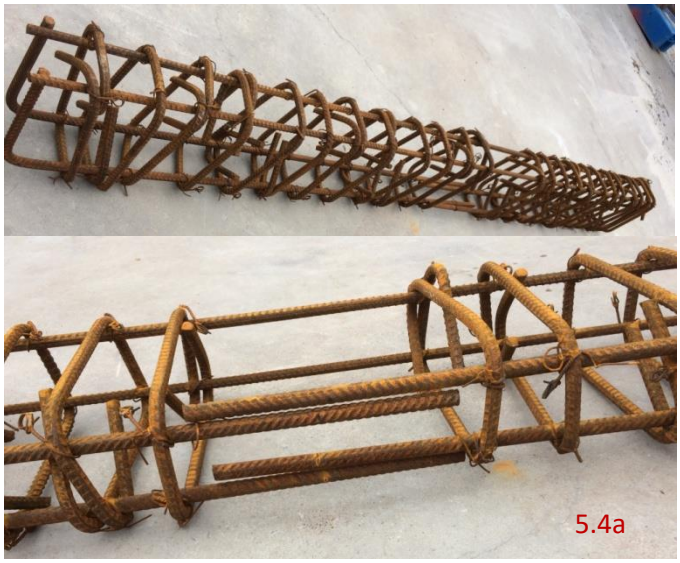

Cages with 2N12 mm tensile reinforcement and 200 mm splice length

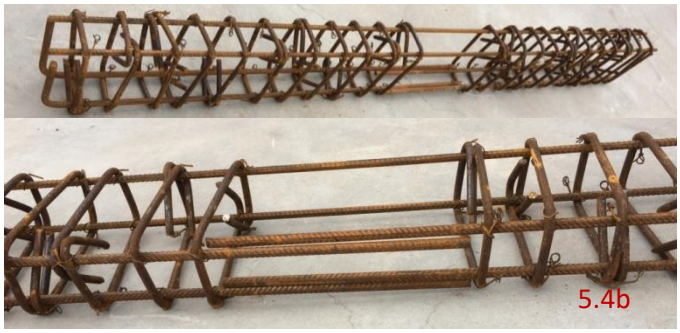

Cages with 2N12 mm tensile reinforcement and 300 mm splice length

Cages with 2N16 mm tensile reinforcement and 200 mm splice length

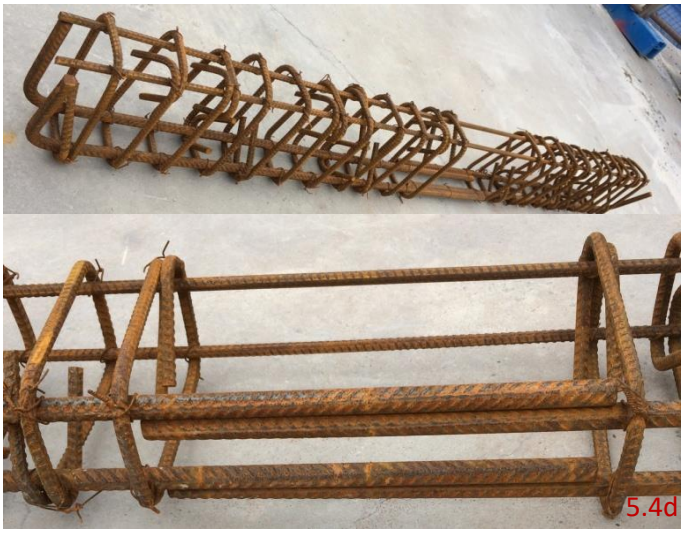

Cages with 2N16 mm tensile reinforcement and 300 mm splice length

Figure 5.4: Prepared reinforcing cages for bond behaviour analysis of beams (a-d)

5.3 Casting and curing of test beams

Reinforced concrete beams were made using 30% FNS as a cement replacement in the concrete mixture. The water to binder ratio of the concrete was 0.6. Steel moulds were used for casting of the beams. The internal surfaces of the moulds were cleaned using a high-pressure water jet. Silicon gel was applied to close any gap at the corner joints in order to prevent possible leaking of fluid during placing and compaction of concrete. Grease was applied inside the moulds for easy demoulding of the specimens after hardening.

Ready mix concrete was used for casting all the specimens. Steel bars were cut to size and welded on the sides and bottom of the reinforcement cages to maintain the correct cover of concrete to the reinforcement. The concrete delivered from a commercial mixing truck was poured into the moulds containing the reinforcement cages and compacted by using an electrically operated pencil vibrator. The specimens were demoulded after one day and wrapped with wet hessian cloth for curing by spraying water for 28 days. Figures 5.5 to 5.8 show the sequence of preparation, casting and curing of the specimens.

Prepared reinforced cages

Placement of cages in the moulds

Figure 5.5: Preparation and placement of the reinforcing cage in the mould

Ready mix concrete

Compaction of concrete

Figure 5.6: Casting of the beam specimens

Finishing of concrete surface

Finished concrete surface

Figure 5.7: Finishing of concrete after placement

Figure 5.8: Curing of the specimens

The beams were then steam-cured at 80 ^{o}C for eight weeks in order to create an accelerated environment for any possible reaction that could occur by hydration of the magnesium contained in FNS. It was expected that the extended steam curing at high temperature would accelerate any possible reaction of magnesium that might cause expansion of concrete and show cracks due to the internal restraints by the reinforcement. The beams were regularly inspected during this accelerated curing period to find out if there were any cracks due to the possible expansive reaction product of magnesium. However, there were no cracks found in the beams after eight weeks of steam curing at 80 ^{o}C.

The beams before steam curing are shown in Figure 5.9. The beams were then tested in three different groups to failure by flexure, shear or bond. It was expected that any reduction of capacity of the beams by cracks due to formation of expansive $Mg(OH)_2$ would be reflected in the load-deflection behaviour and the failure load. The specimens after steam curing are shown in the Figure 5.10.

Figure 5.9: Specimens before steam curing

Figure 5.10: Specimens after steam curing

5.4 Testing of the beams

Four point loading tests were conducted on the steam cured simply supported RC beams for flexure, bond and shear behaviour. After eight weeks of steam curing, they were removed from the chamber and allowed to cool down for one day before testing. The beams were carefully inspected for any cracks after steam curing and before the start of the load tests. No crack was found in any of the beams due to possible expansion by

hydration of the magnesium of the FNS. Mid span deflection, cracking load, crack patterns, ductility and ultimate failure loads were investigated. All the beams were tested using a universal testing machine of 2500 kN capacity. The initial loading rate was 0.5 mm/min and the rate was increased after the yielding load. LVDT was used to measure the deflection at the centre of beam and 450 mm inside from each support. The first cracking load was identified and recorded. The crack propagation was monitored on the beam surface. The flexural, shear and bond capacity of the beams were determined experimentally. The predicted capacities of the beams were calculated by using design codes and compared with the experimentally determined values. The test set up is shown in Figure 5.11.

Figure 5.11: Test set up of the beams

5.5 Results and Discussion

5.5.1 Flexural behaviour

Three beams were manufactured from concrete using 30% FNS as a cement replacement and tested to failure by flexure. The main test variable was the tensile reinforcement ratio, which was 0.79%, 1.26% and 1.99% for the test beams. The investigation was made on load-deflection behaviour, first cracking load, ultimate failure load and ductility of the beam. The mixture proportions are given in section 5.1. All beams contained compressive, tensile and shear reinforcement and were designed to fail in a flexural mode. A four point bending test was conducted on the specimens. Shear span to effective depth ratio was maintained the same in the tests of all three beams.

The load versus mid-span deflection plots of the beams are shown in Figure 5.12. It can be seen from the figure that the load-deflection curves were typical of those usually observed in reinforced concrete beams. Load gradually increased with the increase of deflection until yielding of the tensile reinforcement in all the beams. The initial stiffness of the beam increased with the increase of tensile reinforcement ratio.

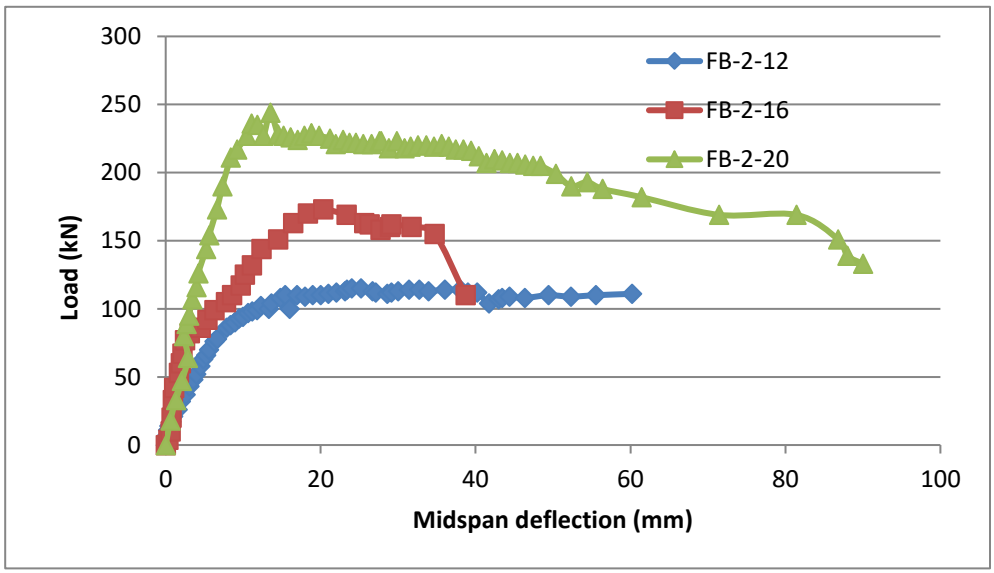

Figure 5.12: Load versus mid-span deflection of the flexural beams

Table 5.6: First crack and ultimate loads of the flexural beams

Beam ID	1st crack load (kN)	Ult. failure load (kN)			Exp. / Predicted	
		Experimental	Predicted AS3600	Predicted ACI318	Exp. / AS3600	Exp. / ACI 318
FB-2-12	30	114	70	70	1.63	1.63
FB-2-16	67	173	118	117	1.47	1.49
FB-2-20	90	244	171	167	1.43	1.46

FB-2-12 = Flexural beam with 2 tensile steel bars of 12mm diameter

The first crack and ultimate loads are given in Table 5.6. The first crack was found to occur in the mid span. The first cracking loads were found to be 30 kN, 67 kN and 90 kN for the beams with reinforcement ratios of 0.79%, 1.26% and 1.99%, respectively. Thus, the first cracking load was found to increase with increase of the tensile reinforcement ratio. More flexural cracks appeared, and the existing cracks widened with the increase of deflection. As shown in Fig. 5.12, all the beams showed significant increase of deflection with a small change of load after yielding of the tensile reinforcement.

As expected, the ultimate load increased with the increase of longitudinal reinforcement ratio. The ultimate failure loads of the beams were 114 kN, 173 kN and 244 kN for the reinforcement ratios of 0.79%, 1.26% and 1.99%, respectively. The variation of first cracking load and ultimate load is shown in Figure 5.13. All the beams finally failed in ductile mode by yielding of the tensile steel and crushing of the compressed concrete in the pure bending moment region. The failure patterns including flexural cracks and crushing of the concrete are shown in Figure 5.14. As shown in Figure 5.12, the ability of the beams to hold load for large deflections after the peak value shows their high ductility in the flexural failure mode.

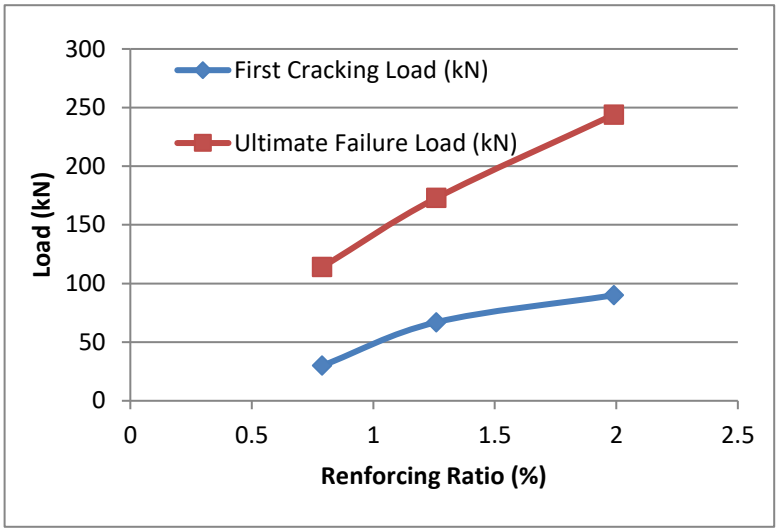

Figure 5.13: Variation of first cracking and ultimate load with reinforcing ratio

FB-2-12

FB-2-16

FB-2-20

Figure 5.14: Beam specimens tested for flexural behaviour

5.5.1.1 Prediction of the ultimate load for flexural failure

The ultimate loads of the test beams were calculated by using the methods of Australian Standard AS3600, 2009 and American Concrete Institute Code ACI 318, 2014. The sample calculations of the ultimate loads by these two methods are given below.

Calculation of the ultimate load of beam FB-2-12

28 days strength of concrete, $f_c' = 29$ MPa,

Yield strength of tensile reinforcement, $f_y = 500$ MPa,

Beam width $b = 150$ mm

Effective depth $d = 214$ mm

Reinforcement area $A_{st} = 226.1\ mm^2$

According to AS 3600 (2009):

Compressive force $C = 0.85 f_c' \gamma d_n b$ where,

γ is used to define the magnitude and location of C

$\gamma = 1.05 - 0.007\, f_c' = 0.847$

$d_n =$ depth of neutral axis

Tensile force, $T = A_{st}\, f_y$

Equating compressive and tensile force, we get $d_n = 36.0$ mm

Lever arm $Z = d - \frac{\gamma d_n}{2} = 200.0$ mm

Moment capacity $M_u = TZ = 22.6\ kN - m$

Shear span to depth ratio $a/d = 3.0$

Total capacity of the beam $= \left(\frac{M_u}{a}\right) * 2 = 70.0$ kN

According to ACI 318-13 (2014):

An average stress of $0.85f_c^{'}$ is used with a rectangular depth of $\beta_1 c$ deep from the top fibre

Compressive force $C = 0.85f_c^{'}(\beta_1 c)\ b$

Tensile force, $T = A_{st}f_y$

Equating compressive and tensile force, we get $\beta_1 c\ = 30.5$ mm

Lever arm $Z = d - \frac{\beta_1 c}{2} = 196.75$ mm

Moment capacity $M_u = TZ = 22.45\ kN - m$

Shear span to depth ratio $a/d = 3.0$

Total capacity of the beam $= \left(\frac{M_u}{a}\right) * 2 = 70.0$ kN

The predicted ultimate loads of the test beams by these two methods are given in Table 5.6 for comparison with the experimentally determined values. It can be seen from the Table 5.6 that the ultimate failure loads obtained from the experiment are higher than those predicted by both AS 3600, 2009 and ACI 318, 2014. The ratio of the test value to predicted value varied from 1.43 to 1.63 using AS 3600. Similarly, the ratio varied from 1.46 to 1.63 using ACI 318. Thus, both the design codes provided conservative predictions of the ultimate loads of the test beams using 30% FNS as a cement replacement.

Overall, no adverse effect of using 30% ground FNS as a cement replacement could be observed in the load-deflection behaviour, ultimate failure load and the failure patterns of the beams tested for failure by flexure.

5.5.2 Shear behaviour

The experimental programme included four beams with 6mm diameter shear reinforcement at 125 and 175mm centres. Shear span to depth ratios of 2.3 and 3.0 were used for both types of specimens. The shear strength of a reinforced concrete beam is a function of the compressive strength of concrete, longitudinal reinforcement percentage and the shear span/depth ratio. Two 24mm diameter bars were used for the tensile reinforcement. The beams were designed and shear reinforcement was provided in such a way that all the beams failed in shear. The experimental results for the beams are shown in Table 5.7 and Figures 5.15 to 5.16. The load at first crack, ultimate failure load, cracking patterns, deflection and failure modes for the tested beams are investigated.

Table 5.7: First crack and ultimate loads of beams tested for shear

Beam ID	Concrete strength (MPa)	1st crack load (kN)	Ultimate failure load (kN) `		Exp./AS 3600
			Experimental	Prediction AS 3600	
S-125-2.3	29	135	230	172	1.33
S-125-3.0	29	130	227	172	1.32
S-175-2.3	29	129	203	148	1.37
S-175-3.0	29	134	186	148	1.26

S-125-2.3 = Beam for shear test with 125 mm stirrup spacing and shear span to depth ratio of 2.3

Deflection started to increase with the increase of the applied load for all the beams. The first crack (diagonal) was observed at shear span for all the beams. With further increase of the load, the first crack did not show to widen enough, and rather inclined shear cracks started to form near the support. All the beams failed in a brittle manner by widening up the shear crack before yielding of the tensile reinforcement.

The experimental results given in Table 5.7 show that there was no significant difference in the first crack load for all the beams. It can be seen that the first crack load

for all the beams varied in a narrow range between 129 kN and 135 kN. It was also observed that the shear capacity varied with the a/d ratio and different stirrup spacing as expected.

From Figures 5.15 and 5.16, it is observed that beams with 125 mm stirrup spacing show higher capacity compared with 175 mm stirrup spacing as expected. The effect of stirrup spacing on the ultimate load was more pronounced than that of shear span to depth ratio. It can be seen that the ultimate load of the beam with a shear span to depth ratio of 2.3 increased from 203 kN to 230 kN due to decrease of the stirrup spacing from 175 mm to 125 mm. Similarly, for the beam with a shear span to depth ratio of 3, the ultimate load increased from 186 kN to 227 kN due to the decrease of stirrup spacing from 175 mm to 125 mm. Photographs of the failed specimens are shown in Figure 5.17. It can be seen that all the beams failed in shear by widening of the diagonal crack. The shear crack angle was found to vary in the range of 25 to 33 degrees with the horizontal. The load-deflection behaviour and failure patterns of the beams were similar to those expected in typical reinforced concrete beams.

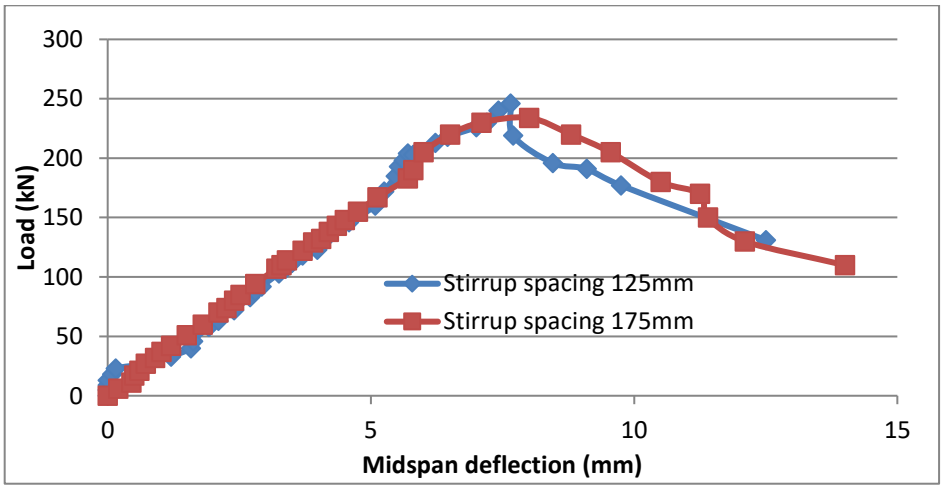

Figure 5.15: Load versus mid-span deflection for a/d ratio 2.3

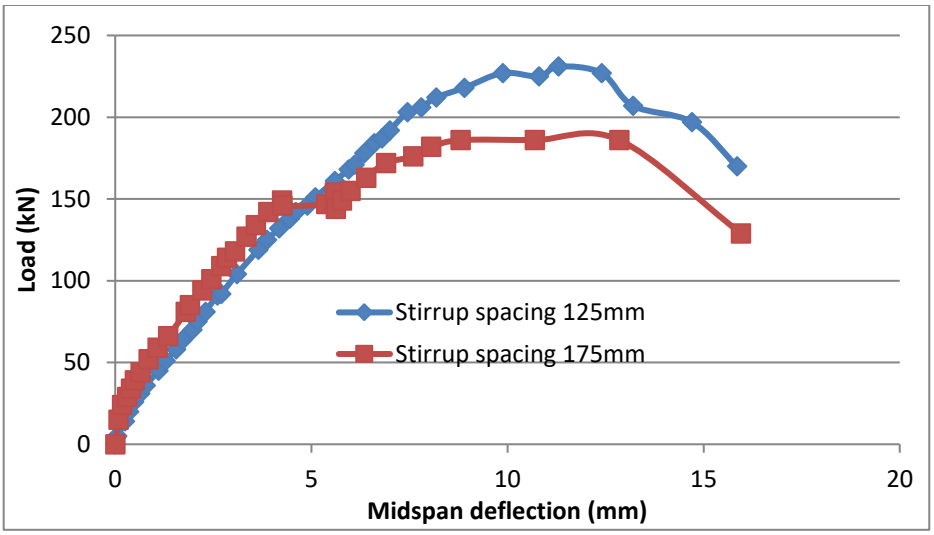

Figure 5.16: Load versus mid-span deflection for a/d ratio 3.0

S-125-3.0

S-175-3.0

S-175-2.3

S-125-2.3

Figure 5.17: Failure patterns of beams tested for shear

5.5.2.1 Prediction of ultimate load in shear

The ultimate loads of the beams tested for shear failure were predicted by using the method of Australian Standard AS 3600, 2009. A sample calculation is shown below as an example of the calculation procedure.

Calculation of the ultimate load of beam S-125-2.3 according to AS 3600 (2009):

28 days concrete strength, $f_c' = 29$ MPa,

Yield strength of tensile reinforcement, $f_y = 500$ MPa,

Yield strength of shear reinforcement, $f_{sy.f} = 250$ MPa,

Beam width $b = 150$ mm

Effective depth $d = 208$ mm

Tensile reinforcement area $A_{st} = 904.3\ mm^2$

Shear reinforcement area $A_{sv} = 56.5\ mm^2$

Shear reinforcement spacing s = 125mm

Contribution to shear strength by the concrete,

$$V_{uc} = \beta_1\beta_2\beta_3 bd\, f_c'^{\frac{1}{3}}\left(\frac{A_{st}}{bd}\right)^{\frac{1}{3}} = 45.0\ kN$$

where, $\beta_1 = 1.1\left(1.6 - \frac{d}{1000}\right) = 1.53$

$\beta_2 = 1, \beta_3 = 1$

Θ_v is taken as 30^o as the shear reinforcement used is close to the minimum amount of shear reinforcement required.

Contribution to shear strength by the shear reinforcement,

$$V_{us} = (A_{sv}\, f_{sy.f}\, d/s)\cot\Theta_v = 40.75\ kN$$

Design maximum load capacity of the beam according to AS 3600, 2009

$= (V_{us} + V_{uc}) * 2 = 172$ kN

The experimentally determined ultimate load for this beam was 230 kN.

The ultimate loads of all the beams were calculated using the same procedure and the predicted values are given in Table 5.7. The ratio of the experimental ultimate load to the predicted value for each beam is given in the table. It can be seen that the ratio is greater than 1.0 for each of the four beams. The ratio varied from 1.26 to 1.35 for the beams. This indicated that the design method of AS3600 resulted in conservative predictions of the ultimate load of the beams failing in shear mode.

Overall, no adverse effect of using the high magnesium FNS as a partial cement replacement was observed on the load-deflection behaviour, shear failure pattern and ultimate load of the beams.

5.5.3 Bond behaviour

Four beams were prepared and tested to study the bond behaviour of reinforced concrete beams containing 30% FNS as a cement replacement. The main variables were the splice length and tensile reinforcement ratio. The main bar diameter was 12 or 16mm and the splice lengths were either 200 mm or 400 mm. All the beams were designed as under-reinforced beams and the basic development length or the splice lengths of the tested beams were less than the required development length according to AS 3600 2009 so that the bond failure/splitting failure would occur before yielding of the bars. No shear reinforcement was provided over the splice zone. Bond failure normally occurs due to either local crushing of the concrete in front of the rib of the bar or splitting of the concrete due to radial cracks around the bar. The experimental results obtained from the tests are given in Table 5.8. The load-deflection diagrams are plotted in Figures 5.18 and 5.19.

Table 5.8: Results for bond behaviour of beams

Beam ID	Concrete strength (MPa)	1st crack load (kN)	Exp. failure load (kN)	Exp. average bond strength (MPa)	Predicted bond strength (MPa)		Exp. / predicted	
					Orangun et al.	Darwin et al.	Orangun et al.	Darwin et al.
B-2-12-200	29	35	45	4.93	4.11	4.0	1.19	1.23
B-2-12-300	29	48	72	5.25	3.67	3.4	1.44	1.55
B-2-16-200	29	47	62	5.22	4.00	4.34	1.31	1.21
B-2-16-300	29	64	68	3.82	3.41	3.45	1.12	1.11

B-2-12-200 – Beam for bond behaviour with 2 tensile reinforcement of 12mm diameter and 200mm splice length

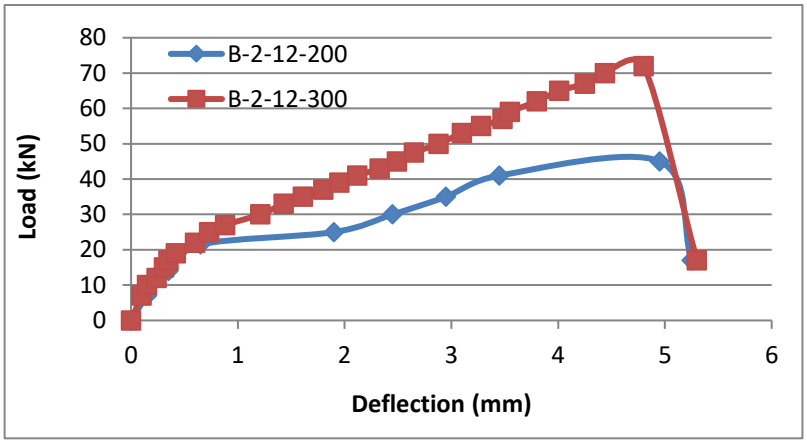

Figure 5.18: Load versus mid-span deflection of beams with 12mm diameter bars

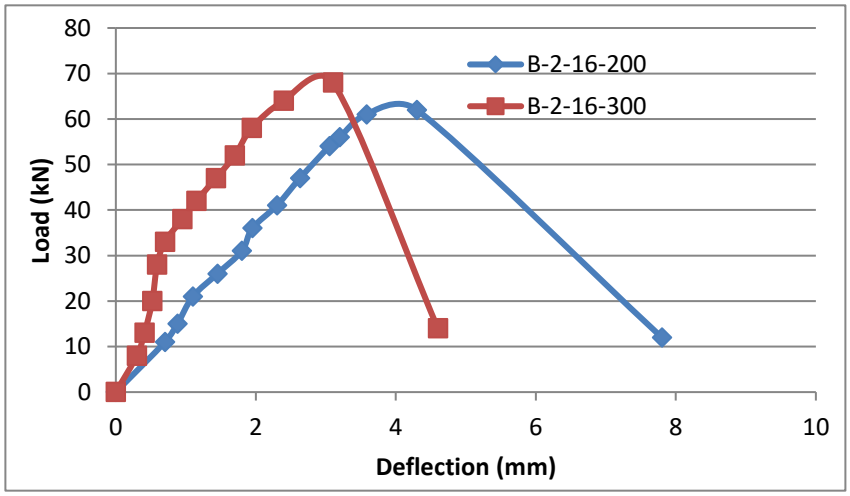

Figure 5.19: Load versus mid-span deflection of beams with 16mm bars

After the start of loading, the first flexural crack (vertical) occurred at the mid-span for all the beams. As given in Table 5.8, the first crack occurred in the beams with 12 mm bars at 35 kN and 48 kN loads for the splice lengths of 200 mm and 300 mm, respectively. Similarly, the first cracks of the beams reinforced with 16 mm bars occurred at loads of 47 kN and 64 kN for splice lengths of 200 mm and 300 mm, respectively. Thus, the first crack load increased with the increase of the splice lengths for both 12 mm and 16 mm bars. With the increase of load, the crack widened, and new cracks started to form.

As the load reached its peak value, splitting cracks initiated in the cover of concrete and the beams suddenly failed by splitting of the concrete in the splice zone. The bond failure of the beams by displacement of cover concrete substrates in the splice zone was similar in all the beams. This can be seen in the photographs of the beams after failure as shown in Figure 5.20. No yielding occurred in any of the tensile bars at failure of the beams. All the beams failed in a brittle manner and the load dropped fast after the peak value as shown in Figures. 5.12 and 5.13. It can be seen from the results given in Table 5.8 that the ultimate load of the beams using 12 mm bars increased from 45 kN to 72 kN by increasing the splice length from 200 mm to 300 mm. Similarly, the ultimate load increased from 62 kN to 68 kN for using 16 mm bars as the tensile reinforcement.

Figure 5.20: Crack pattern and failure mode of beams tested for bond behaviour analysis

5.5.3.1 Ultimate bond strength of the test beams and comparison with predicted values

The bond strengths of the test beams were calculated from the experimentally determined ultimate loads given in Table 5.8. An elastic analysis of the cross-section was carried out in order to determine the tensile force in the reinforcing bar using the bending moment at ultimate load. The average bond stress in the bar was then calculated by dividing the tensile force by the perimeter of the bar in the spliced length. The calculated bond strengths of the beams are given in Table 5.8. An example of the calculation of bond strength from the ultimate load is given below. The bond strengths of the beams were also predicted by using the empirical equations proposed by Orangun

et al. (1997) and Darwin et al. (1992). These equations were shown to provide conservative predictions of the bond strength between OPC concrete with reinforcing steel. Examples of the calculations of bond strengths by these two equations are also shown below.

Calculation of bond strength of beam B-2-12-200 from the ultimate load:

Beam width $b = 150$ mm

Effective depth $d = 214$ mm

Splice length, $L = 200$ mm

Bar diameter, $d_s = 12$ mm

Tensile reinforcement area, $A_s = 226.1\ m^2$

Experimental failure load $P = 45.0$ kN

Shear span to depth ratio $\frac{a}{d} = 3.0$

Modulus of elasticity of steel $E_s = 200\ GPa$

Modulus of elasticity of concrete $E_c = 5000 \times f_c'^{0.5} = 26925$

Modular ratio $n = \frac{E_s}{E_c} = 7.42$

Steel ratio $\rho = \frac{A_s}{bd} = 0.00704$

$k = \sqrt{2\rho n + (\rho n)^2} - \rho n = 0.27$

$j = 1 - \frac{k}{3} = 0.91$

Shear span to depth ratio $\frac{a}{d} = 3.0$

Moment, $M_{max} = \frac{P}{2} \times a = \frac{45}{2} \times 3 \times 0.214 = 14.44$ kN $-$ m

Stress in the tensile steel $f_s = \frac{M_{max}}{A_s jd} = 328.0$ MPa

Bond strength $u = \frac{A_s f_s}{2\pi d_s L} = 4.93$ MPa

Bond strength prediction of beam B-2-12-200 by Orangun et al. (1997):

Bond strength $u = 0.083045\, f_c'^{0.5} \left(1.2 + \frac{3C}{d_s} + \frac{50 d_s}{L}\right) = 4.11$ MPa

where, C = cover = 20 mm

Bond strength prediction of beam B-2-12-200 by Darwin et al. (1992):

Bond strength $u = 0.083045\, f_c'^{0.5} \left(\left(1.06 + \frac{2.12C}{d_s}\right)\left(0.92 + 0.08 \times \frac{C_{max}}{C_{min}}\right) + \frac{75 d_s}{L}\right)$

$= 4.0$ MPa

where,

C = concrete cover

$C_{max} =$ max of (min (side cover, half of bar spacing), bottom cover) $= 20$ mm

$C_{min} =$ min of (bottom or side cover or half of bar spacing) $= 20$ mm

The predicted values of bond strengths of the beams by these two empirical equations are given in Table 5.8. The ratios of the predicted to experimental bond strengths are also given in this table. It can be seen that the ratio of experimental to predicted values by the equation of Orangun et al. (1997) varied from 1.12 to 1.44 for these four test beams. Similarly, the ratio varied from 1.11 to 1.55 for predictions by the equations of Darwin et al. (1992). Thus, both the equations predicted the bond strengths conservatively. Therefore, the equations developed for the bond strength of the reinforcing bars with normal OPC concrete can be used for conservative predictions of the bond strength of reinforced concrete beams using 30% FNS as a cement replacement.

5.6 Summary

This chapter presented the behaviour of reinforced concrete beams containing 30% ground FNS as a cement replacement. The beams were subjected to steam curing at 80 ^{o}C for eight weeks in order to create a favourable environment for any possible reaction of the high magnesium content of the FNS. No cracks or other changes were found in the beams at the end of extended steam curing that could have occurred as a result of the possible reaction of the high magnesium FNS. This observation is consistent with the results presented in the previous chapter where no excessive expansions were observed due to the reaction of the FNS in different tests. The beams were then tested under loads to failure by flexure, shear and bond between concrete and steel reinforcement. The load-deflection and failure behaviours of the beams under these different actions were found to be similar to those usually found in tests of normal concrete beams using OPC as the binder. The analytical methods commonly used for prediction of the ultimate loads of OPC concrete beams under these actions were found to be suitable for conservative predictions of ultimate loads of the test beams. Therefore, no adverse effect of using the high magnesium FNS as a partial replacement of cement was found on the structural behaviour of the reinforced concrete beams.

Chapter 6: CONCLUSIONS

This thesis presented the fresh properties, hardened properties and durability of cement paste, mortar and concrete specimens using high-magnesium ferronickel slag (FNS) as a partial replacement of cement. Particular emphasis was given to the investigation of the possible expansion of concrete due to the high magnesium content of the ferronickel slag. Microstructural investigations were carried out by using SEM, EDS and XRD in order to understand the reaction products and evaluate the properties shown in different tests. Comparison was made between the properties determined for using FNS as a partial replacement of cement with those for using other commercial supplementary cementitious materials such as fly ash and GGBFS. The study also investigated the structural behaviours of reinforced concrete beams cast with concrete containing 30% FNS as a replacement of cement. The major findings of the study are concluded below.

1. Water demand and setting times were not significantly affected by the use of up to 50% FNS as a cement replacement. The strength activity indices of FNS at 7 and 28 days were 74% and 84%, respectively. Therefore, the pozzolanic activity of FNS is comparable to that of a class F fly ash.

2. No negative effects of FNS on the expansion of the specimens were found in the Le-Chatelier expansion test, autoclave expansion test and extended heat curing tests. The specimens using FNS showed less expansion than the control cement paste specimens and specimens containing 5% or 10% reactive MgO. This is attributed to the reduced free lime content in the mixes using FNS as a partial cement replacement. The expansions were well below the 5% and 0.8% limits set by the standards for the Le-Chatelier and autoclave tests, respectively. Therefore, the use of up to 50% FNS as a cement replacement did not cause deleterious expansion in spite of its high magnesium content.

3. The leaching assessment of ground FNS showed that the concentrations of leachable heavy metals were far below the limits set by ASLP (AS4439.3),

TCLP (US EPA- 1311) and DAO-35 for protected water (1990). Thus, the use of FNS as a partial cement replacement is considered environmentally safe.

4. For 20% cement replacement by FNS, the 28 day mortar compressive strength decreased from 35 MPa to 29 MPa and at 90 days it decreased from 37 MPa to 35 MPa. For 50% FNS replacement, mortar compressive strength decreased from 35 MPa to 23 MPa and 37 MPa to 25 MPa at 28 and 90 days, respectively. Similarly, 20% FNS concrete specimens showed 66 MPa and 75 MPa compressive strengths at 28 and 90 days, respectively. Specimens with 50% FNS achieved 51 MPa and 57 MPa while the control specimens had 73 MPa and 76 MPa at 28 and 90 days, respectively. Compressive strength decreased with the increase of cement replacement by FNS, however, the difference was less at 90 days, as is generally found for other supplementary cementitious materials.

5. The flexural and splitting tensile strengths of 20% FNS concrete were also very close to those of the control concrete. At 90 days, 20% FNS showed flexural strength of 10.8 MPa and splitting tensile strength of 5.58 MPa where the control specimens showed 10.84 MPa and 6.0 MPa, respectively.

6. Very small changes occurred in the drying shrinkage of concrete after 120 days. With the incorporation of 20% FNS in concrete mixes, drying shrinkage decreased at the early ages as compared to the control mixture. An increasing trend of drying shrinkage was observed in concrete specimens as the compressive strength decreased considerably for 30% to 65% FNS contents. A small variation was observed for 20% FNS replacement. No cracks were observed due to the high drying shrinkage in the specimens with the higher amount of FNS. The increase of drying shrinkage with the increase of FNS content may be attributed to the higher fineness of ground FNS than cement. The experimentally measured 90-day shrinkage values also showed the same trend except the specimens using 20% FNS. The ratio of the experimental 90-day shrinkage to that predicted by the Australian Standard varied between 0.73 and

0.88. This shows that the Australian Standard can be used for conservative prediction of drying shrinkage of the specimens using ground FNS as a partial cement replacement. No adverse effect on expansion was observed up to 58 months due to the incorporation of FNS as a cement replacement in concrete.

7. Water absorption of concrete using FNS as a partial replacement of cement was found to vary in the range of 3.29 % to 4.17%, which is considered low or average as per VicRoad's (2007) specification and BS1881, 2011. The volume of permeable voids of concrete was found to be less than 12%, which is considered good as per VicRoad's specification. Sorptivity was in the range of 0.005-0.009, which is considered very low. FNS reduced the chloride ion penetrability and all the mixtures with FNS were either in the low or very low category according to the ASTM C1202, 2012 classification.

8. The XRD, SEM and EDS analysis showed no trace of expansive $Mg(OH)_2$ in the hydration product though the FNS had a high magnesium content. This is because the magnesium was present in the form of stable forsterite ferroan as shown by the XRD results. The amorphous silica present in the slag contributed to the late-age strength development of the specimens. Thus, the soundness and compressive strength development of the ground ferronickel slag was found comparable to those of other commonly used supplementary cementitious materials such as class F fly ash.

9. Reinforced concrete beams made with concrete containing 30% FNS as a cement replacement and steam cured at 80 ^{o}C for eight weeks did not show any cracks due to the possible expansion of the hydration of magnesium contained in FNS. No difference was observed in the load-deflection curve, cracking and failure patterns of the beams tested to fail in flexure, shear and bond due to the use of high magnesium FNS and high temperature steam curing for prolonged duration. The ultimate loads predicted by common methods for flexural, shear and bond failure were found to be conservative when compared with the test results.

Therefore, the design standards for traditional cement concrete are suitable for the conservative design of reinforced concrete beams made of concrete using ground FNS as a partial cement replacement.

10. Overall, no adverse effects of using the high-magnesium FNS as a partial cement replacement were found on the fresh properties and expansion of the specimens. The rate of strength development of concrete using FNS was found comparable with that for using other common supplementary cementitious materials such as class F fly ash. Results of the tests related to durability indicated a good level of durability of concrete using FNS as a partial cement replacement. Structural behaviour of reinforced concrete beams using 30% FNS was the same as those for beams using traditional OPC concrete. Therefore, the use of ground FNS as a partial replacement of cement is considered a viable option for the production of green concrete.

RECOMMENDATIONS FOR FUTURE WORKS

This study could be extended by using FNS as a binder for geopolymer concrete. After establishing the early age fresh properties, research could be extended to exploring the strength and durability properties of the geopolymer containing different percentages of FNS.

REFERENCES:

AASHTO M 307 (2013). Specification for silica fume used in cementitious mixtures.

Abdul Razak, H. and Wong, H.S. (2004). Strength estimation model for high-strength concrete incorporating metakaolin and silica fume.

ACI 233 R03. (2000). Slag Cement in Concrete and Mortar, Detroit, Michigan.

Ahmed, S., Bolatito A., and Christopher F. (2017). Structure and properties of mortar and concrete with rice husk ash as partial replacement of ordinary Portland cement – A review.

American Concrete Institute ACI Committee. (2011). Building Code Requirements for Structural Concrete ACI 318-08 and Commentary 318R-11. ACI 318-08/318R-11. American Concrete Institute, Farmington Hills, MI, USA.

ACI 318. (2014). Building code requirements for structural concrete and commentary.

AS 1012.13 (1992). Methods of testing concrete. Methods 13: Determination of the drying shrinkage of concrete for samples prepared in the field or in the laboratory. SAI Global Limited.

AS 4439.3. (1997). Wastes, sediments and contaminated soils Part 3: Preparation of leachates - Bottle leaching procedure. SAI Global Limited.

AS 3972. (2010). General Purpose and Blended Cements SAI Global Limited. SAI Global Limited.

AS 3582.1. (2016). Supplementary cementitious materials Part 1: Fly ash. SAI Global Limited.

AS 3582.2. (2001). Supplementary cementitious materials for use with Portland and blended cement Slag - Ground granulated iron blast-furnace. SAI Global Limited.

AS 3582.3. (2002). Supplementary cementitious materials for use with Portland and blended cement - Amorphous silica. SAI Global Limited.

AS 3583.9. (1991). Methods of test for supplementary cementitious materials for use with portland cement - Determination of magnesia content . SAI Global Limited.

AS 3582.2. (2001). Supplementary cementitious materials for use with portland and blended cement - Slag - Ground granulated iron blast-furnace . SAI Global Limited.

AS 2350.5. (2006). Methods of testing portland, blended and masonry cements - Determination of soundness. SAI Global Limited.

AS 1012.3.1. (2014). Methods of testing concrete - Determination of properties related to the consistency of concrete - Slump test. SAI Global Limited.

AS 1012.2. (2014). Methods of testing concrete - Preparing concrete mixes in the laboratory. SAI Global Limited.

AS 1012.9. (1999). Methods of testing concrete Determination of the compressive strength of concrete specimens. SAI Global Limited.

AS 1012.10. (2000). Methods of testing concrete Determination of indirect tensile strength of concrete cylinders. SAI Global Limited.

AS 1012.11. (2000b). Methods of testing concrete Determination of the modulus of rupture. SAI Global Limited.

AS 1012.21. (1999a). Methods of testing concrete Determination of water absorption and apparent volume of permeable voids in hardened concrete. SAI Global Limited.

AS 4439.3. (1997). Wastes, sediments and contaminated soils - Preparation of Lechates - Bottle Leaching Procedure. Australian Standard.

AS 3972. (2010). General purpose and blended cements. SAI Global Limited.

AS 2758.1. (2014a). Aggregates and rock for engineering purposes - Part 1: Concrete aggregates. SAI Global Limited.

AS 2350.3. (2006). Methods of testing portland, blended and masonry cements - Normal consistency. SAI Global Limited.

AS 2350.4. (2006). Methods of testing portland, blended and masonry cements - Methods of testing portland, blended and masonry cements - Setting time. SAI Global Limited.

AS 2350.12. (2006). Methods of testing portland, blended and masonry cements - Preparation of a standard mortar and moulding of specimens. SAI Global Limited.

AS 3583.4. (1991). Methods of test for supplementary cementitious materials for use with portland cement part 4 - determination of autoclave expansion. SAI Global Limited.

AS 3600. (2009). Concrete structures. SAI Global Limited.

ASTM C618-12a. (2012). Standard specification for Coal Fly Ash and Raw or Calcined Natural Pozzolan for Use in Concrete. ASTM International.

ASTM C150. (2012). Standard specification for Portland cement. ASTM International.

ASTM C618-08a. (2006). Standard specification for coal fly ash and raw or calcined natural pozzolan for use in concrete. ASTM International.

ASTM C150-97a. (1998). ASTM specification for Portland cement. ASTM International, 100 Barr Harbor Drive, West Conshohochen.

ASTM C618-98. (1999). ASTM specification for coal fly ash and raw or calcined natural pozzolan for use as a mineral admixture in concrete. ASTM International, 100 Barr Harbor Drive, West Conshohochen, PA.

ASTM C595. (2018). Standard specification for blended hydraulic cements.

ASTM C618. (2017a). Standard specification for coal fly ash and raw or calcined natural pozzolan for use in concrete.

ASTM C618. (2017a). Standard specification for coal fly ash and raw or calcined natural pozzolan for use in concrete.

ASTM C1240 (2015). Standard Specification for Silica Fume Used in Cementitious Mixtures.

ASTM C109. (2013). Standard Test Method for Compressive Strength of Hydraulic Cement Mortars (Using 2-in. or [50-mm] Cube Specimens). ASTM International.

ASTM C204-11. (2013). Standard Test Methods for Fineness of Hydraulic Cement by Air-Permeability Apparatus, ASTM International.

ASTM C1202-12. (2012). Standard Test Method for Electrical Indication of Concrete's Ability to Resist Chloride Ion Penetration, ASTM International.

ASTM C311. (2013). Standard Test Methods for Sampling and Testing Fly Ash or Natural Pozzolans for Use in Portland-Cement Concrete. ASTM International.

ASTM C494/C494M. (2008a). Standard Specification for Chemical Admixtures for Concrete

ASTM C1585. (2013). Standard Test Method for Measurement of Rate of Absorption of Water by Hydraulic-Cement Concretes.

ASTM C1437. (2015). Standard Test Method for Flow of Hydraulic Cement Mortar.

Atis, C.D., and Bilim, C. (2007). Wet and dry cured compressive strength of concrete containing ground granulated blast-furnace slag. Build. Environ. 42(8), 3060–3065.

Atul (2012). Use of Non-Conventional Material in Pavement. M. Tech Thesis submitted in SHIATS, Allahabad.

Babaiefar, S. (2007). The Durability Assessment of Concrete made with Rice Husk Ash (RHA) in Sulphate Environment (M.Sc. thesis). University of Guilan, Iran.

Barnett, S.J., Soutsos, M.N., Millard,S.G., Bungey, J.H. (2006). Strength development of mortars containing ground granulated blast-furnace slag: effect of curing temperature and determination of apparent activation energies, Cem. Concr. Res. 36, 434–440.

Babu, K.G., Kumar, V.S.R. (2000). Efficiency of GGBFS in concrete. Cem. Concr. Res., 30(7), 1031–1036.

Basheer, P.A.M., Gilleece, P.R.V., Long, A.E., McCarter, W.J. (2002). Monitoring electrical resistance of concretes containing alternative cementitious materials to assess their resistance to chloride penetration. Cem. Concr. Compos. 24(5), 437–449.

Behra, G.C., Mohanty, M., Bagh, S.R., Sarker I., and Singh, S. (2011). Slag as Coarse Aggregate and Its effect on Mechanical properties of concrete. International Journal of Earth Sciences and Engineering, 4(6), 899-902.

Bendapudi, S.C.K. (2011). Contribution of fly ash to the properties of mortar and

concrete. Int. J. Earth Sci. Eng. 04 (06 SPL), 1017-1023.

Bhanja, S., and Sengupta, B. (2005). Influence of silica fume on the tensile strength of concrete. Cement and concrete research, Jadavpur University Kolkata, West Bengal, India.

Bouikni, A., Swamy, R.N., Bali, A. (2009). Durability properties of concrete containing 50% and 65% slag. Construct. Build. Mater. 23(8), 2836–2845.

Brooks, J.J., Megat Johari, M.A., Mazloom, M. (2000). Effect of admixtures on the setting times of high-strength concrete. Cem. Concr. Compos., 22 (4), 293–301.

British Standards Institution. (1997b). BS 8110: Part I, Structural Use of Concrete: Code of Practice for Design and Construction.

Newman, J.B. and Choo, B.S. (2003). Advanced concrete technology. Constituent materials.

BS 1881-122. (2011). Testing concrete: Part 122, method for determination of water absorption.

BS EN 197-1. (2011). Cement. Composition, specifications and conformity criteria for common cements.

BS EN 1338. (2003). Concrete paving blocks. Requirements and test methods.

Butterworth (2003). Advanced concrete Technology, Constituent materials, Technology and Engineering.

Cement Concrete & Aggregates Australia. (2009). Chloride resistance of concrete. Retrieved from www.ccaa.com.au on 10 July 2016.

Cheron, M., Lardinois, C. (1968). In: Proceedings of the 5th International Congress on the Chemistry of Cement, Tokyo, vol. IV, 277–285.

Cheng, A., Huang, R., Wu, J.K., Chen, C.H. (2005). Influence of GGBFS on durability and corrosion behavior of reinforced concrete. Mater. Chem. Phys., 93, 404–411.

Chung, D.D.L. (2002). Review improving cement-based materials by using silica fume. Journal of material science, composite materials research laboratory, state university of New York at Buffalo, USA.

Chopra, D., Siddique, R., Kunal, M. (2015). Strength, permeability and microstructure of self-compacting concrete containing rice husk ash. Biosyst. Eng., 130, 72–80.

Chindaprasirta, P., Kanchandaa, P., Sathonsaowaphaka, A., Cao, H.T. (2007). Sulfate resistance of blended cements containing fly ash and rice husk ash. Constr. Build. Mater., 21 (6), 1356–1361.

Chengyou, Wu., Hongfa, Yu., Jinmei, D., and Zheng, L. (2014). Effects of Material Ratio, Fly Ash, and Citric Acid on Magnesium Oxysulfate Cement. ACI Materials Journal, 111(3), 291-297.

Coutinho, J. S. and Papadakis, V. G. (2011). Rice Husk Ash – Importance of Fineness for its Use as a Pozzolanic and Chloride-Resistant Material. International Conference on Durability of Materials and Components, Porto, Portugal.

CSA A3001-03. (2003). Cementitious materials for use in concrete, National standards of Canada.

Darwin, D., McCabe, S. L., Idun, E.K. and Schoenekase, S.P. (1992). Development length criteria: bars not confined by transverse reinforcement. ACI Struct J, 89(6), 709–20.

Daube, J., Bakker, R. (1986). Portland blast-furnace slag cement: a review. Blended Cement, ASTM-STP 897,5–14.

DAO-35 (1990). DENR administrative order no. 35 pursuant to provisions of Sec. 6 of PD 984 (Pollution Control Decree of 1976).

Dabai, M.U., Muhammad, C., Bagudo, B.U., Musa, A. (2009). Studies on the effect of rice husk ash as cement admixture. Nigerian J. Basic Appl. Sci., 17 (2), 252–256.

Deng, M., Cui, X., Liu, Y., and Tang, M. (1990). Expansive Mechanism of Magnesia as an Additive of Cement. Journal of Nanjing Institute of Chemical Technology, 12(4), 1-11.

Demotica, J.S., Amparado Jr. R. F., Malaluan, R.M., and Demayo, C. G. (2012). Characterization and leaching assessment of Ferronickel slag from a smelting plant in Iligan City. International Journal of Environmental Science and Development, 3(5), 470-474.

Dimitrioglou, N., Tsakiridis, P.E., Katsiotis, N.S. (2016). Production and Characterization of Concrete Paving Blocks Containing Ferronickel Slag as a Substitute for Aggregates. Waste Biomass Valor, 7, 941.

Duchesne, J., and Berubet, M.A. (1995). Effect of supplementary cementing materials on the composition of cement hydration products, Advn Cem Bas Mat, 2, 43-52.

Elahi, A., Basheer, P.A.M., Nanukuttan, S.V., Khan, Q.U.Z. (2010). Mechanical and durability properties of high performance concretes containing supplementary cementitious materials. Constr. Build. Mater., 24(3), 292–299.Escalante-Garcia, J., Erdogan O., Mustafa E. (2016). Utilization and efficiency of ground granulated blast furnace slag on concrete properties – A review. Constr. Build. Mater., 105, 423-434.

Feng, Q., Yamamichi, H., Shoya, M., Sugita, S. (2004). Study on the pozzolanic properties of rice husk ash by hydrochloric acid pretreatment. Cem. Concr. Res., 34 (3), 521–526.

Foong, K. Y., Alengaram, U. J., Jumaat, M. Z., and Mo, K. H. (2015). Enhancement of the mechanical properties of lightweight oil palm shell concrete using rice husk ash and manufactured sand. Journal of Zhejiang University-SCIENCE A (Applied Physics & Engineering, 16 (1), 59–69.

Ganeshbabu, K., and Suryaprakash, P.V. (1995). Efficiency of Silica Fume in Concrete. Cement and Concrete Research, 25(6), 1273-1283.

Gafoori, N. and Diawareand, H. (2007). Strength and Wear Resistance of Sand -Replaced Silica Fume Concrete, ACI Materials Journal, 104(2), 206-214.

Ganesan, K., Rajagopal, K., & Thangavel, K. (2007). Evaluation of bagasse ash as supplementary cementitious material. Cement and Concrete Composites, 29(6), 515-524.

Guneyisi, E., and Gesoglu, M. (2008). A study on durability properties of high-performance concretes incorporating high replacement levels of slag, Mater. Struct. 41, 479–493.

Hakkari, S. (2011). Effects of mineral admixture on concrete. http://www.academia.edu/1049451/Effects_Of_Mineral_Admixture_On_Concrete.

Hanson. (2010). REGEN The Strength Behind Sustainable Concrete. Hanson Cement, Heidelberg cement group, London.

Habeeb, G.A., Fayyadh, M.M. (2009). Rice husk ash concrete: the effect of RHA average particle size on mechanical properties and drying shrinkage. Aust. J. Basic Appl. Sci., 3 (3), 1616–1622.

Habeeb, G.A., Mahmud, H.B. (2010). Study on properties of rice husk ash and its use as cement replacement material. Mater. Res., 13 (2), 185–190.

Henrist, C., Mathieu, J.P., Vogels, C., Rulmont, A., Cloots, R. (2003). Morphological study of magnesium hydroxide nanoparticles precipitated in dilute aqueous solution. Journal of Crystal Growth, 249, 321–330.Helmuth, R. (1987). Fly Ash in Cement and Concrete, Portland Cement Association, Skokie, 36-61.

Hemmings, R., and Berry, E. (1988). On the glass in coal fly ashes: recent advances. In: Presented at the MRS Symposium, Pittsburg,USA, p. 3.

Hemalatha, T., and Ramaswamy, A. (2017). A review on fly ash characteristics – Towards promoting high volume utilization in developing sustainable concrete, Journal of Cleaner Production, Volume 147, 546-559.

Hui-sheng, S., Bi-wan, X., Xiao-chen, Z. (2009). Influence of mineral admixtures on compressive strength, gas permeability and carbonation of high performance concrete. Construct. Build.Mater., 23(5), 1980–1985.

Hwang, C. L., and Chandra, S. (2016). The Use of Rice Husk Ash in Concrete.

Hwang, C.L., Bui, L.A., Chun-Tsum, C. (2011). Effect of rice husk ash on the strength and durability characteristics of Concrete. Constr. Build. Mater., 25 (9), 3768–3772.

http://www.ecocem.ie. Concrete mix design using GGBFS. Ecocem Ireland Ltd. Dublin.

Karim, M.R., Zain, M.F.M., Jamil, M., Lai, F.C. (2013). Fabrication of a non-cement composite binder by using slag, palm oil fuel ash and rice husk ash with sodium hydroxide as an activator. Constr. Build. Mater., 49, 894–902.

Kartini, K., Mahmud, H.B., Hamidah, M.S., (2010). Absorption and permeability performance of Selangor rice husk ash blended grade 30 concrete. J. Eng. Sci. Technol., 5 (1), 1–16.

Katkhuda,H., Hanayneh, B., Shatarat, N. (2009). Influence of Silica Fume on High Strength lightweight Concrete. World Academy of Science, Engineering and Technology, 34, 781-788.

Kadri, E.H. and Duval, R. (1998). Influence of Silica Fume on the Workability and Compressive Strength of High Performance Concrete. Cement and Concrete Research 28(4) , 533-547.

Katsiotis, N.S., Tsakiridis, P.E., Velissariou, D. (2015). Utilization of Ferronickel Slag as Additive in Portland Cement: A Hydration Leaching Study. Waste Biomass Valor, 6, 177.

Khatib, J.M., Hibbert, J.J. (2005). Selected engineering properties of concrete incorporating slag and metakaolin, Constr. Build. Mater., 19 (6), 460–472.

Khan, M.I. and Siddique, R. (2011). Utilization of silica fume in concrete: Review of durability properties. Construction and Building materials, 57(30-35).

Khan, S.M., and Ayers, M.E. (1995). Minimum Length of Curing of Silica Fume Concrete. Journal of Materials in Civil Engineering, 7(3), 134-139.

Khassaf, S.I., Jasim, A.T., Mahdi, F.K. (2014b). Investigation the properties of concrete containing rice husk ash to reduction the seepage in canals. Int. J. Sci. Technol. Res., 3 (4), 348–354.

Kobayakawa, M., Hwang, K., Hanehara, S., Tomosawa, F. (1998). Influence of severalfactors on pozzolanic reaction of fly ash. Summ. Tech. Pap. Annu. Meet. Archit. Inst. Jpn A-1, 633-634.

Köksal, F., and Sahin, Y. (2008). Combined effect of silica fume and steel fibre on the mechanical properties of high strength concretes. Construction and Building Materials, 22(8), 1874–80.

Kumar, L., Li, W.Z., Vannoy, C.H., Leblank, R.M., Wang, D.Z. (2009). Synthesis, characterization and optical properties of $Mg(OH)_2$ micro-/nanostructure and its conversion to MgO. Ceramics International, 35, 3355–3364.

Lamond, J. F., Pielert, J. H.(2006). Expansive Mechanism of Magnesia as an Additive of Cement and Concrete-making Materials, ASTM International, 169(4).

Lam, L.,Wong, Y., Poon, C. (1998). Effect of fly ash and silica fume on compressive and fracture behaviors of concrete. Cem. Concr. Res. 28, 271-283.

Le, H.T., Nguyen, S.T., Ludwig, H. (2014). A study on high performance fine-grained concrete containing rice husk ash. Int. J. Concr. Struct. Mater., 8 (4), 301–307.

Liu, Y., Zhang, K., Zhao, E.F.H., and Liu, F. (2017). Synthesis of geopolymer composites from a mixture of ferronickel slag and fly ash. IOP Conf. Series: Materials Science and Engineering, 182 012038.

Lingling, X., and Min, D. (2005). Dolomite used as raw material to produce MgO-based expansive agent, Cement and Concrete Research, 35, 1480-1485.

Liwu M., Panesar, D.K. (2013). Accelerated carbonation–A potential approach to sequester CO2 in cement paste containing slag and reactive MgO. Cement & Concrete Composites, 43, 69–77.

Liwu, M., and Daman, K. P. (2012). Effects of accelerated carbonation on the microstructure of Portland cement pastes containing reactive MgO. Cement and Concrete Research, 42, 769-777.

Li, G., Zhao, X. (2003). Properties of concrete incorporating fly ash and ground granulated blastfurnace slag. Cem. Concr. Compos., 25(3), 293–299.

Luo, R., Cai, Y., Wang, C., Huang, X. (2003). Study of chloride binding and diffusion in GGBFS concrete. Cem. Concr. Res. 33(1), 1–7.

Malhotra, V. (1986). Superplasticized fly ash concrete for structural applications. Concr. Int. 8, 28-31.

Malhotra, V.M. (1990). Durability of concrete incorporating high-volume of low-calcium (ASTM Class F) fly ash. Cem. Concr. Compos. 12, 271-277.

Marthong, C. (2012). Effect of rice husk ash (RHA) as partial replacement of cement on concrete properties. Int. J. Eng. Res. Technol., 1 (6), 1–8.

Mahmud, H.B., Bahri, S., Yee, Y.W., Yeap, Y.Y. (2016). Effect of rice husk ash on the strength and durability of high strength performance concrete. World Acad. Sci. Eng. Technol., 10 (3), 375–380.

Mahmud, H.B., Malik, M.F.A., Kahar, R.A., Zain, M.F.M., Raman, S. N. (2009). Mechanical properties and durability of normal and water reduced high strength 60 grade concrete containing rice husk ash. J. Adv. Concr. Technol., 7 (1), 21–30.

Malhotra, V.M. and Metha, P.K. (2005). High-Performance High-Volume Fly Ash Concrete: Materials, Mixture Proportioning, Properties, Construction practice, and Case Histories.

Mehta, P.K. (1977). Properties of Blended Cements Made from Rice Husk Ash. ACI Journal, 440-442.

Megat Johari, M.A., Brooks, J.J., Kabir, S., Rivard, P. (2011). Influence of supplementary cementitious materials on engineering properties of high strength concrete. Constr. Build. Mater, 25, 2639–2648.

Mo, L., Deng, M. (2010a). Effects of calcination condition on expansion property of MgO-type expansive agent used in cement-based materials, Cement and Concrete Research, 40, 437-446.

Mo, L., Deng, M. (2010b). Potential Approach to Evaluating Soundness of Concrete Containing MgO-Based Expansive Agent, ACI Materials Journal, 197(2), 99-105.

Mo, L., Deng, M., Wang, A. (2012). Effects of MgO-based expansive additive on compensating the shrinkage of cement paste under non-wet curing conditions. Cement & Concrete Composites, 34, 377–383.

Mo, L., Deng, M., Tang, M. (2010). Potential approach to evaluating soundness of concrete containing MgO-Based expansive agent. ACI Materials Journal, 107(2), 9-105.

Mo, L. and Panesar, D.K. (2013). Accelerated carbonation - A potential approach to sequester CO2 in cement paste containing slag and reactive MgO. Cem. Concr. Com., 43, 69-77.

Muhl, A. (2003). The use of supplementary cementing materials in residential concrete, Master's thesis, University of Toronto.

Narmluk, M., Nawa, T. (2011). Effect of fly ash on the kinetics of Portland cement hydration at different curing temperatures. Cem. Concr. Res. 41, 579-589.

Nader, G., and Hamidou, D. (2007). Strength and Wear Resistance of Sand -Replaced Silica Fume Concrete. ACI Materials Journal, 104(2), 206-214.

Nair, D., Fraaij, A., Klaassen, A., and Kentgens, A. (2008). A structural investigation relating to the pozzolanic activity of rice husk ashes. Cement and Concrete Research (Elmsford), 38(6), 861-869.

Newman, J.B., Choo, B. S. (2003). Advanced concrete technology, Constituent materials.

Neville, A. M. (1996). Properties of concrete (4th and Final ed.). New York, USA: John Wiley & Sons, Inc.

Nguyen, V.T., Van Ye, G., Breugel, K., Fraaij, A.L.A., Bui, D.D. (2011a). The study of using rice husk ash to produce ultra-high performance concrete. Constr. Build. Mater., 25 (4), 2030–2035.

Nguyen, V.T. (2011). Rice Husk Ash as Mineral Admixture for Ultra Performance Concrete (Ph.D thesis). Delft University of Technology, Delft.

Nkinamubanzi, P.C., Baalbaki, M., Bickley, J., Aitcin, P.C. (1998). The use of slag for making high performance concrete, in: Sixth NCB International Seminar on Cement and Building Materials, XIII, NCB, New Delhi, 13–39.

Sharp, J. (1998). Effect of temperature on the hydration of the main clinker phases in Portland cements: Part II, blended cements. Cem. Concr. Res. 28, 1259-1274.

Snelson, D., Wild, S. (2011). Setting times of Portland cement–metakaolin–fly ash blends. Journal of Civil Engineering and Management, 17(1), 55-62.

Olorunsogo, F.T. (1998). Particle size distribution of GGBFS and bleeding characteristics of slag cement mortars. Cem. Concr. Res. 28(6), 907–919.

Oner, A., Akyuz, S. (2007). An experimental study on optimum usage of GGBFS for the compressive strength of concrete. Cem. Concr. Compos. 29(6), 505–514.

Orangun, C.O., Jirsa, I.O. and Breen, J.E. (1977). A reevaluation of test data on development length and splices. ACI Journal, Proceedings, 74(3), 114–22.

Özbay, E., Erdemir, M., and Durmuş, H.I. (2016). Utilization and efficiency of ground granulated blast furnace slag on concrete properties – A review, In Construction and Building Materials, 105, 423-434.

Pappadakis, V.G., Antiohos, S., and Tsimas, S. (2002). Supplementary cementing materials in concrete: Part II: A fundamental estimation of the efficiency factor, Cement and Concrete Research, 32(10), 1533-1538.

Pawade Prashant, Y., Nagarnaik, P.B., Pande, A.M. (2011) Influence of Silica fume in enhancement of compressive strength, flexural strength of steel fibers concrete and their relationship. International Journal of Civil and Structural Engineering, 2(1), 43-55.

Peiwei, G., Xiaolin, L., Shaochun, J., Hui, Z., and Chunxing, G., (2008). Using a new composite expansive material to decrease deformation and fracture of concrete, Materials Letters, 62, 106-108.

Poon, C., Lam, L., Wong, Y. (2000). A study on high strength concrete prepared with large volumes of low calcium fly ash. Cem. Concr. Res. 30, 447-455.

Poon, C.S., Kou, S.C., Lam L. (2006). Compressive strength, chloride diffusivity and porestructure of high performance metakaolin and silica fume concrete. Constr. Build. Mater., 20(10), 858–865.

Poon, C.S., Wong, Y., Lam, L. (1997). The influence of different curing conditions on the pore structure and related properties of fly-ash cement pastes and mortars. Constr. Build. Mater. 11, 383-393.

Ramakrishnan, V., and Srinivasan, V. (1982). Silica Fume in Fibre Reinforced Concrete. Indian Concrete Journal, 326-334.

Rashid, M.H. (2016). Strength behavior of cement mortar assimilating rice husk ash. Int. J. Adv. Agric. Environ. Eng., 3 (2), 288–293.

Roy, D.K.S and Sil, A. (2012). Effect of Partial Replacement of Cement by Silica Fume on Hardened Concrete. International Journal of Emerging Technology and Advanced Engineering, 2(8), 472-475.

Sakr, K. (2006). Effects of silica fume and Rice husk Ash on the Properties of Heavy Weight Concrete. Journal of Materials in Civil Engineering, 18(3), ASCE, 367 -376.

Safiuddin, M. (2008). Development of Self-consolidating High Performance Concrete Incorporating Rice Husk Ash (Ph.D thesis). University of Waterloo.

Safiuddin, M., West, J.S., Soudki, K.A. (2011). Flowing ability of the mortars formulated from self-compacting concretes incorporating rice husk ash. Constr. Build. Mater., 25 (2), 973–978.

Salas, A., Delvasto, S., Gutierrez, R.M., and Lange D. (2009). Comparison of two processes for treating rice husk ash for use in high performance concrete. Cement and Concrete Research, 39(9), 773–778.

Sakoi Y., Minoru, Aba., Tsukinaga Y., and Nagataki S. (2013). Properties of Concrete used in ferronickel Slag Aggregate. Third international conference on sustainable construction materials and technologies. August 18-21, Kyoto research park, Kyoto, Japan.

Sato, T., Watanabe, K., Ota, A., Minoru, Aba., and Sakoi, S. (2011). Influence of excessive bleeding on frost succeptibility of concrete incorporating ferronickel slag as aggregate. 36th Conference on our World in concrete & structures, Singapore, August 14-16.

Saha, A.K. and Sarker, P.K. (2017a). Compressive strength of mortar containing ferronickel slag as replacement of natural sand. Procedia engineering, 171. 689-694.

Saha, A.K. and Sarker, P.K. (2016). Expansion due to alkali-silica reaction of ferronickel slag fine aggregate in OPC and blended cement mortars. Construction and Building Materials, 123, 135–142.

Saha, A.K. and Sarker, P.K. (2017b). Sorptivity and chloride permeability of concrete using ferronickel slag as fine aggregate. Concrete 2017, Advances in Concrete materials and Structures, 22-25 October 2017, Adelaide, South Australia.

Saha, A.K. and Sarker, P.K. (2017c). Sustainable use of ferronickel slag fine aggregate and fly ash in structural concrete: Mechanical properties and leaching study. Journal of Cleaner Production, 162, 438-448.

Scheetz, B.E. and Earle, R. (1998). Current Opinion in Solid State & Material Science, 3, 510-520.

Shariq, M., Prasad, J. and Abbas, H. (2016). Creep and drying shrinkage of concrete containing GGBFS. Cem. Concr. Compos., 68, 35-45.

Sivasundaram, V., Malhotra, V.M. (1992). Properties of concrete incorporating low quantity of cement and high volumes of ground granulated slag, ACI Mater. J., 89, 554–563.

Siddique, R., and Khan, M.I. (2011). Supplementary cementing materials, Springer-Verlag Berlin Heidelberg.

Singha, D.K.R., and Amitava, S. (2012). Effect of Partial Replacement of Cement by Silica Fume on Hardened Concrete. International Journal of Emerging Technology and Advanced Engineering, 2(8), 472-475.

Soutsos, M.N. (2004). Using recycled demolition waste in concrete building blocks. Proceedings – Institution of Civil Engineers Engineering Sustainability, 157 (3), 139–148.

Sua-iam, G., Makul, N. (2013). Use of unprocessed rice husk ash and pulverized fuel ash in the production of self-compacting concrete. IERI Procedia 5, 298–303.

Tasong, W.A., Wild, S., Tilley, R.J.D. (1999). Mechanism by which ground granulated blast furnace slag prevents sulfate attack of lime stabilized kaolinite. Cem. Concr. Res. 29(7), 975–982.

Tanyildizi, H., Coskun, A. (2008). Performance of lightweight concrete with silica fume after high temperature. Construction and Building Materials, 22(10), 2124–2129.

Talsania1, S., Pitroda, J., Vyas, C.M. (2015). Effect of rice husk ash on properties of pervious concrete. Int. J. Adv. Eng. Res. Stud., 4 (2), 296–299.

Tanijaya, J., and Hardjito, D. (2007). The short-term properties of nickel slag aggregate high strength concrete. Proceedings of the conference on sustainable building south-east Asia (SB07SEA), 337-343.

Tokuhashi, K., Shoya, M., Aba, M., and Sugita, S. (2001). Application of slag fine aggregate to produce self-compacting concrete. 26th Conference on our World in concrete & structures, Singapore, August 27-28.

US EPA 1311 (1992). Toxicity characteristics leaching procedure (TCLP).

VicRoads (2007). Test methods for the assessment of durability of concrete- Technical Note (TN 89). Melbourne: VicRoads.

Vinothan, K.G., Baskar, G. (2015). Study of structural behaviour on pozzolanic material (Rice Husk). Int. J. Civ. Eng. Technol., 6 (9), 31–46.

Wan, H., Shui, Z., Lin, Z. (2004). Analysis of geometric characteristics of GGBFS particles and their influences on cement properties. Cem. Concr. Res. 34(1), 133–137.

Wainwright, P.J., Ait-Aider, H.: The influence of cement source and slag additions on the bleeding of concrete. Cem. Concr. Res. 25(7), 1445–1456 (1995).

Wainwright, P.J., Rey, N. (2000). The influence of ground granulated blast furnace slag (GGBFS) additions and time delay on the bleeding of concrete. Cem. Concr. Compos. 22(4), 253–257.

Wan, H., Shui, Z., Lin, Z. (2004). Analysis of geometric characteristics of GGBFS particles and their influences on cement properties. Cem. Concr. Res. 34(1), 133–137.

Wu, X.F., Hu, G.S., Wang, B.B., Yang, Y.F. (2008). Synthesis and characterization of superfine magnesium hydroxide with monodispersity. Journal of Crystal Growth, 310, 457–461.

Xie, Y., Liu, B., Yin, J., & Zhou, S. (2002). Optimum mix parameters of high-strength self-compacting concrete with ultrapulverized fly ash. Cement and Concrete Research, 32(3), 477-480.

Yim, H.J., Kim, J.H., Han, S.H. and Kwak, H.G. (2015). Influence of Portland cement and ground-granulated blast-furnace slag on bleeding of fresh mix. Constr. Build. Mater.,80, 132-140.

Yogendran, Y., Langan, B.W., Haque, M.N., Ward, M.A. (1987). Silica fume in High Strength Concrete. ACI Materials Journal, 84(2), 124-129.

Yuan, M., and Tang, M. (1984). Mechanism of the Autogeneous Expansion of the Concrete of Changbaishan Dam in Jilin Province, Journal of Nanjing Institute of Chemical Technology, 2, 38-45.

Yu, J.C., Xu, A., Zhang, L., Song, R., Wu, L. (2004). Synthesis and Characterization of Porous Magnesium Hydroxide and Oxide Nanoplates. J. Phys. Chem., 108, 64-70.

Zhang, M. H., Lastra, R., & Malhotra, V. M. (1996). Rice-husk ash paste and concrete: Some aspects of hydration and the microstructure of the interfacial zone between the aggregate and paste. Cement and Concrete Research, 26(6), 963-977.

"Every reasonable effort has been made to acknowledge the owners of copyright materials. I would be pleased to hear from any copyright owner who has been omitted or incorrectly acknowledged."

APPENDICES

APPENDIX A: Material properties

Table A.1 Sieve analysis of fine and coarse aggregate

Fine aggregate				Coarse aggregate			
Sieve size (mm)	Cumulative % retained	Cumulative % passing	FM	Sieve size (mm)	Cumulative % retained	Cumulative % passing	FM
6.75	0	100		38	0	100	
4.75	0	100		19	60	40	
2.36	0	100		9.5	100	0	
1.18	2	98		4.75	100	0	
0.6	13	87	1.94	2.36	100	0	7.6
0.3	81	19		1.18	100	0	
0.15	98	2		0.6	100	0	
0.075	100	0		0.3	100	0	
-	-	-		0.15	100	0	

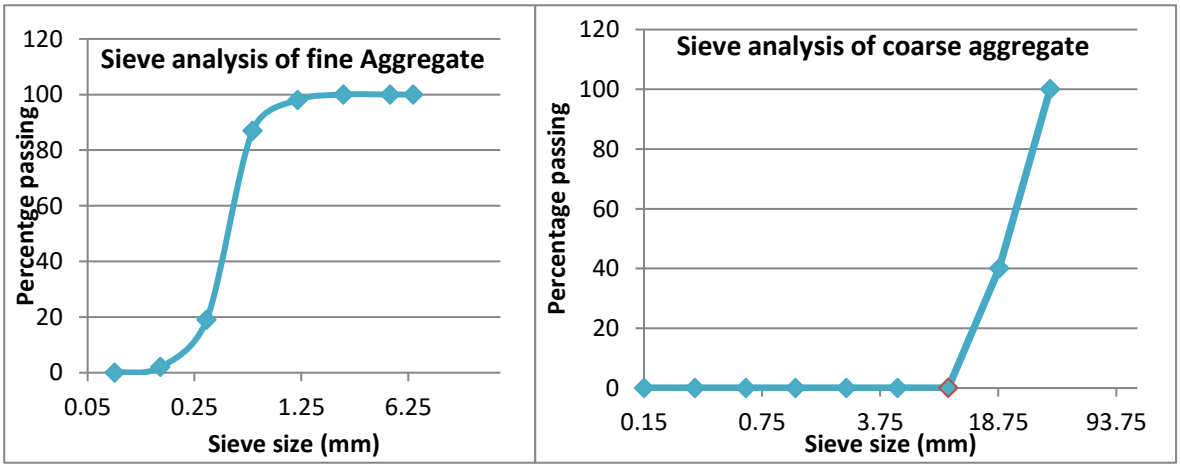

Figure A.1 Sieve analysis of aggregates

APPENDIX B: Fresh and Early Age Properties

Figure B.1 Flow test of mortar

Table B.1 Normal consistency and setting time

Composition	Water for Normal Consistency (%)	Initial setting time (min)	Final setting time (min)
100C	30	130	190
20FNS 80C	29	130	200
30FNS 70C	28	130	200
40FNS 60C	27.5	140	200
50FNS 50C	27	130	200
40FNS 10GGBFS 50C	29	150	220
65FNS 35C	27	150	230

Table B.2 Flow of mortar

Mix Composition		Flow (%)
Cement	100%	70%
FNS	20%	75%
	30%	77%
	40%	78%
	50%	80%
GGBFS	20%	60%
	30%	62%
	40%	64%
	50%	65%
FA	20%	70%
	30%	80%
	40%	81%
	50%	83%

Table B.3 Le-Chatelier expansions of FNS and cement paste

Composition	Expansion (%)
100C	1.0
20FNS 80C	0.75
30FNS 70C	0.58
40FNS 60C	0.45
50FNS 50C	0.49
65FNS 35C	0.42

Table B.4 Le-Chatelier expansions of different SCM

Composition	Expansion (%)
40FNS 60C	0.45
40FA 60C	0.58
40FA 60GGBFS	0.42

Table B.5 Le-Chatelier expansions of FNS and cement paste containing MgO

Composition	MgO (%)	Expansion (%)
50FNS 50C	5.0	0.75
50FNS 50C	10.0	1.1
100C	5.0	1.9
100C	10.0	3.1

Table B.6 Expansion by accelerated heat and ambient curing

Composition	MgO (%)	Expansion (%)	
		Ambient curing	Heat cured at $80\ ^{o}C$
Control (100C)	0	0.33	0.37
30FNS 70C	0	0.32	0.35
50FNS 50C	0	0.32	0.35
100C	5.0	0.46	0.51
100C	10.0	0.62	0.69

APPENDIX C: Strength and durability properties

Table C.1 Compressive strength of mortar specimens

Composition	Mean compressive strength (MPa)			
	3 Days	14 Days	28 Days	90 Days
0FNS 100C	23	33	35	37
20FNS 80C	16	24	29	35
30FNS 70C	16	23	28	32
40FNS 60C	12	19	24	27
50FNS 50C	11	17	23	25

Table C.2 Slump and compressive strength of concrete

Composition	Slump (mm)	Mean compressive strength (MPa)		
		7 Days	28 Days	90 Days
0FNS 100C	160	61	73	76
20FNS 80C	80	57	66	75
30FNS 70C	100	43	55	67
40FNS 60C	110	41	54	56
40FNS 10GGBFS 50C	75	36	50	54
50FNS 50C	80	32	51	57
65FNS 35C	130	19	37	43

Table C.3 Drying shrinkage of concrete specimens

Control (100C)		20FNS 80C		30FNS 70C		40FNS 60C		50FNS 50C		65FNS 35C		40 FNS 10 GGBFS 50C	
Days	Drying Shrinkage (10^{-6})	Days	Drying Shrinkage (10^{-6})	Days	Drying Shrinkage (10^{-6})	Days	Drying Shrinkage (10^{-6})	Days	Drying Shrinkage (10^{-6})	Days	Drying Shrinkage (10^{-6})	Days	Drying Shrinkage (10^{-6})
0	0	0	0	0	0	0	0	0	0	0	0	0	0
7	52	7	156	7	228	7	104	7	140	7	238	7	52
14	118	15	160	15	234	14	134	14	260	15	366	14	224
21	164	22	175	22	253	21	128	21	274	22	470	21	300

28	212	29	178	29	280	28	174	28	326	29	482	28	322
35	222	36	185	36	372	35	262	36	368	35	496	35	330
42	244	44	194	44	304	42	324	43	418	42	528	43	384
50	284	53	205	53	320	50	362	56	436	49	540	50	424
57	332	60	210	60	333	57	420	63	456	56	552	63	422
64	333	67	220	67	346	64	420	70	460	63	542	70	416
70	334	73	222	73	359	70	418	77	466	71	536	77	440
77	342	80	224	80	373	77	444	84	480	78	550	84	456
84	345	87	232	87	379	84	450	92	492	85	586	91	454
91	348	94	244	94	384	91	454	99	490	92	580	99	450
98	378	101	252	101	408	98	470	106	496	99	582	106	452
106	396	109	270	109	415	106	488	113	489	106	575	113	456
113	394	116	285	116	420	113	490	120	480	113	578	120	460
120	392	123	289	123	423	120	488	127	482	120	572	127	458
127	390	130	300	130	416	127	489	134	470	127	569	134	462
134	396	137	315	137	400	134	480	141	475	134	566	141	468
141	389	145	322	145	408	141	485	148	476	145	568	148	460
148	398	152	332	152	394	148	472	155	465	152	560	155	465
155	395	159	330	159	401	155	474	166	462	159	551	162	470
162	392	166	332	166	410	162	465	173	470	166	545	173	474
169	382	173	340	173	419	169	450	180	466	173	540	180	478
180	378	180	349	180	423	180	452	186	462	180	534	186	474
186	381	186	365	186	429	186	452	201	471	186	550	201	466
201	375	201	360	201	414	201	455	216	474	201	555	216	468
216	372	216	375	216	409	216	458	231	479	216	565	231	471
231	385	231	380	231	403	231	464	245	482	231	580	245	476
245	393	245	371	245	394	245	471	260	484	245	595	260	480
260	406	260	365	260	399	260	478	275	504	260	576	275	484
275	420	275	368	275	406	275	495	280	499	275	605	280	490
280	398	280	365	280	398	280	475	305	510	280	586	305	510
305	414	305	370	305	410	305	498	320	492	305	580	320	480
320	384	320	374	320	392	320	465	335	502	320	594	335	485
335	375	335	379	335	396	335	468	350	526	335	603	350	482
350	386	350	378	350	405	350	462	365	532	350	610	365	500
365	384	365	371	365	393	365	470	380	544	365	626	380	524
380	404	380	379	380	395	380	478	396	550	380	629	396	530
396	420	396	365	396	388	396	506	412	532	396	636	412	534
412	426	412	359	412	390	412	510	427	562	412	645	427	526
427	414	427	351	427	385	427	518	457	554	427	660	457	530
457	420	457	357	457	383	457	520	487	540	457	656	487	529
487	415	487	345	487	395	487	519	517	549	487	651	517	540
517	410	517	340	517	380	517	509	547	556	517	655	547	544

547	396	547	331	547	385	547	502	577	560	547	640	577	541
577	398	577	325	577	374	577	491	607	550	577	634	607	536
607	380	607	330	607	383	607	488	637	536	607	643	637	539
637	375	637	310	637	370	637	494	667	531	637	646	667	543
667	349	667	305	667	375	667	499	697	539	667	654	697	544
697	354	697	293	697	364	697	471	727	544	697	660	727	554
727	334	727	299	727	370	727	464	757	541	727	635	757	559
757	319	757	295	757	361	757	473	787	537	757	630	787	553
787	308	787	319	787	355	787	466	817	533	787	633	817	549
817	325	817	329	817	349	817	450	847	528	817	625	847	540
847	331	847	323	847	359	847	459	877	535	847	610	877	545
877	327	877	315	877	364	877	446	890	524	877	616	890	542
897	312	898	330	898	353	897	454	950	530	898	620	950	540
957	318	958	325	958	360	957	449	1010	522	958	618	1010	543
1017	330	1018	315	1018	365	1017	445	1070	528	1018	624	1070	550
1077	322	1078	320	1078	368	1077	435	1130	534	1078	627	1130	538
1137	317	1138	318	1138	375	1137	434	1190	533	1138	615	1190	544
1197	325	1198	328	1198	372	1197	439	1250	520	1198	610	1250	551
1257	315	1258	310	1258	380	1257	448	1310	518	1258	619	1310	549
1317	320	1318	305	1318	382	1317	438	1369	496	1318	623	1369	534
1338	314	1378	300	1378	394	1338	430	1471	475	1378	618	1471	510
1440	320	1480	330	1480	400	1440	435	1563	436	1480	625	1563	498
1532	326	1572	352	1572	396	1532	440	1688	445	1572	640	1688	515
1657	320	1697	325	1697	385	1657	455	1772	422	1697	655	1776	506
1780	304	1761	360	1761	410	1780	448			1765	648		

Table C.4 Water absorption and AVPV

Composition	Immersed water absorption Ai (%)		Boiled water absorption Ab (%)		AVPV (%)	
	28 Days	90 Days	28 Days	90 Days	28 Days	90 Days
Control (100C)	3.29	3.65	3.33	3.39	8.7	8.14
20FNS 80C	3.67	3.68	3.81	3.83	8.87	8.61
30FNS 70C	4.12	4.17	3.61	3.64	8.99	8.72
40FNS 60C	3.75	3.72	3.84	3.9	8.89	9.23
40FNS 10GGBFS 50C	3.69	3.63	3.75	3.76	8.75	9.02
50FNS 50C	3.84	3.78	3.72	3.75	9.04	8.95
65FNS 35C	4.1	4.11	4.06	4.03	9.65	9.6

Table C.5 Sorptivity

Composition	Sorptivity	
	28 Days	90 Days
Control	0.0083	0.0074
20 FNS 80C	0.0087	0.0069
30 FNS 70C	0.0088	0.0073
40 FNS 60C	0.0083	0.0066
40 FNS 10GGBFS 50C	0.0082	0.0061
50 FNS 50C	0.0073	0.0065
65 FNS 35C	0.0053	0.0062

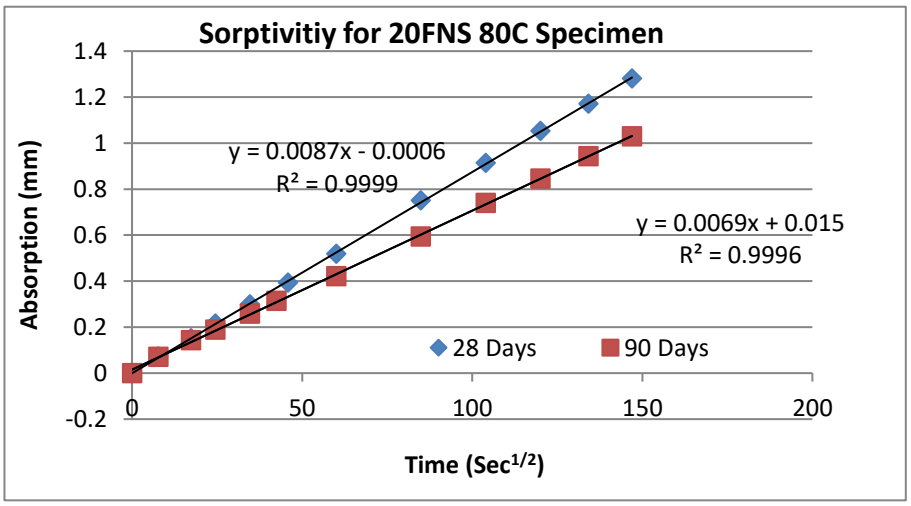

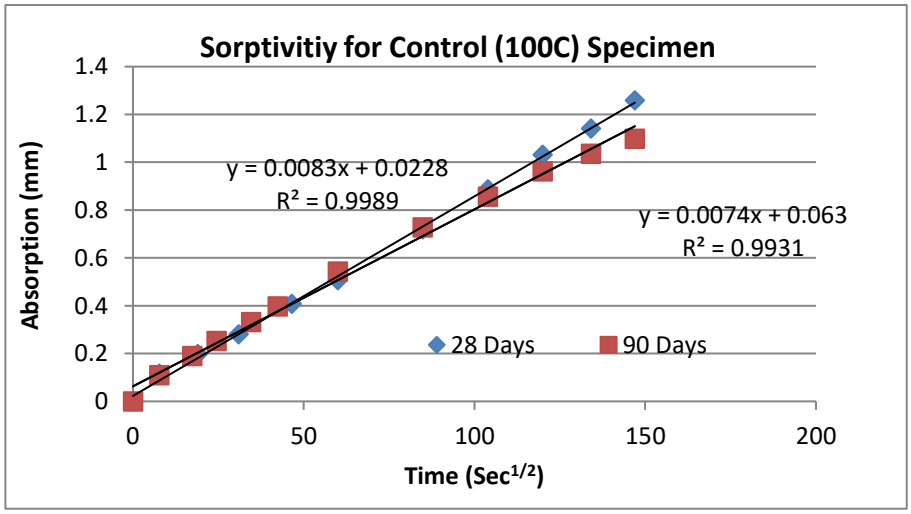

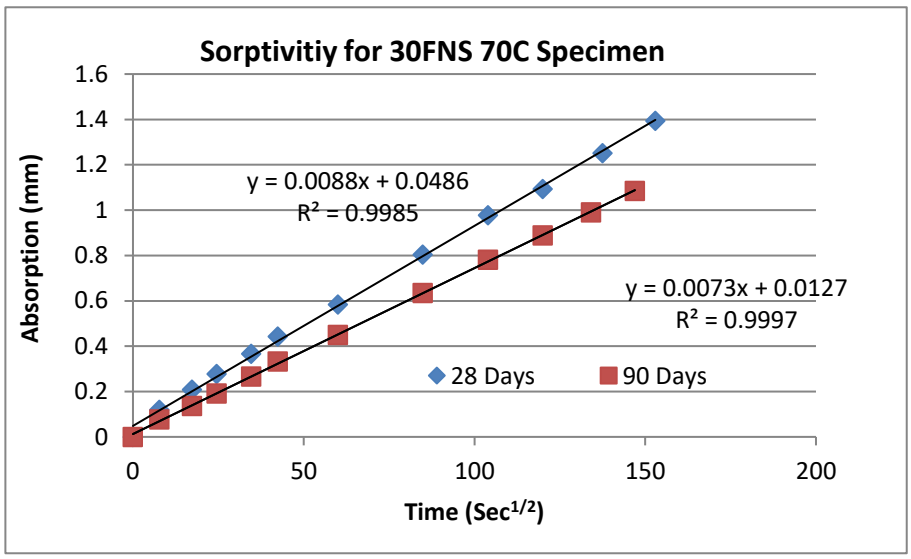
Sorptivitiy for 30FNS 70C Specimen
Absorption (mm)
1.6
1.4
1.2
1
0.8
0.6
0.4
0.2
0
y = 0.0088x + 0.0486
R² = 0.9985
y = 0.0073x + 0.0127
R² = 0.9997
28 Days
90 Days
0
50
100
150
200
Time (Sec1/2)

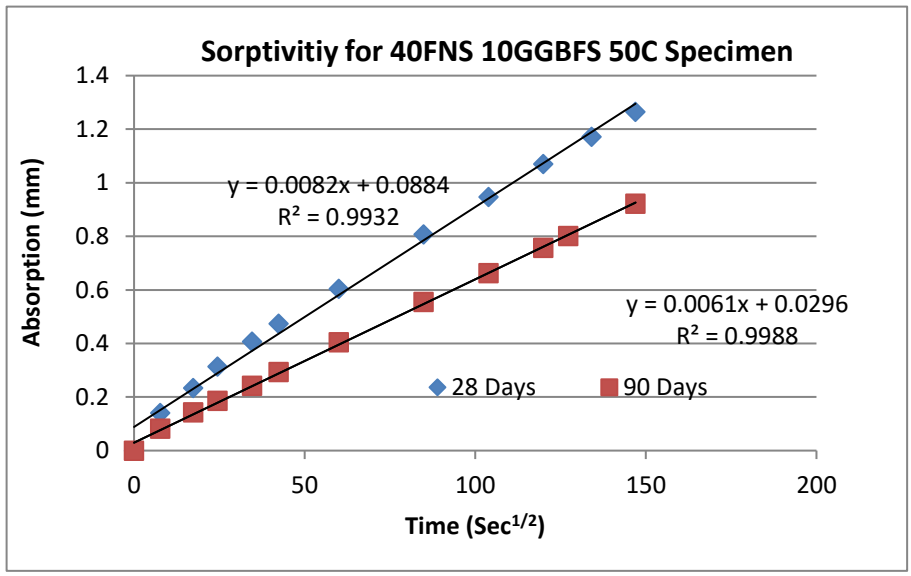
Sorptivitiy for 40FNS 10GGBFS 50C Specimen
Absorption (mm)
1.4
1.2
1
0.8
0.6
0.4
0.2
0
y = 0.0082x + 0.0884
R² = 0.9932
y = 0.0061x + 0.0296
R² = 0.9988
28 Days
90 Days
0
50
100
150
200
Time (Sec1/2)

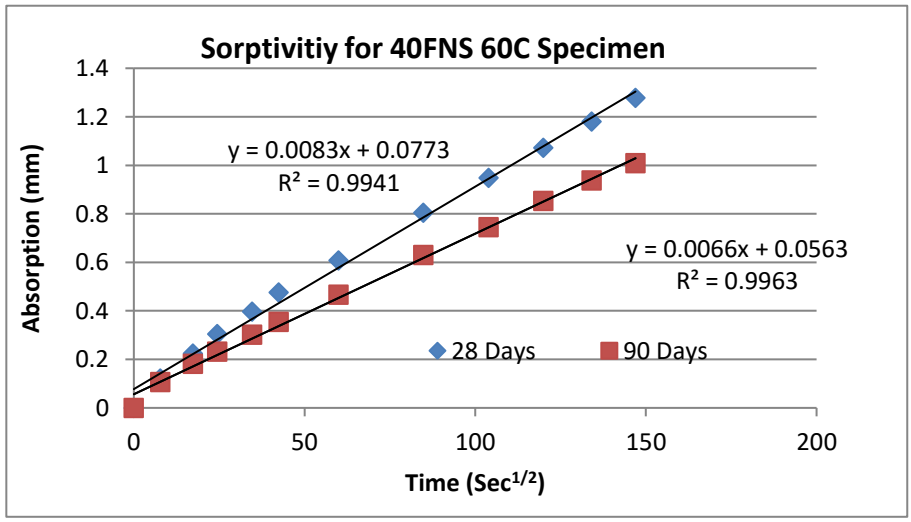
Sorptivitiy for 40FNS 60C Specimen
Absorption (mm)
1.4
1.2
1
0.8
0.6
0.4
0.2
0
y = 0.0083x + 0.0773
R² = 0.9941
y = 0.0066x + 0.0563
R² = 0.9963
28 Days
90 Days
0
50
100
150
200
Time (Sec1/2)

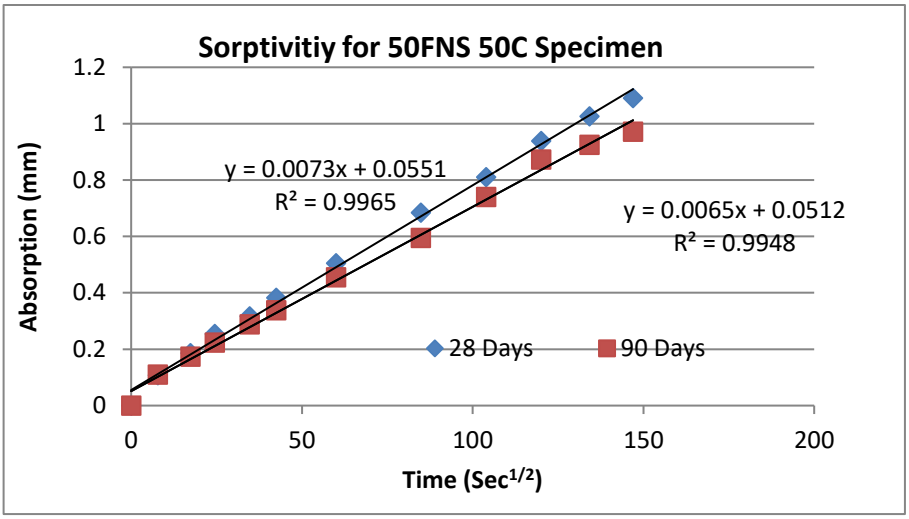

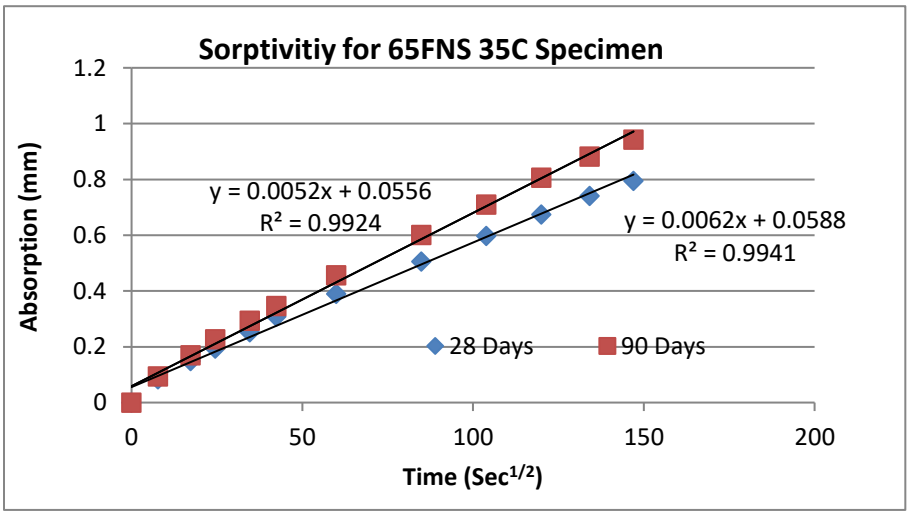

Table C.6 Rapid chloride penetrability test result

Type	Chloride Penetration			
	28 Days	Classification	90 Days	Classification
Control	1590	Low	1258	Low
20FNS 80C	1520	Low	715	Very low
30FNS 70C	1815	Low	958	Very low
40FNS 60C	1503	Low	1065	Low
40FNS 10GGBFS	1120	Low	856	Very low
50FNS 50C	1254	Low	713	Very low
65FNS 35C	1059	Low	508	Very low

APPENDIX D: Results of tested beams

Beam F-2-12 (a/d=3, effective span 1800 mm)

Load (kN)	Deflection (left) (mm)	Deflection (mid) (mm)	Deflection (right) (mm)
0	0	0	0
7	0.17	0.16	0.18
11	0.3	0.3	0.2
14	0.42	0.45	0.32
17	0.58	0.68	0.48
21	0.8	0.94	0.69
26	1.24	1.52	1.22
32	1.55	1.95	1.5
37	1.99	2.55	2.1
43	2.4	3.05	2.38
48	2.78	3.55	2.82
52	3.05	3.93	3.12
58	3.45	4.45	3.5
63	3.74	4.82	4.8
66	4	5.2	5.08
70	4.28	5.56	5.35
76	4.78	6.27	5.87
78	5.02	6.62	6.1
86	5.85	7.85	7
88	6.18	8.35	7.3
90	6.5	8.9	7.73
93	6.88	9.45	8.1
94	7.15	9.95	8.5
97	7.58	10.6	8.93
98	7.9	11.15	9.35
99	8.28	11.78	9.78
102	8.53	12.25	10.12
100	8.58	13.3	10.18
104	8.8	13.63	10.4
108	9.43	14.78	11.25
110	9.82	15.4	11.75
100	10.1	16	12.1
110	10.8	16.95	12.7
109	11.5	17.95	13.5
110	12.15	18.95	14.2
110	12.95	20	14.92
111	13.6	21	15.42
112	14.3	22	16.1
113	15.1	23.12	16.82
114	16.05	23.38	17.6
115	17.45	24	18.01

115	18.3	25.2	18.8
113	19.4	26.68	19.75
112	20.3	27.1	20.5
111	21.3	28.6	21.5
112	22.35	29.1	22.35
113	23.4	30	23.28
114	24.25	31.4	24.12
114	24.7	32.7	24.6
113	25.7	33.9	25.6
114	26.8	36	26.1
114	27.9	38	26.22
112	28.85	39	27
112	30	40.2	28
104	31.3	41.7	29.35
107	32.4	42.95	29.9
108	35.9	43.4	31
109	36.8	44.35	32.7
108	37.3	46.35	33.4
110	38.2	49.4	34.15
109	39.5	52.3	35.2
110	40.1	55.5	36.8
111	41.5	60.2	38.9

Beam F-2-16 (a/d=3, effective span 1800 mm)

Load (kN)	Deflection (left) (mm)	Deflection (mid) (mm)	Deflection (right) (mm)
0	0	0	0
4	0.15	0.31	0.05
10	0.3	0.62	0.2
20	0.45	0.75	0.25
33	0.78	0.91	0.65
42	1.1	1.05	0.98
53	1.6	1.7	1.19
60	1.85	1.95	1.56
67	2.2	2.15	1.75
77	2.63	2.48	2.22
82	2.8	3.11	2.49
86	3.14	4.48	2.68
92	3.9	5.35	2.99
99	4.65	6.28	3.5
105	4.9	7.77	3.85
110	5.23	8.55	4.29
117	5.55	9.68	4.5
125	5.93	10.2	4.93

132	6.35	11.1	5.48
144	7.1	12.35	6.4
151	8.75	14.5	7.22
163	9.65	16.45	7.88
170	10.33	18.35	8.98
173	11.35	20.3	9.8
169	12.6	23.35	11.2
163	12.98	25.6	12.68
162	14.6	26.3	13.3
158	15.4	27.7	15.9
160	17.05	28.95	16.4
162	19.4	29.1	18.2
160	21.4	31.7	20.1
155	22.4	34.7	22.9
110	25	38.7	23.88

Beam F-2-20 (a/d=3, effective span 1800 mm)

Load (kN)	Deflection (left) (mm)	Deflection (mid) (mm)	Deflection (right) (mm)
0	0	0	0
18	0.75	0.6	0
33	1.35	1.3	0.15
47	1.9	2.08	0.82
64	2.42	2.85	1.5
80	2.8	2.35	2.1
89	3	2.7	3.15
95	3.2	3	3.45
107	3.55	3.42	3.73
116	3.9	3.95	4.1
126	4.5	4.2	4.4
144	4.75	5.2	5
154	5.1	5.6	6.35
173	5.9	6.6	7.1
190	6.4	7.32	7.7
211	7.3	8.4	8.5
217	7.75	9.2	9
227	8.72	10.45	10.85
236	9.15	11.05	11.2
235	9.7	11.8	11.7
227	10.24	12.6	12.2
244	10.85	13.5	12.75
228	11.55	14.5	13.28
227	12	15.2	13.7
226	12.7	16.1	14.15
224	13.25	17	14.6
227	13.9	17.9	15.1

229	14.4	18.8	15.6
227	15	19.8	15.05
225	15.8	21.2	16.2
221	16.15	21.95	17.1
224	16.8	22.9	17.2
222	17.1	23.7	18.1
222	17.6	24.55	18.5
221	18.12	25.5	19
221	18.7	26.55	19.55
223	18.3	27.6	20.2
223	18.8	27.8	20.8
218	19.38	28.8	21.2
223	19.9	29.8	21.75
218	20.3	30.8	22.1
219	21.3	31.6	23
220	21.9	32.55	23.7
220	22.4	33.6	24.2
219	23	34.6	24.75
221	23.58	35.6	25.35
219	24	36.5	25.8
217	24.5	37.4	26.2
217	25.05	38.4	27.8
216	25.6	39.4	28.3
212	26.15	40.4	28.82
207	26.8	41.4	29.45
210	27.3	42.4	29.9
209	28.05	43.4	30.55
207	28.6	44.4	36
207	29.1	45.4	36.6
206	29.9	46.4	37.15
205	30.9	47.4	37.65
205	31.9	48.35	38.5
199	32.9	50.35	39.5
190	33.9	52.35	40.75
193	35.9	54.4	41.9
188	36.15	56.4	42.6
182	39.5	61.4	43.1
169	44	71.4	44.5
151	49.3	86.8	55.3
139	52	88	56.2
133	53	90	59.8

S-125-3 (a/d=3, effective span 1800 mm)

Load (kN)	Deflection (left) (mm)	Deflection (mid) (mm)	Deflection (right) (mm)
0	0	0	0
4	0.1	0.02	0.04
5	0.15	0.05	0.08
14	0.32	0.25	0.12
20	0.4	0.35	0.2
26	0.52	0.48	0.3
31	0.65	0.64	0.4
36	0.85	0.78	0.5
45	0.97	1.1	0.7
51	1.17	1.28	0.9
58	1.29	1.55	1.08
64	1.45	1.72	1.17
70	1.55	1.97	1.3
75	1.67	2.1	1.4
81	1.87	2.3	1.55
91	1.95	2.6	1.88
92	2.22	2.7	1.9
104	2.6	3.1	2.1
119	2.77	3.65	2.33
125	2.97	3.87	2.54
132	3.17	4.18	3
138	3.37	4.45	3.18
142	3.49	4.6	3.3
146	3.75	4.9	3.5
151	3.93	5.1	3.8
161	4.36	5.6	4.08
168	4.63	5.95	4.35
171	4.73	6.1	4.48
178	4.96	6.35	4.75
184	5	6.6	4.98
187	5.34	6.8	5.08
192	5.51	7	5.2
203	5.86	7.45	5.6
206	6.14	7.8	6
212	6.36	8.18	6.25
218	6.94	8.9	7.1
227	7.94	9.88	7.9
225	8.64	10.8	8.1
231	8.94	11.3	8.45
227	9.46	12.4	9.5

207	9.86	13.2	10.5
197	10.96	14.7	11.6
170	11.9	15.85	14.9

S-125-2.3 (a/d=2.3, effective span 1800 mm)

Load (kN)	Deflection (left) (mm)	Deflection (mid) (mm)	Deflection (right) (mm)
0	0	0	0
5	0.2	0	0
9	0.35	0	0
13	0.35	0	0
18	0.4	0.08	0
23	0.45	0.15	0
27	0.5	0.75	0.1
33	0.6	1.2	0.12
40	0.75	1.58	0.2
46	0.78	1.62	0.25
58	1	1.92	0.5
63	1.1	2.1	1
72	1.3	2.4	1.15
83	1.55	2.7	1.45
88	1.6	2.8	1.5
92	1.7	2.92	1.6
103	1.9	3.25	2
107	2	3.38	2.08
112	2.12	3.5	2.12
118	2.25	3.7	2.28
123	2.35	3.98	2.4
135	2.6	4.2	2.88
146	2.9	4.58	3.2
160	3.28	5.08	3.65
172	3.33	5.25	3.73
185	3.39	5.47	3.87
193	3.43	5.53	4.02
198	3.47	5.62	4.27
204	3.5	5.7	4.6
203	3.6	5.8	4.85
213	3.9	6.22	5.22
218	4.07	6.45	5.5
226	4.4	7	6.08
230	4.75	7.5	6.5
219	4.9	7.85	7.2

196	5.1	8.45	7.9
191	5.45	9.1	8.9
177	5.85	9.75	9.85
131	7.6	12.5	13.05

S-175-3 (a/d=3, effective span 1800 mm)

Load (kN)	Deflection (left) (mm)	Deflection (mid) (mm)	Deflection (right) (mm)
0	0	0	0
9	0.05	0.17	0.1
14	0.18	0.3	0.2
19	0.25	0.4	0.26
24	0.35	0.5	0.34
29	0.45	0.65	0.49
37	0.6	0.85	0.67
44	0.75	1.08	0.71
51	0.95	1.35	0.88
66	1.28	1.8	1.33
70	1.38	1.9	1.41
79	1.6	2.22	1.7
86	1.78	2.45	1.85
94	1.95	2.7	1.99
99	2.08	2.85	2.15
103	2.2	3.05	2.24
112	2.4	3.35	2.44
119	2.6	3.58	2.67
127	2.85	3.9	2.89
134	3.2	4.25	3.29
131	4.22	4.26	4.19
132	4.32	5.38	4.36
139	4.55	5.6	4.59
129	4.58	5.62	4.57
134	4.65	5.78	4.69
140	4.8	6	4.87
148	5.1	6.4	5.14
157	5.58	6.9	5.51
161	6.38	7.6	5.35
167	6.9	8.05	6.65
171	7.8	8.8	7.88
171	9.7	10.7	9.79
171	11.6	12.85	11.4
114	14.01	15.95	14.1

S-175-2.3 (a/d=2.3, effective span 1800 mm)

Load (kN)	Deflection (left) (mm)	Deflection (mid) (mm)	Deflection (right) (mm)
0	0	0	0
6	0.1	0.2	0.15
11	0.25	0.45	0.2
17	0.32	0.5	0.35
21	0.35	0.6	0.55
27	0.45	0.72	1.05
32	0.58	0.9	1.15
37	0.65	1.02	1.25
42	0.8	1.2	1.45
51	1	1.5	1.7
60	1.2	1.8	1.9
70	1.45	2.1	2.17
74	1.55	2.25	2.27
80	1.62	2.4	2.4
85	1.75	2.52	2.5
94	1.92	2.8	2.95
107	2.2	3.2	3.15
110	2.3	3.3	3.8
114	2.37	3.4	4.3
122	2.6	3.7	4.55
129	2.75	3.9	4.85
132	2.85	4.05	4.95
138	3	4.2	5
143	3.1	4.35	5.25
148	3.2	4.5	5.35
155	3.4	4.75	5.6
167	4.1	5.12	6.05
183	4.5	5.7	6.1
211	5.7	5.8	6.15
224	5.9	6	6.2
234	6.3	6.5	6.21
245	6.7	7.1	6.71
261	7.15	8	8.85
258	7.7	8.8	9.9
212	7.85	9.55	10.9
200	8.85	10.5	11.95
191	9.15	11.25	12.3
184	9.45	11.4	14.25
174	10.35	12.1	17.2
128	10.45	14	17.85

B-2-12-200 (a/d=3, effective span 1800 mm)

Load (kN)	Deflection (left) (mm)	Deflection (mid) (mm)	Deflection (right) (mm)
0	0	0	0
7	0.11	0.15	0.2
14	0.3	0.35	0.35
21.5	0.55	0.65	0.52
25	1.12	1.9	1.22
30	2.08	2.45	2.11
35	2.4	2.95	2.43
41	2.75	3.45	2.82
45	3.9	4.95	3.75
17	4.9	5.25	4.95

B-2-12-300 (a/d=3, effective span 1800 mm)

Load (kN)	Deflection (left) (mm)	Deflection (mid) (mm)	Deflection (right) (mm)
0	0	0	0
7	0.05	0.1	0.3
10	0.07	0.15	0.41
12	0.09	0.24	0.53
15	0.1	0.31	0.59
17	0.12	0.35	0.7
19	0.15	0.42	0.83
22	0.18	0.6	1.01
25	0.21	0.73	1.11
27	0.23	0.88	1.2
30	0.38	1.21	1.36
33	0.6	1.43	1.58
35	0.72	1.61	1.63
37	0.85	1.8	1.85
39	0.95	1.95	1.93
41	1.05	2.12	2.1
43	1.23	2.33	2.29
45	1.31	2.49	2.35
47.5	1.38	2.65	2.45
50	1.53	2.88	2.55
53	1.65	3.1	2.76
55	1.75	3.28	2.88
57	1.86	3.48	3.08
59	1.93	3.55	3.15
62	2.06	3.8	3.3
65	2.23	4.01	3.43

67	2.35	4.25	3.6
70	2.44	4.44	3.7
72	2.7	4.8	3.9
17	3.02	5.3	4.57

B-2-16-200 (a/d=3, effective span 1800 mm)

Load (kN)	Deflection (left) (mm)	Deflection (mid) (mm)	Deflection (right) (mm)
0	0	0	0
11	0.68	0.7	0.5
15	0.85	0.88	0.75
21	1.03	1.1	1.1
26	1.3	1.45	1.25
31	1.5	1.8	1.55
36	1.65	1.95	1.8
41	1.9	2.3	1.95
47	2.12	2.63	2.19
54	2.4	3.05	2.5
56	2.5	3.2	2.63
61	2.75	3.58	2.79
62	3.4	4.3	3.7
12	4	7.8	4.19

B-2-16-300 (a/d=3, effective span 1800 mm)

Load (kN)	Deflection (left) (mm)	Deflection (mid) (mm)	Deflection (right) (mm)
0	0	0	0
8	0.12	0.3	0.15
13	0.19	0.41	0.19
20	0.25	0.52	0.24
28	0.32	0.59	0.27
33	0.4	0.7	0.3
38	0.61	0.95	0.55
42	0.75	1.15	0.7
47	0.86	1.43	0.89
52	1.1	1.7	1.1
58	1.45	1.94	1.5
64	1.63	2.4	1.72
68	1.92	3.1	2.5
14	2.4	4.6	3.2

APPENDIX E: Attribution of research outputs

Article 1:

Rahman, M.A., Sarker, P.K. and Shaikh, F.A.U. (2015). Fresh and Early-Age Properties of Cement Pastes and Mortars Blended with Nickel Slag. *27th Biennial National Conference of the Concrete Institute of Australia in conjunction with the 69th RILEM Week*, Aug 30 2015. Melbourne, Australia.

Authors and full affiliations:

MA Rahman, Phd Student, Department of Civil Engineering, Curtin University, WA

PK Sarker, Associate Prof., Department of Civil Engineering, Curtin University, WA

FAU Shaikh, Associate Prof., Department of Civil Engineering, Curtin University, WA

Name of Co-author	Literature review	Experimental design/concept	Data collection	Discussion	Paper writing
PK Sarker		x		x	x
I acknowledge that these represent my contribution to the above research output. *(Signature)*					
FAU Shaikh		x		x	x
I acknowledge that these represent my contribution to the above research output. *(Signature)*					

Article 2:

Rahman, M.A., Sarker, P.K., Shaikh, F.A.U., Saha, A.K. (2017). Soundness and compressive strength of Portland cement blended with ground granulated ferronickel Slag. *Construction and Building Materials*, 140: 194-202.

Authors and full affiliations:

MA Rahman, Phd Student, Department of Civil Engineering, Curtin University, WA

PK Sarker, Associate Prof., Department of Civil Engineering, Curtin University, WA

FAU Shaikh, Associate Prof., Department of Civil Engineering, Curtin University, WA

AK Saha, Phd Student, Department of Civil Engineering, Curtin University, WA

Name of Co-author	Literature review	Experimental design/concept	Data collection	Discussion	Paper writing
PK Sarker		x		x	x
I acknowledge that these represent my contribution to the above research output. *(Signature)*					
FAU Shaikh		x		x	x
I acknowledge that these represent my contribution to the above research output. *(Signature)*					
AK Saha			x		
I acknowledge that these represent my contribution to the above research output. *(Signature)*					

APPENDIX F: Permission for reusing figures

F.1 License for figure 2.1

ELSEVIER LICENSE
TERMS AND CONDITIONS

Mar 23, 2019

This Agreement between Curtin University -- Muhammad Ashiqur Rahman ("You") and Elsevier ("Elsevier") consists of your license details and the terms and conditions provided by Elsevier and Copyright Clearance Center.

License Number	4546430384792
License date	Mar 12, 2019
Licensed Content Publisher	Elsevier
Licensed Content Publication	Construction and Building Materials
Licensed Content Title	Influence of Portland cement and ground-granulated blast-furnace slag on bleeding of fresh mix
Licensed Content Author	Hong Jae Yim,Jae Hong Kim,Seong Ho Han,Hyo-Gyoung Kwak
Licensed Content Date	Apr 1, 2015
Licensed Content Volume	80
Licensed Content Issue	n/a
Licensed Content Pages	9
Start Page	132
End Page	140
Type of Use	reuse in a thesis/dissertation
Portion	figures/tables/illustrations
Number of figures/tables /illustrations	1
Format	both print and electronic
Are you the author of this Elsevier article?	No
Will you be translating?	No
Original figure numbers	Figure 1
Title of your thesis/dissertation	Study of the use of ferronickel slag in concrete
Expected completion date	Jul 2019
Estimated size (number of pages)	170
Requestor Location	Curtin University Kent Street, Bentley Perth, Western AUstralia 6102 Australia Attn: Muhammad Ashiqur Rahman
Publisher Tax ID	GB 494 6272 12
Total	**0.00 USD**
Terms and Conditions	

F.2 License for figure 2.2

SPRINGER NATURE LICENSE
TERMS AND CONDITIONS

Mar 23, 2019

This Agreement between Curtin University -- Muhammad Ashiqur Rahman ("You") and Springer Nature ("Springer Nature") consists of your license details and the terms and conditions provided by Springer Nature and Copyright Clearance Center.

License Number	4546431305188
License date	Mar 12, 2019
Licensed Content Publisher	Springer Nature
Licensed Content Publication	Materials and Structures
Licensed Content Title	A study on durability properties of high-performance concretes incorporating high replacement levels of slag
Licensed Content Author	Erhan Güneyisi, Mehmet Gesoğlu
Licensed Content Date	Jan 1, 2007
Licensed Content Volume	41
Licensed Content Issue	3
Type of Use	Thesis/Dissertation
Requestor type	academic/university or research institute
Format	print and electronic
Portion	figures/tables/illustrations
Number of figures/tables /illustrations	1
Will you be translating?	no
Circulation/distribution	<501
Author of this Springer Nature content	no
Title	Study of the use of ferronickel slag in concrete
Institution name	Curtin University
Expected presentation date	Jul 2019
Portions	Figure 4
Requestor Location	Curtin University Kent Street, Bentley Perth, Western AUstralia 6102 Australia Attn: Muhammad Ashiqur Rahman
Billing Type	Invoice
Billing Address	Curtin University Kent Street, Bentley Perth, Australia 6102 Attn: Muhammad Ashiqur Rahman
Total	**0.00 USD**

F.3 License for figure 2.3

ELSEVIER LICENSE
TERMS AND CONDITIONS

Mar 23, 2019

This Agreement between Curtin University -- Muhammad Ashiqur Rahman ("You") and Elsevier ("Elsevier") consists of your license details and the terms and conditions provided by Elsevier and Copyright Clearance Center.

License Number	4546440076857
License date	Mar 12, 2019
Licensed Content Publisher	Elsevier
Licensed Content Publication	Cement and Concrete Research
Licensed Content Title	Strength development of mortars containing ground granulated blast-furnace slag: Effect of curing temperature and determination of apparent activation energies
Licensed Content Author	S.J. Barnett,M.N. Soutsos,S.G. Millard,J.H. Bungey
Licensed Content Date	Mar 1, 2006
Licensed Content Volume	36
Licensed Content Issue	3
Licensed Content Pages	7
Start Page	434
End Page	440
Type of Use	reuse in a thesis/dissertation
Intended publisher of new work	other
Portion	figures/tables/illustrations
Number of figures/tables /illustrations	1
Format	both print and electronic
Are you the author of this Elsevier article?	No
Will you be translating?	No
Original figure numbers	Figure 1
Title of your thesis/dissertation	Study of the use of ferronickel slag in concrete
Publisher of new work	Curtin University
Expected completion date	Jul 2019
Estimated size (number of pages)	170
Requestor Location	Curtin University Kent Street, Bentley Perth, Western AUstralia 6102 Australia Attn: Muhammad Ashiqur Rahman
Publisher Tax ID	GB 494 6272 12
Total	**0.00 USD**
Terms and Conditions	

F.4 License for figure 2.4

ELSEVIER LICENSE
TERMS AND CONDITIONS

Mar 23, 2019

This Agreement between Curtin University -- Muhammad Ashiqur Rahman ("You") and Elsevier ("Elsevier") consists of your license details and the terms and conditions provided by Elsevier and Copyright Clearance Center.

License Number	4546440409475
License date	Mar 12, 2019
Licensed Content Publisher	Elsevier
Licensed Content Publication	Cement and Concrete Composites
Licensed Content Title	Effects of MgO-based expansive additive on compensating the shrinkage of cement paste under non-wet curing conditions
Licensed Content Author	L. Mo,M. Deng,A. Wang
Licensed Content Date	Mar 1, 2012
Licensed Content Volume	34
Licensed Content Issue	3
Licensed Content Pages	7
Start Page	377
End Page	383
Type of Use	reuse in a thesis/dissertation
Intended publisher of new work	other
Portion	figures/tables/illustrations
Number of figures/tables /illustrations	1
Format	both print and electronic
Are you the author of this Elsevier article?	No
Will you be translating?	No
Original figure numbers	Figure 8
Title of your thesis/dissertation	Study of the use of ferronickel slag in concrete
Publisher of new work	Curtin University
Expected completion date	Jul 2019
Estimated size (number of pages)	170
Requestor Location	Curtin University Kent Street, Bentley Perth, Western AUstralia 6102 Australia Attn: Muhammad Ashiqur Rahman
Publisher Tax ID	GB 494 6272 12
Total	**0.00 USD**
Terms and Conditions	